

HYDRODYNAMICS AND CONTROL IN THERMAL-FLUID NETWORKS

A Dissertation

Submitted to the Graduate School
of the University of Notre Dame
in Partial Fulfillment of the Requirements
for the Degree of

Doctor of Philosophy

by

Walfre Franco, B.S., M.S.

Mihir Sen, Director

Graduate Program in Aerospace and Mechanical Engineering

Notre Dame, Indiana

July 2003

HYDRODYNAMICS AND CONTROL IN THERMAL-FLUID NETWORKS

Abstract

by

Walfre Franco

Theoretical, numerical and experimental studies of hydraulic, thermal and control aspects in fluid networks are presented. First, a one-dimensional differential-algebraic nonlinear model, based on first principles, representing the time-dependent behavior in networks is developed. A thermal-hydraulic analysis of a small network with three common control strategies for heating and cooling of buildings is carried out. *PID* controllers are used to respond to changes in the thermal load. The temperature difference between the chiller supply and return water is used as a criterion for comparison.

Next, an experimental hydronic network featuring these control methodologies is used to complement the theoretical study by including all the complexities of the problem, such as valves hysteresis, dynamic time constants, imperfect actuators and imperfect sensors. Stability and reachability issues arise during the control process as a consequence of changing the thermal load. The importance of location and selection of the hardware used for control becomes evident.

Control hardware placement is addressed next. The discrete space of possible locations for a specific layout is explored in order to find the best configuration. The hardware elements are a control valve and two booster pumps. Pumping action is divided among the two pumps to be able to look at different combinations. The

change in operating conditions and the output reachabilities of the control system are used as criteria to compare the relative merits of different configurations.

Finally, the mathematical model is extended to the study of large, possibly infinite, self-similar networks configured in the form of a regular branching tree. Each branch of the tree bifurcates with a constant diameter and length ratio. Since the local Reynolds number changes at every generation, the flow may transition from laminar to turbulent or relaminarize from turbulent to laminar. The global stability of the steady flow is demonstrated for friction laws for which viscous forces are nondecreasing functions of the flow rate, otherwise the flow may oscillate. In addition the control properties of the network hydrodynamics are investigated using valves and pumps as control elements to manipulate branch flow rates and nodal pressures.

A Vera, mi cronopio favorito.

CONTENTS

FIGURES	vi
TABLES	x
ACKNOWLEDGEMENTS	xi
NOMENCLATURE	xii
CHAPTER 1: BACKGROUND	1
1.1 Science of networks	2
1.1.1 Fractal dimension	4
1.1.2 Bifurcating networks	6
1.2 Linear control theory	9
1.2.1 State controllability	10
1.2.2 Output controllability	10
1.2.3 Observability	10
1.3 Control in bifurcating networks	11
1.4 Systems of differential algebraic equations	12
1.4.1 Linear systems	12
1.4.2 Linear stability	12
1.4.3 Bounded control	13
1.4.4 Nonlinear systems	14
1.5 Hydronic systems	15
1.5.1 Cooling networks	17
1.5.2 Optimization of hardware placement and selection	18
1.6 Objectives of dissertation	19
1.7 Scope of dissertation	21
CHAPTER 2: MATHEMATICAL MODEL	23
2.1 Hydraulic components	23
2.2 Thermal balance	25
2.3 Network principles	28
2.4 Open-circuit fluid networks	28

2.5	Closed-circuit fluid networks	29
CHAPTER 3: HEATING AND COOLING OF BUILDINGS		32
3.1	Thermal control strategies	34
3.1.1	Variable flow	34
3.1.2	Constant flow	34
3.1.3	Constant temperature difference	34
CHAPTER 4: EXPERIMENTAL HYDRONIC NETWORK		36
4.1	Heating circuit	36
4.2	Cooling circuit	39
4.3	Data acquisition and processing	44
CHAPTER 5: NUMERICAL STUDY OF THERMAL CONTROL STRATE- GIES		48
5.1	Generalized network configuration	49
5.2	Integral control	51
5.3	Open-loop control	53
5.4	Dynamics and feedback control	56
5.5	Comparison of strategies	62
5.6	Discussion	66
CHAPTER 6: EXPERIMENTAL STUDY OF THERMAL CONTROL STRATE- GIES		68
6.1	Proportional-integral-derivative control	69
6.2	Experimental methodology	72
6.3	Steady state and dynamics of control valves	72
6.4	Dynamics of feedback control response	75
6.4.1	Primary heating and cooling loops	75
6.4.2	Secondary loops	80
6.4.3	Stable and unstable control	84
6.4.4	System reachability	84
6.5	Comparison of control strategies	88
6.5.1	Temperature effect on chiller	88
6.5.2	Pressure drop effect on primary loop	89
6.5.3	Temperature effect on hot loop side	89
6.6	Discussion	93
CHAPTER 7: SELECTION AND PLACEMENT OF HARDWARE		95
7.1	Steady-state mathematical model	96
7.1.1	Hydraulic components	96
7.1.2	Thermal modeling	97
7.1.3	Network principles	97
7.2	Statement of problem	98

7.2.1	Hardware configurations	98
7.2.2	Bounded thermal control	100
7.2.3	Network performance	100
7.3	Computations	101
7.3.1	Control valve on supply pipe	103
7.3.2	Control valve on coil inlet pipe	107
7.3.3	Control valve on bypass pipe	110
7.4	Optimal configuration	110
7.5	Discussion	113
CHAPTER 8: HYDRODYNAMICS OF REGULAR TREE NETWORKS . .		115
8.1	Topology	116
8.2	Mathematical model	118
8.3	Steady-state analysis	119
8.3.1	Large networks	119
8.3.2	Infinite networks	120
8.4	Global stability of steady flow	121
8.4.1	Network of two generations	127
8.4.2	Network of three generations	128
8.4.3	Network of N_g generations	131
8.5	Unstable flow	132
8.5.1	Single branch	133
8.5.2	Branching network	134
8.6	Hydrodynamic control	141
8.6.1	Control by means of valves	141
8.6.2	Control by means of individual pumps	143
8.6.3	From differential algebraic to differential equations	144
8.6.4	State R-controllability and output controllability	148
8.7	Discussion	150
CHAPTER 9: CONCLUSIONS AND RECOMMENDATIONS		152
9.1	Modeling, simulation and experiments in hydronic networks	152
9.2	Strategies for thermal control	152
9.3	Selection and placement of control hardware	153
9.4	Bifurcating networks	154
9.4.1	Flow dynamics	154
9.4.2	Control properties	155
9.5	Recommendations	155
9.6	Significance of this research	157
REFERENCES		158

FIGURES

1.1	Seven Bridges of Königsberg.	2
1.2	A view of Tug river basin in West Virginia (Rinaldo <i>et al.</i> , 1998). . .	7
1.3	Arterial circulation system. Source: AMA's <i>Current Procedural Terminology</i> , Revised 1998 Edition. CPT is a trademark of American Medical Association.	8
1.4	Steam and chilled water network at Notre Dame campus.	16
2.1	Coil leaving air temperature using -- distributed and — lumped parameter models.	26
2.2	Open loop flow circuit.	30
2.3	Closed loop flow circuit.	31
3.1	(a) Variable flow, <i>VF</i> . (b) Constant flow, <i>CF</i> . (c) BRDG-TNDR, <i>BT</i> . Broken lines represent control signals.	33
4.1	Experimental hydronic network.	37
4.2	Experimental network layout.	38
4.3	Water heater.	40
4.4	Water-water shell-tube heat exchanger.	41
4.5	Water-water compact heat exchanger.	42
4.6	Variable speed pump.	43
4.7	Booster pump.	45
4.8	Pneumatic control valve.	47
5.1	Generalized network layout.	50
5.2	Leaving air temperature as function of valve closing parameter for three different air velocities; — * — <i>VF</i> and — ▷ — <i>CF</i> ; $T_a^E = 30^\circ\text{C}$. . .	54

5.3	Leaving air temperature as function of valve closing parameter for three different entrance air temperatures; $- * -VF$ and $- \triangleright -CF$; $U_a = 10$ m/s.	55
5.4	Network behavior, BT method: (a) Δp_{bp} and T_w^L ; (b) T_a^L ; $T_a^E = 30^\circ\text{C}$, $U_a = 10$ m/s.	57
5.5	Method $- * -VF$ and $- \triangleright -CF$: (a) mass flow rates, (b) leaving air temperature; $T_a^E = 30^\circ\text{C}$, $U_a = 10$ m/s, $v_2 = 0.76$	58
5.6	Method BT : (a) mass flow rates, (b) leaving air temperature, (c) leaving water temperature, (d) pressure drop in bypass; $T_a^E = 30^\circ\text{C}$, $U_a = 10$ m/s, $v_1 = 0.46$, $v_3 = 0.54$	59
5.7	Dynamic response of control system to drop in air velocity, method $- * -VF$ and $- \triangleright -CF$; $\bar{T}_a^L = 26^\circ\text{C}$, $T_a^E = 30^\circ\text{C}$	60
5.8	Dynamic response of control system to drop in air velocity, BT method; $\bar{T}_w^L = 5.5^\circ\text{C}$, $\Delta \bar{p}_{bp} = 20000$ N/m ² ; $T_a^E = 30^\circ\text{C}$	61
5.9	Temperature drop in chiller as function of air velocity; $- \circ -BT$, $- \triangleright -CF$, $- * -VF$	63
5.10	Temperature drop in chiller as function of air entering temperature; $- \circ -BT$, $- \triangleright -CF$, $- * -VF$	64
5.11	ΔT_{ch} dynamics; $- \circ -BT$, $- \triangleright -CF$, $- * -VF$	65
6.1	Steady state pressure drop $\Delta p_{V_{10}}$ as function of input signal v_{10} ; $- \circ -$ opening, $- + -$ closing.	73
6.2	Steady and dynamic flow rate q_4 as function of input signal v_7 ; $- \circ -$ opening, $- + -$ closing. Arrows indicate direction of dynamic path.	74
6.3	Secondary water flows and heat exchanger inlet temperature T_{21} on heating loop: $- \circ -BT$, $- \triangleright -CF$, $- * -VF$. Dashed vertical lines are instants at which thermal load is changed.	76
6.4	Supply temperature T_1 and pressure drop Δp_{P_4} across pump on primary cooling loop: $- \circ -BT$, $- \triangleright -CF$, $- * -VF$. Dashed vertical lines are instants at which thermal load is changed.	78
6.5	Main loop flow q_1 , heat exchanger inlet flows q_9 , q_6 and q_3 , and supply flows q_5 and q_2 to secondary on cooling loop: $- \circ -BT$, $- \triangleright -CF$, $- * -VF$. Dashed vertical lines are instants at which thermal load is changed.	79
6.6	Heat exchangers outlet temperatures on heating loop: $- \circ -BT$, $- \triangleright -CF$, $- * -VF$. Dashed vertical lines are instants at which thermal load is changed.	81

6.7	Secondary return temperatures and pressure drop Δp_{V_8} across V_8 on cooling loop: $- \circ -BT$, $- \triangleright -CF$, $- * -VF$. Dashed vertical lines are instants at which thermal load is changed.	83
6.8	V_{12} phase space for VF when $t > 4500$ s.	85
6.9	V_9 phase space for CF when $t > 4500$ s.	86
6.10	V_{11} during operation for VF	87
6.11	ΔT_{ch} as a function of hot water flow rates q_8 , q_7 and q_4 : $- \circ -BT$, $- \triangleright -CF$, $- * -VF$	90
6.12	Return temperatures from secondaries on cooling side T_4 , T_{10} and T_{20} , and outlet temperatures on heating side T_8 , T_{14} and T_{18} as a function of hot water flow rates q_8 , q_7 and q_4 : $- \circ -BT$, $- \triangleright -CF$, $- * -VF$	91
6.13	Pressure drop Δp at secondaries in cooling loop: $- \circ -BT$, $- \triangleright -CF$, $- * -VF$. Dashed vertical lines are instants at which thermal load is changed.	92
7.1	Subcircuit layout.	99
7.2	ΔT_w^R and ΔT_a^L for different v ; $\diamond = [1, j, k, B]$, $+ = [2, j, k, B]$, $\square = [3, j, k, B]$	102
7.3	ΔT_w^R and ΔT_a^L for different v ; $\circ = [1, 1, 3, B]$, $* = [1, 2, 1, B]$, $\Delta = [1, 3, 2, B]$. Arrows indicate direction of increasing B	104
7.4	Temperatures as a function of B for $[1, j, k, B]$: $* - T_a^L(v_{op})$, $* - T_a^L(v_{cl})$, $\circ - T_w^R(v_{op})$, $\circ - T_w^R(v_{cl})$	106
7.5	ΔT_w^{af} and ΔT_a^L for different v ; $\circ = [2, 1, 3, B]$, $* = [2, 2, 1, B]$, $\Delta = [2, 3, 2, B]$. Arrows indicate direction of increasing B	108
7.6	Temperatures as a function of B for $[2, j, k, B]$: $* - T_a^L(v_{op})$, $* - T_a^L(v_{cl})$, $\circ - T_w^R(v_{op})$, $\circ - T_w^R(v_{cl})$	109
7.7	ΔT_w^{af} and ΔT_a^L for different v ; $\circ = [3, 1, 3, B]$, $* = [3, 2, 1, B]$, $\Delta = [3, 3, 2, B]$. Arrows indicate direction of increasing B	111
7.8	Temperatures as a function of B for $[3, j, k, B]$: $* - T_a^L(v_{op})$, $* - T_a^L(v_{cl})$, $\circ - T_w^R(v_{op})$, $\circ - T_w^R(v_{cl})$	112
8.1	Schematic of tree with branches.	117
8.2	Length as function of scaling parameter.	122
8.3	Lateral area as function of scaling parameter.	123
8.4	Tube volume as function of scaling parameter.	124

8.5	R as function of scaling parameter.	125
8.6	Ratio S/R as function of scaling parameter.	126
8.7	Network with two generations.	127
8.8	Analytical $- + -$ and numerical $- \circ -$ frequency as function of ϵ . . .	135
8.9	Pipe dynamics for $\epsilon = 0.05$	136
8.10	Pipe resistance F as function of q	137
8.11	Flow rates for network with four generations when second generation oscillates.	138
8.12	Nodal pressures for network with four generations when second generation oscillates.	139
8.13	ϵ - β plane for 10 generation network where first branch Reynolds number is eleven times Re_c	140
8.14	Flow into and out of junction k	144

TABLES

5.1	DIMENSION OF PIPES IN GENERALIZED NETWORK.	52
6.1	<i>PID</i> CONTROLLERS GAINS.	70
8.1	RANKS OF CONTROLLABILITY MATRICES.	149

ACKNOWLEDGEMENTS

I thank Professor Mihir Sen for this unique journey of learning, for lighting the flame of scientific curiosity and for believing in his students. I believe that his philosophy, mentoring and friendship bring out the best in all of his students and make a deep and lasting impression on their lives.

I am thankful to my co-advisor Professor K.T. Yang for all his valuable feedback and insightful comments on the philosophy of research. I extend my gratitude to Professor Bill Goodwine for his always welcome and acute remarks on my research project. I also thank Professor John Renaud for his support.

I thank Rod McClain for designing and building the experimental facility and for reading my dissertation. Thanks are also given to Kevin Peters for his punctual and very professional assistance.

I would like to give special mention to my wife, Bridget Franco, for her unflagging support and patience and to my mother, Belinda Consuegra, for her encouragement throughout my academic life. I thank my family for believing in me. Thanks to the friends I have made here at Notre Dame - those who have already moved on, those leaving and those staying - for sharing all the ups and downs of our graduate school journey.

I would like to acknowledge the support of the National University of Mexico (UNAM) for providing funding during my graduate studies at the University of Notre Dame. I also acknowledge BRDG-TNDR for their financial support.

NOMENCLATURE

A	area (m^2)
B	pump partition parameter
BT, CF, VF	control configurations
c	specific heat (J/kg K)
d	pipe diameter (m)
e	error
F	flow resistance
f	friction factor
H	head (m)
HT	water heater
HX	heat exchanger
h	heat transfer coefficient ($\text{W/m}^2 \text{K}$)
K	loss coefficient
k_P	proportional gain (Volts)
k_I	integral gain (Volts/s)
k_D	derivative gain (Volts s)
l	pipe length (m)
M	mass (kg)
MV	manual valve
\dot{m}	mass flow (kg/s)
N_b	number of total branches

N_g	number of generations
N_n	number of total nodes
N_o	number of outputs
N_p	number of pumps
Nu	Nusselt number
P	pump
\mathcal{P}	total pressure rise (N/m ²)
Pr	Prandtl number
p	pressure (N/m ²)
Δp	pressure drop (N/m ²)
q	volumetric flow (m ³ /s)
T	temperature (°C)
ΔT_{ch}	temperature difference across chiller (°C)
r_i	number of branches in generation i
Re	Reynolds numbers
S	volume (m ³)
t	time (s)
U	velocity (m/s)
V	valve
v	signal from valve (Volts)

Subscripts and superscripts

a	air
bp	bypass
c	critical
cc	cooling coil

<i>ch</i>	chiller
<i>cl</i>	closed
<i>E</i>	entering
<i>f</i>	final
<i>in</i>	inlet
<i>L</i>	leaving
<i>l</i>	left
<i>out</i>	outlet
<i>op</i>	open
<i>R</i>	return
<i>r</i>	right
<i>rf</i>	refrigerant
<i>ref</i>	reference
<i>sat</i>	saturation
<i>S</i>	supply
<i>t</i>	tube
<i>w</i>	water
0	initial

Greek symbols

α	thermal diffusivity (m ² /s)
β	scaling parameter
ζ	total efficiency of air side surface
θ	scaling parameter
κ	thermal conductivity (W/m K)
ν	kinematic viscosity (m ² /s)

ξ	period
ρ	water density (kg/m ³)
σ	roughness of duct wall (m)
τ	time constant (s)
ϕ	frequency

CHAPTER 1

BACKGROUND

A common practice in trying to understand the behavior of complex systems, such as social, economic, biological and natural systems, is to study their different components. In many cases this approach has successfully explained the properties of individual components. However, when the pieces are put together our understanding of the system behavior might fall short. The little or lack of understanding may be due to the fact that important interplay between components is ignored or underestimated. The world, besides being complex, is highly interconnected. Artificial or engineering systems are by no means free from this complexity, the difference is that we build each component but together they become overwhelming. Among several reasons for achieving a better understanding of complex interconnected systems are to be able to predict and/or regulate them. In many systems regulation of a specific process is a fundamental part of their basic functions. Consider as examples societies, stock markets, the human body and heating and cooling of buildings.

The scope of this dissertation includes the control in thermal and fluid networks. Networks geometrically small and irregular are considered, as well as large, regular and self-similar ones. Thus, there are many different motivations and implications in studying these systems but all within the context of networks and control. The nature of the investigation makes necessary to step outside of the traditional thermal sciences methods and theory. Loosely speaking the thermal sciences provide the

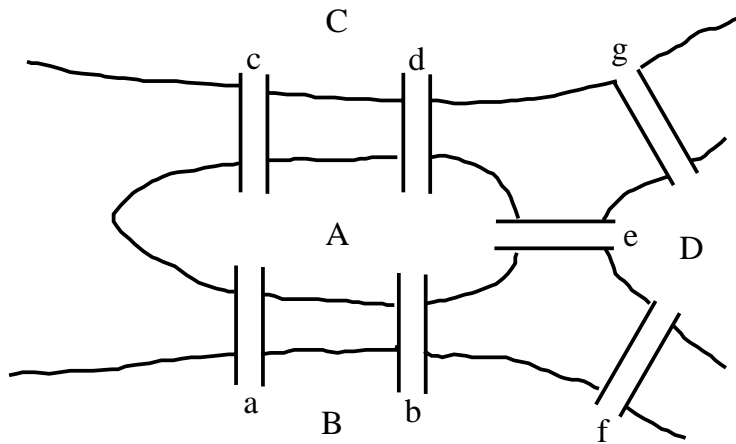


Figure 1.1. Seven Bridges of Königsberg.

problem that is tackled by a combination of local and external tools and concepts. There are many disciplines and areas of knowledge that have contributed to this work. Some of the most important are reviewed in the following sections.

1.1 Science of networks

Networks are not new to the scientific community. Transportation and communication problems have always challenged the mankind. The Pregel river ran through the city of Königsberg in Eastern Prussia such that in its center was an island. The river separated into two branches at the island. Seven bridges were built so that the people of the city could get from one part to another. The people of Königsberg used to entertain themselves by wondering whether or not one could walk around the city crossing each bridge only once. Figure 1.1 illustrates the seven bridges of Königsberg. In 1736 Leonhard Euler mathematically demonstrated that there is no solution for such a problem. In solving such a dilemma Euler laid the foundations of the development of a new branch on mathematics known as graph theory (Biggs *et al.*, 1976). Graph theory studies the mathematical

properties of graphs, such as size, degree, paths, cycles, distances, diameters and regularity among others (Balakrishnan and Ranganathan, 2000). A graph G is an ordered collection of vertices that may or may not be connected to each other by edges; i.e. $G = (V(G), E(G), I_G)$, where $V(G)$ is a nonempty set of vertices, $E(G)$ a disjoint set of edges from $V(G)$ and I_G is an incidence map that associates each element of $E(G)$ to $V(G)$. The number of edges incident at a vertex is the degree of the vertex. A graph is regular if every vertex has the same degree. Graph theory has successfully been used for solving problems of shortest-paths, timetables and connectors. It has also been used in social psychology, Harary *et al.* (1965) studied the social relationships between people within a particular group.

Recently the study of networks has taken a new shift. Barabási (2002) proposed Networks as a new science whose backbone is to study the way they emerge, develop, look like and impact our understanding of complex systems. The author investigated the World Wide Web, Hollywood movie stars, airports and metabolic pathways concluding that these networks are scale-free. The number of vertices with n edges or links follows a power law distribution, i.e. there are a few vertices highly connected. As a consequence, removing 80% of the least connected nodes would have a small effect on the network. However removing some of those highly connected vertices could be a disaster. Boguña *et al.* (2003) studied the spreading of infections in complex population networks. They showed that scale free networks have a null epidemic threshold and always show a finite fraction of infected individuals. This weakness was also found in immunization strategies that can be successfully developed only by taking into account the inhomogeneous connectivity properties of scale-free networks. Strogatz (2001) claims that complex networks pervade all of science. In addition to investigate the structure of networks, the author explores the collective dynamics of the system given the individual dynamics of components

and coupling architecture. Csete and Doyle (2002) identify the complexity of highly interconnected artificial and biological systems as a consequence of convergent evolution of the system. They propose that there is a deep and necessary interplay between complexity and robustness, modularity, feedback and fragility. Thorsen *et al.* (2002) used microfluidic large-scale integration to construct the fluidic analog of a comparator array and a memory storage device. Large-scale integration technology is used to built complex integrated circuits containing hundreds to thousands individual components. The chips contain flow networks with thousands of micromechanical valves and hundreds of individually addressable chambers. A valve multiplexor, which is a combinatorial array of binary patterns, allows complex fluid manipulations with a minimal number of controlled inputs.

1.1.1 Fractal dimension

In Euclidean geometry the dimension of an object has an integer value, e.g. a point has dimension zero, a line has dimension one, the interior of a triangle has dimension two and the interior of a pyramid has dimension three. This concept of dimension is related to coordinate geometry because it is the minimum number of coordinates needed to describe all points contained in an object. A different concept of dimension relates the dimension of the space to the way it can be divided by boundaries, e.g. a curve can be divided by cuts of zero dimension therefore has dimension one. A generalization of this concept is the Hausdorff (1919) definition of dimension, which is not restricted to integer values. To each set $E \subset \mathbb{R}^n$ corresponds a topological dimension D defined as

$$D = \lim_{\gamma \downarrow 0} \frac{\ln N_\gamma}{\ln \gamma^{-1}} \quad (1.1)$$

where N_γ is the number of boxes of side γ necessary to cover the set E . If D is not an integer the dimension is said to be fractal. There are different methods to

compute D and sometimes different definitions of dimension are used. A fractal can be defined as a set whose dimension is greater than its topological dimension in the Euclidean space. An essential property of a fractal object is self-similarity, that is it looks the same in any scale. The Koch curve is an example of a fractal with perfect self similarity.

Many natural and biological systems exhibit a fractal nature; branches of trees, river basins, leaf veins, coast lines, etc. Several researchers have used the concept of fractals to calculate the dimension of natural and biological systems under the hypothesis that systems exhibiting a fractal geometry sometimes represent reality better than their Euclidean counterpart. West *et al.* (1997) proposed a fractal model to explain the origin of allometric scaling relations in biology. Allometric relations are power laws characteristic of organisms; a biological variable Y is typically related to the body mass M as $Y = Y_0 M^b$. The model describes the transport of materials through space-filling fractal networks of branching tubes which minimize energy dissipation and have terminal tubes that are invariant to body size. The authors compared their model predictions to empirical observations of the cardiovascular and respiratory system. A few studies about the fractal nature of the vascular and respiratory system are provided by the literature (Zamir, 1999, 2001; Gutierrez, 2002; Grasman *et al.*, 2003). Artificial networks within this geometry have also been studied. Pence (2002) compared the wall temperature and pressure distribution of a fractal-like channel network to that of a straight channel network. It was assumed that the hydrodynamic and thermal boundary layer redevelop at each bifurcation. The flow was laminar and the thermal properties were constant. The fractal-like array yielded 60% lower pressure drop and a 30°C lower temperature under the same total flow rate and pumping power conditions. In a similar study, Chen and Cheng (2002) investigated the increased cooling capacity and decreased power requirement

in fractal trees in comparison to traditional parallel channels for the cooling of a microelectronic chip.

1.1.2 Bifurcating networks

Trees are a very common form of flow networks in natural, biological and artificial systems. A common engineering example is the piping that distributes water in a city. The water is pumped from the source to the end user through a series of pipes of decreasing cross-sectional areas and lengths. A similar network provides heating and cooling fluids in district and building climate-control systems. In nature the collection of water in a river basin is through streams and tributaries of different flow rates. Figure 1.2 illustrates the basin of the Fella river in Italy. The mammalian vascular systems and bronchial trees also have similar configurations. Figure 1.3 illustrates the arterial circulation system which distributes oxygenated blood to the body. Many of these trees not only have flow but also transport of a scalar such as heat or species concentration. The bronchial system is one example where mass is transferred and building heating/cooling system another that works with heat.

Though there have been many studies of flows in branching trees, the geometrical complexity of an irregular tree with a large number of generations has precluded the demonstration of general results. The magnitude of the problem can be reduced, however, by assuming simplifications in the dynamics and regularity in the geometry. Most studies of blood flow assume that the flow rate is proportional to the longitudinal pressure gradient in a blood vessel (Cohn, 1954; Berne and Levy, 1998; Gafiychuk and Lubashevsky, 2001). While this assumption does not take into account entry effects, flow separation near bifurcations, elasticity of the walls and other observed phenomena, these studies provide a starting point for analysis of more complex networks. A comprehensive overview of the mechanics of vascular

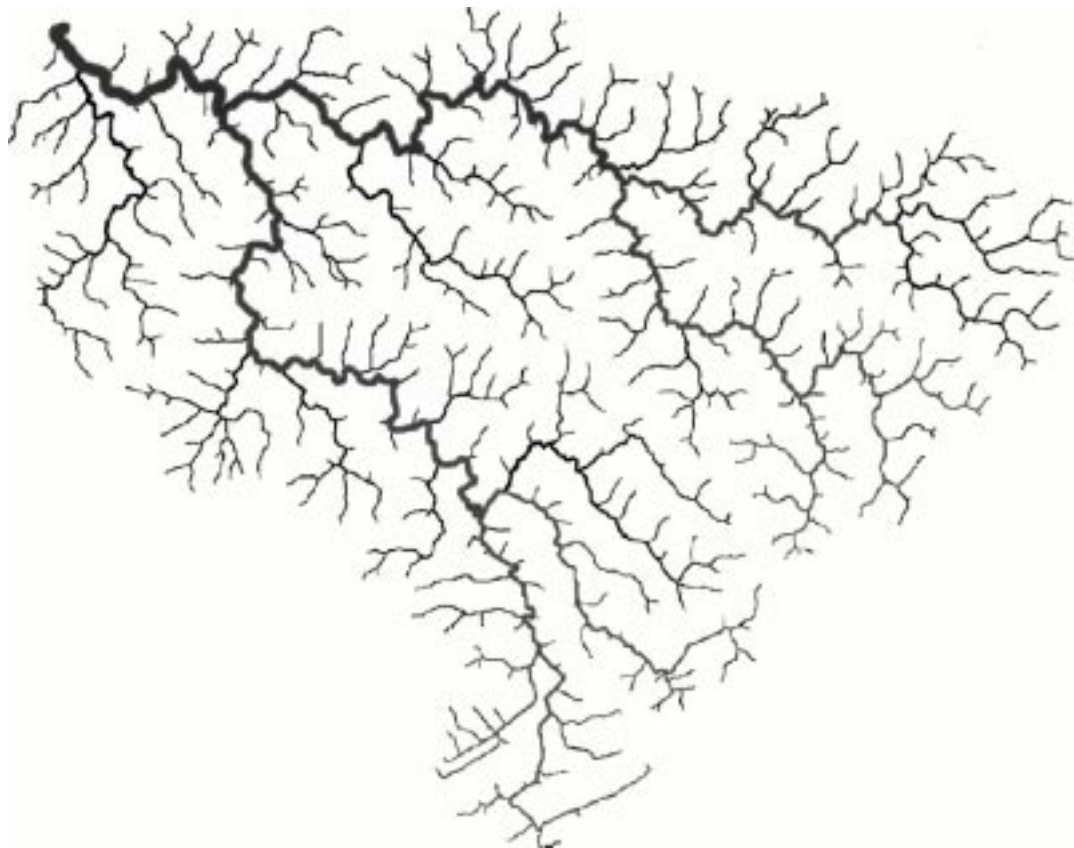


Figure 1.2. A view of Tug river basin in West Virginia (Rinaldo *et al.*, 1998).

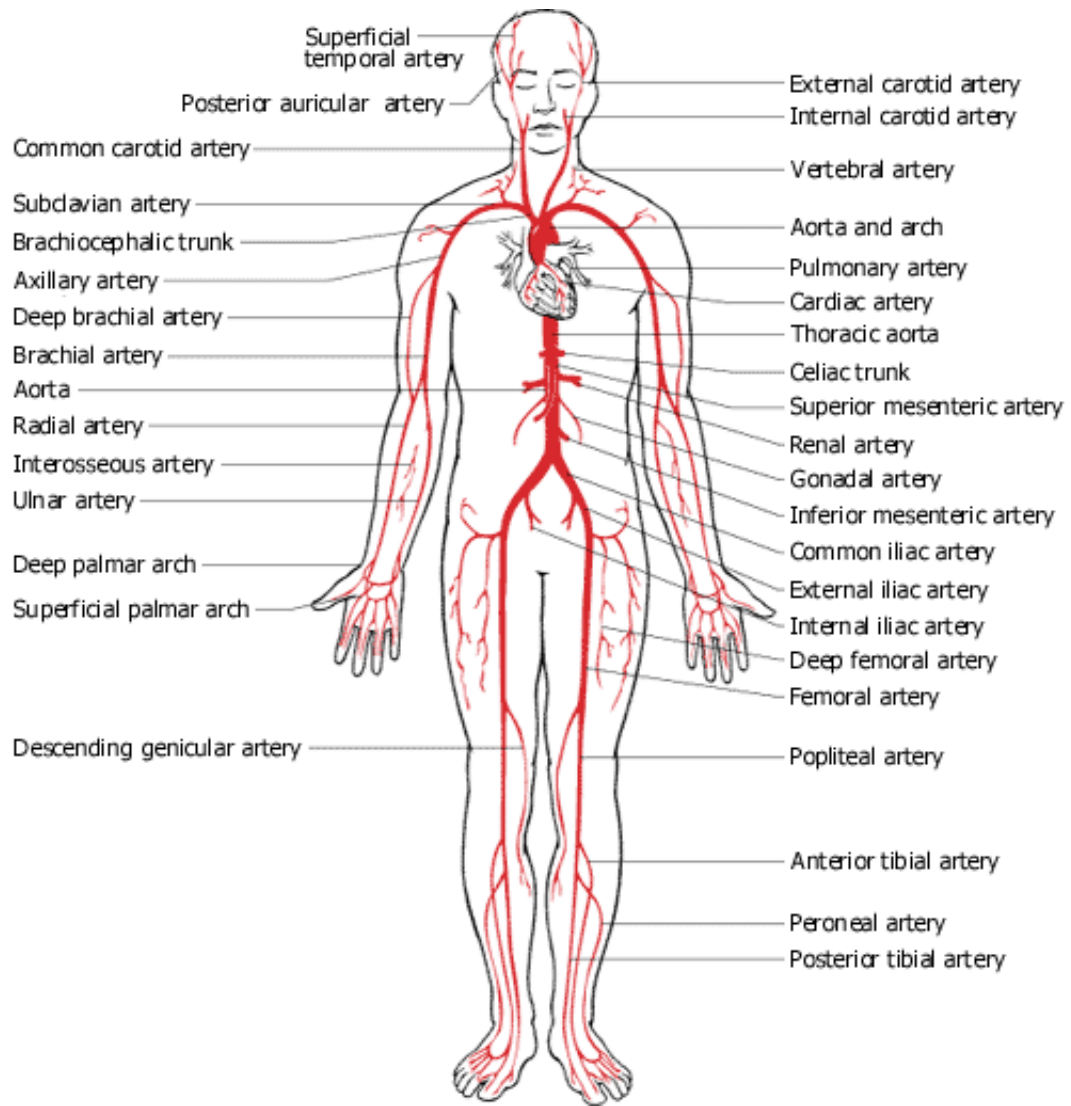


Figure 1.3. Arterial circulation system. Source: AMA's *Current Procedural Terminology*, Revised 1998 Edition. CPT is a trademark of American Medical Association.

networks is given by Pedley (2000). Using a simplified approach, Bejan and Errera (1997) studied the heat transfer from a fractal piping network within a porous environment. Bejan (2000) also studied the tree architecture of the volume-to-point path such that the flow resistance is minimal in flow systems, like in hot water distribution piping.

Numerous studies in branching trees are restricted to the laminar region of the flow for simplicity of the problem. However, not surprisingly, the flow may go from turbulent to laminar or from laminar to turbulent as the geometry changes. Thus transition from one regime to the other becomes relevant for tree networks and flow phenomena like relaminarization may occur (Narasimha and Sreenivasan, 1979; Iida and Nagano, 1998; Greenblatt and Moss, 1999). Ohmi, Iguchi and Urahata (1982a) while characterizing a pulsating flow observed differences between the accelerating and decelerating phase of the flow; relaminarization of the flow was seen in the accelerating phase on the velocity wave forms. In a following publication Ohmi *et al.* (1982b) reported a similar phenomenon for oscillatory flows; turbulent bursts in the decelerating phase on the velocity wave forms.

1.2 Linear control theory

The behavior of many linear control systems can be described by

$$\dot{\mathbf{x}}(t) = \mathbf{A} \mathbf{x}(t) + \mathbf{B} \mathbf{u}(t), \quad (1.2)$$

$$\mathbf{y}(t) = \mathbf{C} \mathbf{x}(t) + \mathbf{D} \mathbf{u}(t), \quad (1.3)$$

where t is time, $\mathbf{x}(t) \in \mathbb{R}^n$ represents the state of the system, $\mathbf{u}(t) \in \mathbb{R}^m$ is the input variable and $\mathbf{y}(t) \in \mathbb{R}^p$ is the output of the system. The matrices $\mathbf{A} \in \mathbb{R}^{n \times n}$, $\mathbf{B} \in \mathbb{R}^{n \times m}$, $\mathbf{C} \in \mathbb{R}^{p \times n}$ and $\mathbf{D} \in \mathbb{R}^{p \times m}$, which completely determine the system will be taken to be time independent.

1.2.1 State controllability

If there is a control vector $\mathbf{u}(t)$ such that the state vector $\mathbf{x}(t)$ reaches a pre-specified value in a finite period of time then the state vector is controllable. For instance, consider a pump attached to a pipe entrance, if there is a set of pumping loads such that the pressure at the outlet reaches specific values then the outlet pressure is controllable. It can be shown (Paraskevopoulos, 2002) that the state of the system is controllable if and only if the matrix

$$\mathbf{M} = \left[\mathbf{B} : \mathbf{A}\mathbf{B} : \mathbf{A}^2\mathbf{B} : \dots : \mathbf{A}^{n-1}\mathbf{B} \right], \quad (1.4)$$

where $\mathbf{M} \in \mathbb{R}^{n \times nm}$ is of rank n .

1.2.2 Output controllability

The output vector $\mathbf{y}(t)$ is controllable if there is a control vector $\mathbf{u}(t)$ such that the output variable $\mathbf{y}(t)$ reaches a prestablished value in a finite period of time. As an example, consider again the pump attached to the pipe; through the pump the pressure drop across the pipe can be varied and, thus, the flow rate. The control theory states that the output of the system is controllable if and only if the matrix

$$\mathbf{N} = \left[\mathbf{D} : \mathbf{C}\mathbf{B} : \mathbf{C}\mathbf{A}\mathbf{B} : \mathbf{C}\mathbf{A}^2\mathbf{B} : \dots : \mathbf{C}\mathbf{A}^{n-1}\mathbf{B} \right], \quad (1.5)$$

where $\mathbf{N} \in \mathbb{R}^{p \times (n+1)m}$ is of rank p .

1.2.3 Observability

The system is observable if the vector of initial conditions $\mathbf{x}(t_0)$ can be determined from $\mathbf{u}(t)$ and $\mathbf{y}(t)$. If one element of the vector of initial conditions cannot be determined then the whole system is unobservable. If the initial outlet pressure

can be determined from the flow and pump pressure then the system is observable. The control theory states that $\mathbf{x}(t)$ is observable if and only if the matrix

$$\mathbf{R}^T = \left[\mathbf{C}^T : \mathbf{A}^T \mathbf{C}^T : (\mathbf{A}^T)^2 \mathbf{C}^T : \dots : (\mathbf{A}^T)^{n-1} \mathbf{C}^T \right], \quad (1.6)$$

where $\mathbf{R} \in \mathbb{R}^{n \times np}$ is of rank n .

1.3 Control in bifurcating networks

Control is an inherent part of the use of many trees. In the cardiovascular system, for instance, control of the blood pressure through baroreflexive feedback prevents neurogenic syncope in normal humans (Morillo and Villar, 1997), while control in water distribution systems is obtained by individual pumps at all levels of the tree (Brion and Mays, 1991). Seebacher (2000) investigated the effect of heart rate on heating and cooling in two reptiles by calculating the heat transfer in a microvascular branching network. Varga, Hangos and Szigeti (1995) derived necessary and sufficient conditions for structural controllability and observability of heat exchanger networks. The authors state that for linear systems with either time-varying or time-invariant parameters it is sufficient to check the connectability of the network to determine the structural controllability and observability of the heat exchanger network. Structural means that instead of numerically given matrices the corresponding structure matrices were considered (Reinschke, 1988), the elements of a structure matrix are either fixed at zero or indeterminate values. Among other similar studies, Dager and Zuazua (2001) investigated the controllability of a tree-shaped network of vibrating strings, finding a necessary and sufficient condition for approximate controllability of the system when the control acts on the root of the tree.

1.4 Systems of differential algebraic equations

Many physical phenomena and engineering applications are modeled by a set of coupled differential and algebraic equations. The differential algebraic equations (DAE) are often referred to as a singular, descriptor or generalized state space system. DAE arise as dynamic models of mechanical, electrical and chemical engineering applications. For instance, standard dynamic balances of mass, momentum and energy give explicit differential equations. Thermodynamic relations, empirical correlations, steady state relations are algebraic equations. There is a significant amount of literature devoted to the study of this type of systems (Dai, 1989; Brenan *et al.*, 1996; Kumar, 1999).

1.4.1 Linear systems

A linear system is described by

$$\mathbf{E} \dot{\mathbf{x}}(t) = \mathbf{A} \mathbf{x}(t). \quad (1.7)$$

If the matrix \mathbf{E} is nonsingular the relation is equivalent to a standard ordinary differential equation (ODE) system. If \mathbf{E} is singular Equation (1.7) is a DAE system. The solution characteristics of the DAE are determined by the corresponding matrix pencil $\mathbf{L} = (\omega \mathbf{E} - \mathbf{A})$ where $\omega \in \mathbb{C}$. If the characteristic polynomial of \mathbf{L} is not identically zero the matrix pencil is said to be regular and the system is solvable (Dai, 1989).

1.4.2 Linear stability

The system (1.7) is stable in the Lyapunov sense if and only if all the roots of the characteristic polynomial of the matrix pencil lie on the left half complex plane. That is if

$$\Omega \subset \mathbb{C}^-, \quad (1.8)$$

where Ω is the set that contains the roots of the polynomial

$$h(\omega) = |\omega \mathbf{E} - \mathbf{A}|. \quad (1.9)$$

1.4.3 Bounded control

Consider the linear DAE system described by

$$\mathbf{E} \dot{\mathbf{x}}(t) = \mathbf{A} \mathbf{x}(t) + \mathbf{B} \mathbf{u}(t), \quad (1.10)$$

$$\mathbf{y}(t) = \mathbf{C} \mathbf{x}(t) + \mathbf{D} \mathbf{u}(t), \quad (1.11)$$

where $\mathbf{x}(t) \in \mathbb{R}^n$ represents the state of the system, $\mathbf{u}(t) \in \mathbb{R}^m$ is the input variable and $\mathbf{y}(t) \in \mathbb{R}^p$ is the output of the system. The matrices $\mathbf{A} \in \mathbb{R}^{n \times n}$, $\mathbf{B} \in \mathbb{R}^{n \times m}$, $\mathbf{C} \in \mathbb{R}^{p \times n}$, $\mathbf{D} \in \mathbb{R}^{p \times m}$ and $\mathbf{E} \in \mathbb{R}^{n \times n}$, which completely determine the system are taken to be time independent. \mathbf{E} is singular. If the system is regular, there exist nonsingular matrices \mathbf{P} and \mathbf{Q} such that Equation (1.10) is decomposed into a slow and fast subsystem (Gantmacher, 1974)

$$\dot{\mathbf{x}}_1(t) = \mathbf{A}_1 \mathbf{x}_1(t) + \mathbf{B}_1 \mathbf{u}(t), \quad (1.12)$$

$$\mathbf{K} \dot{\mathbf{x}}_2(t) = \mathbf{x}_2(t) + \mathbf{B}_2 \mathbf{u}(t), \quad (1.13)$$

where $\mathbf{x}_1(t) \in \mathbb{R}^{n_1}$, $\mathbf{x}_2(t) \in \mathbb{R}^{n_2}$ and the nilpotent matrix $\mathbf{K} \in \mathbb{R}^{n_2 \times n_2}$. The state response for this system is

$$\mathbf{x}_1(t) = e^{\mathbf{A}_1 t} \mathbf{x}_1(0) + \int_0^t e^{\mathbf{A}_1(t-\tau)} \mathbf{B}_1 \mathbf{u}(\tau) d\tau, \quad (1.14)$$

$$\mathbf{x}_2(t) = - \sum_{i=0}^{q-1} \mathbf{K}^i \mathbf{B}_2 \mathbf{u}^{(i)}(t). \quad (1.15)$$

The control input $\mathbf{u}(t)$ is $q - 1$ times piecewise continuously differentiable. When $t > 0$, the state response $\mathbf{x}(t)$ is uniquely determined by the initial condition $\mathbf{x}_1(0)$, control input $\mathbf{u}(\tau)$, $0 \leq \tau \leq t$, and time point t . Therefore any vector $\mathbf{w} \in \mathbb{R}^n$

in a n -dimensional vector space is reachable if there are an initial condition $\mathbf{x}_1(0)$, admissible control input $\mathbf{u}(t) \in \mathbb{C}_p^{q-1}$ and $t_1 > 0$ such that

$$\mathbf{x}(t_1) = \begin{bmatrix} \mathbf{x}_1(t_1) \\ \mathbf{x}_2(t_2) \end{bmatrix} = \mathbf{w}. \quad (1.16)$$

The system is controllable if and only if the matrices

$$\mathbf{M}_1 = \begin{bmatrix} \mathbf{B}_1 \vdots \mathbf{A}_1 \mathbf{B}_1 \vdots \mathbf{A}_1^2 \mathbf{B}_1 \vdots \dots \vdots \mathbf{A}_1^{n_1-1} \mathbf{B}_1 \end{bmatrix}, \quad (1.17)$$

$$\mathbf{M}_2 = \begin{bmatrix} \mathbf{B}_2 \vdots \mathbf{K} \mathbf{B}_2 \vdots \mathbf{K}^2 \mathbf{B}_2 \vdots \dots \vdots \mathbf{K}^{q-1} \mathbf{B}_2 \end{bmatrix}, \quad (1.18)$$

are of rank n_1 and n_2 , respectively (Dai, 1989). $\mathbf{M}_1 \in \mathbb{R}^{n_1 \times n_1 m_1}$ and $\mathbf{M}_2 \in \mathbb{R}^{n_2 \times n_2 m_2}$. The system is R-controllable when \mathbf{M}_1 is full rank and \mathbf{M}_2 is not. This implies that the state vector $\mathbf{x}(t)$ is partially controllable.

1.4.4 Nonlinear systems

Consider the function

$$F(\dot{\mathbf{x}}(t), \mathbf{x}) = 0. \quad (1.19)$$

It is an implicit ODE system if the Jacobian $\partial f_i / \partial x_j$ is nonsingular, otherwise it is an implicit DAE. Many nonlinear DAE systems arise naturally as

$$\dot{\mathbf{x}} = f(\mathbf{x}), \quad (1.20)$$

$$0 = g(\mathbf{x}). \quad (1.21)$$

The index η of a DAE system is the number of times the algebraic equations have to be differentiated to convert the DAE to a set of ODEs. The index provides a measure of the singularity of the DAE. A problem in the numerical solution of DAE is the need for consistent initial conditions that satisfy the algebraic relations and do not violate the Differential equations. For arbitrary initial conditions $\mathbf{x}(0)$ the system exhibits an impulsive behavior at $t = 0$. This is a common cause of failure in

numerical simulations of these type of systems. In control situations, $\dot{\mathbf{x}} = f(\mathbf{x}, \mathbf{u})$, the solution may also depend on the time derivatives of the inputs \mathbf{u} (Kumar, 1999).

1.5 Hydronic systems

Hydronic systems are thermal-fluid networks which convey heat through a piping arrangement. In general these systems are very large and irregular branching networks essential to buildings and complex apartments. The main circuits of the chilled water and steam network at Notre Dame campus are shown in Figure 1.4.

The hydronic system's purpose is to achieve and maintain specific temperature conditions at the terminal users by means of heat exchangers. In general, a control system in a hydronic network comprises three elements: (1) a sensor, (2) a controller and (3) an actuator, usually a valve. There are three basic ways of controlling the output from a coil:

1. The flow to the coil is modulated as a function of the control variable.
2. The flow through the coil remains constant and the inlet temperature is modulated as a function of the control variable.
3. A combination of the two previous one: the flow is modulated to a minimum value while the supply temperature is maintained constant. A minimum flow recirculating pump is started in a blending bypass, resulting in varying flow and sliding temperature under low load operation.

PID type controllers are widely used in these control processes and require constant attention for optimal control. More than 90% of the control loops in the industry are of this type (Åström and Karl, 1995; Yu, 1999) and in most cases they are poorly tuned. As a consequence the research trend in this respect is on either *PID* controllers or alternative control techniques.

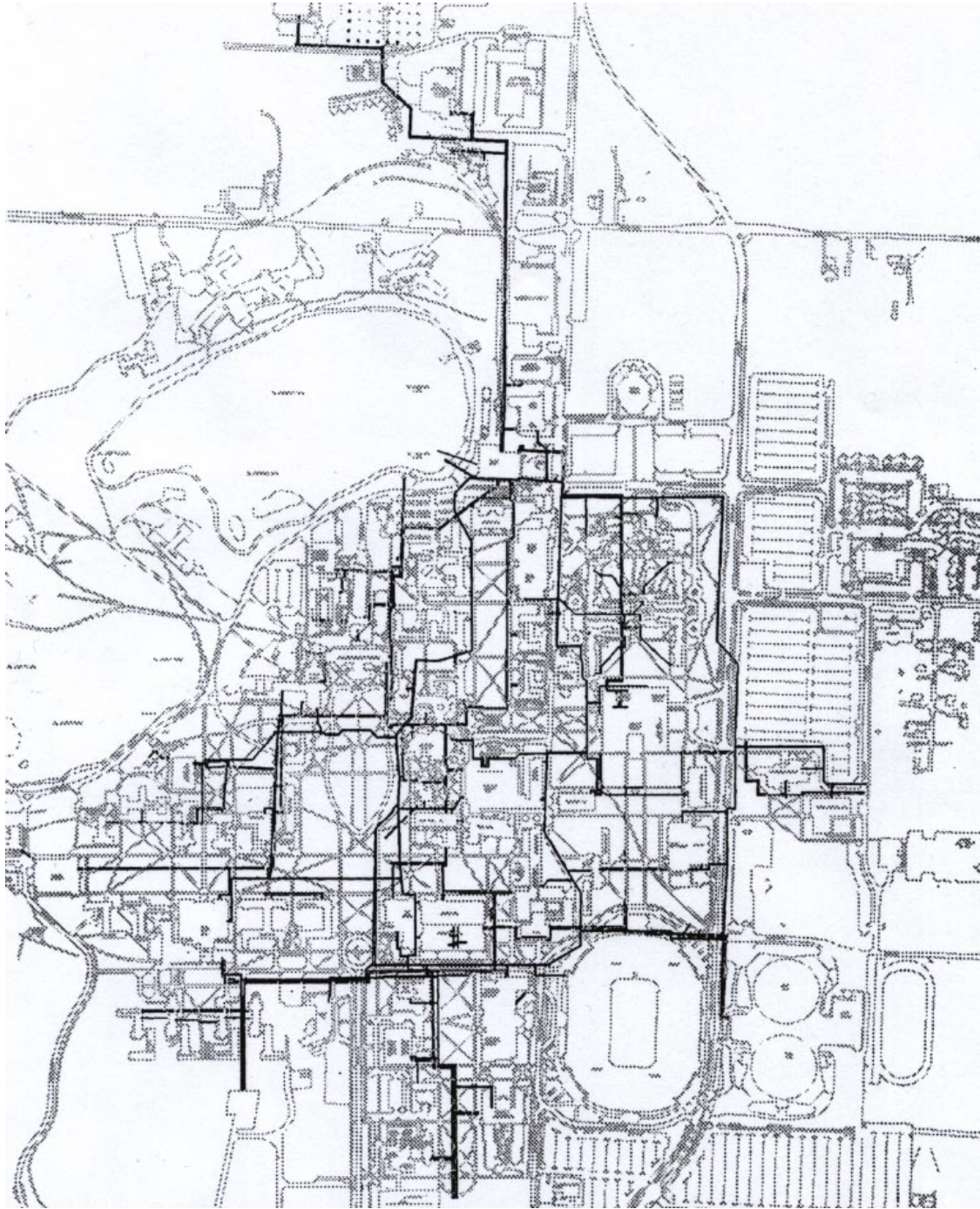


Figure 1.4. Steam and chilled water network at Notre Dame campus.

1.5.1 Cooling networks

The task of a chilled-water cooling system is to remove the heat generated within a conditioned space or process. Heat is extracted at a terminal unit cooling coil and transferred to water which is then conveyed through the piping network to the evaporator side of a chiller, or bank of chillers. Several cooling coils are usually connected to the same chiller. Heat is removed at the chiller from the water by a refrigerant and eventually discharged to the atmosphere. The chilled water is circulated back to the cooling coil. A control system adjusts the flow rate of chilled water to the cooling coil or its temperature according to the thermal load. This can be done in many different ways with specific advantages claimed for each method.

An important point of concern in the design and operation of chilled water plants is ΔT_{ch} , which is the difference in temperature of the water entering and leaving the chiller. A common situation encountered during the operation of a chilled water plant is that ΔT_{ch} is frequently not at its design value but is changing according to the thermal load. As a consequence, pumps and chillers are usually put online and taken offline to meet the demand in an inefficient fashion. This gives rise to situations for which the system was not designed and therefore to new problems. For example, a change in chilled water flow might unbalance the system producing changes in chilled-water delivery to distant terminal users. This is not an unusual situation, especially in large systems.

There are many reasons why ΔT_{ch} could be different from its design value, among them dirty cooling coils, insufficient shutoff capability of the control valves, reset of the chilled water supply temperature, faulty controls, or poorly controlled blending stations. It is a problem when ΔT_{ch} is below the design capacity of the chiller, and from the causes mentioned it can be inferred that it is a combined design, control, operation and maintenance problem. This has come to be known as the “low ΔT

central plant syndrome” (Kirsner, 1995b). The literature has descriptions where this situation arises (Kirsner, 1995a), and suggests practical recommendations to prevent and overcome it (Kirsner, 1995a; Avery, 1998; Fiorino, 1999; Avery, 2000, 2001). Among the solutions proposed are: a variable primary flow system with oversized variable-speed chiller pumps and distributed system pumping; control of chiller capacity with a bypass check valve to prevent mixing the return water with supply water; high temperature differences at the cooling coils from proper design, installation, operation and maintenance of cooling coils, control valves, control systems, and distribution systems. An appropriate control system should thus take ΔT_{ch} and its time variation into account; i.e. control strategies with small changes in ΔT_{ch} are desirable.

1.5.2 Optimization of hardware placement and selection

A significant necessary amount of energy is consumed by high rises and building complexes in which heating, ventilating and air conditioning (*HVAC*) systems do not work properly. For distributed hydronic heating and cooling systems, thermal-fluid networks play an essential role, and it is vital for this reason that their performance be well understood and optimized. Several optimization problems related to the hydraulics of *HVAC* systems have been addressed by previous authors. For example, there are studies on the optimum sizing of channels (Coker, 1991; Tosun and Akşin, 1993; Capps, 1995). In a recent publication Söylemez (2000) reported formulas to determine optimum channel sizes including the effects of economic parameters. Similarly Costa *et al.* (2000) used simulated annealing to optimize the pipe diameters and pump sizes of a piping system. Asiedu *et al.* (2000) used a genetic algorithm to design an *HVAC* air system including duct sizes, variable operating conditions and variable utility rates. Reis *et al.* (1997) addressed the problem of appropriate

location of control valves in a water supply network and their settings via genetic algorithms to maximize leakage reduction for specific nodal demands and reservoir levels. Carlson-Skalak *et al.* (1998) proposed an object-orientated algorithm based on genetic algorithms to design a piping system in which fluid was delivered to three machines at given hydraulic conditions. While the most recent technologies, for instance artificial neural networks and fuzzy logic, are being used to develop *HVAC* control strategies in commercial buildings (Hordeski, 2001), few studies have focused on the network layout and its effect on the system. In the design of *HVAC* systems it is vital to optimize the selection and placement of the hardware by using cost and operation criteria.

1.6 Objectives of dissertation

The goals of the research project stated in this section are presented as general and specific objectives. The former refers to the overall goals of the personnel of the Hydraulics Laboratory and the progress that has been made by several graduate students over the last few years. The latter corresponds to the research undertaken by the present author. The specific goals achieved in this dissertation represent a contribution to a more general long term goal.

It is necessary to put this research in context in order to comprehend its contribution. Previous dissertations within this research group have focused in the study of the dynamics, control and optimization of heat exchangers and its components. Zhao (1995) examined experimentally the steady and dynamic performance of a single-row heat exchanger. Romero-Méndez (1998) studied tube-to-tube conduction through fins and the hydrodynamics and heat transfer in the plane-fin and tube geometry. Experimental visualization of the flow between fins was also performed. Díaz (2000) applied Artificial Neural Networks to simulate the steady and dynamic

behavior of heat exchangers, and to control the fluid temperature. Pacheco-Vega (2002) used global regression and soft computing methods to investigate enhancement in accuracy of heat rate predictions in compact-fin heat tube heat exchangers. Alotaibi (2003) determined the dynamic response and controllability of heat exchangers and long ducts. All of them studied specific heat transfer components. After achieving a good understanding of heat exchangers as devices, this dissertation takes the outlined research to the next level: heat exchangers are put together to constitute a thermal network.

The specific objective of this dissertation is to study the control of the hydrodynamics and heat transfer in networks by means of theoretical, numerical and experimental methods. First, small and irregular systems that constitute a technological application are investigated. The goal is to compare three different control techniques commonly used in heating and cooling of buildings; to assess their relative merits and disadvantages respect a specific criterion. Next, the problem of component placement is explored. The goal is to investigate if the location of hardware affects the system performance and to what extent. Finally, networks are generalized to large, regular and geometrical self-similar systems within a branching topology. The goal is to study the hydrodynamics, control mechanism and control properties in tree networks that bifurcate with a constant diameter and length ratio.

For the simulation of thermal and fluid networks, the objective is to develop simple but realistic network and component models that allow the investigation of large systems. It is also an objective to perform experimental studies to complement the analysis and to provide information about phenomena that simulations cannot account for.

1.7 Scope of dissertation

The scope of this dissertation is the study of hydrodynamics, heat transfer and control aspects in thermal-fluid networks for which the transport of a scalar is an essential function, in particular to study thermal control in chilled-water cooling networks, and the hydrodynamics and control of flow in branching networks.

The study begins with the development of simple but realistic models of network components, such as pipes, pumps, valves and cooling coils. Then, a thermal-fluid network small in size, closed circuit and irregular in topology is considered; that is, analytical and experimental studies of a specific cooling network featuring three commonly used thermal control strategies are performed. The inherent restrictions imposed on the simulation by the experiments is then relaxed to address a more general problem that involves a subcircuit of the cooling network.

The study is then extended to investigate large, open circuit and regular networks. After investigating small systems, it is natural to consider large systems. This step involves some complications that must be addressed to make the research feasible. As a consequence, the small and large system analyses may look unrelated. It is also a possibility that some physical phenomena become relevant as the problem changes, therefore the approach may be different. For the study of large networks the topology is simplified to consider regular systems that are self-similar. This simplification allows numerical simulations, calculations and theoretical analysis of large networks. Transport systems within this topology are a very common form of open circuit flow networks, for instance water distribution piping systems, the vascular and respiratory system, and the collection of water in river basins. Consequently, theoretical studies of possible flow scenarios, stability of flow, and control properties of flow in tree networks are carried out. Specific simplifying assumptions on the geometry of the network are used to make the problem tractable. The goal

is to gain insightful understanding of the flow physics and to develop analytical techniques before addressing more complex thermal-fluid networks.

CHAPTER 2

MATHEMATICAL MODEL

In this Chapter analytical models for the network and hydronic components are developed. Next, the methodology for modeling the hydrodynamics of closed and open circuit systems is addressed.

For the analysis of thermal-hydraulic networks it is necessary to have a mathematical model representing the time-dependent behavior of the system. Equations for the components in the network such as pipes, valves, pumps and heat exchangers are described next and then combined into a network model. The assumptions are that the velocity and temperature are uniform over the cross section of a pipe and the parameters for the heat exchangers are lumped. The fluid density and the diameter of each pipe are also assumed constant. Differences in height between different parts of the network are neglected.

2.1 Hydraulic components

The momentum equation for flow in a pipe is

$$\frac{dU_w}{dt} = \frac{\Delta p}{\rho l} - \left(\frac{1}{2} \frac{f}{d} + \frac{K}{l} \right) U_w |U_w|, \quad (2.1)$$

where $U_w(t)$ is the mean water velocity in the pipe, Δp is the pressure difference along the length l of the pipe and is defined to be positive in the flow direction, ρ is the water density, and d is the pipe diameter. The friction factor f depends on the flow Reynolds number defined by $Re_d = |U_w| d / \nu$, where ν is the kinematic viscosity.

The flow is assumed laminar for $Re_d < 2300$ with $f = 64/Re_d$. For turbulent flow, $Re_d \geq 2300$ and the Haaland (1983) formula

$$f = \frac{0.3086}{\left[\ln \left\{ \frac{6.9}{Re_d} + \left(\frac{\sigma}{3.7d} \right)^{1.11} \right\} \right]^2}, \quad (2.2)$$

is used, where σ/d is the relative roughness of the pipe with $\sigma = 4.6 \times 10^{-5}$ m.

The loss coefficient K for a valve V is approximated by

$$K = 60 \frac{v^{2.8}}{1 - v}, \quad (2.3)$$

corresponding to a fit to published curves for a typical globe valve (Lyons, 1982; White, 1986). v is the valve signal input or closing fraction, so that $v = 0$ is fully open and $v = 1$ is completely closed. The signal is dimensionless in the analytical study and has voltage as unit in the experimental study. To avoid singularities during solution of the equations the highest closing value used is $v = 0.99$, which allows a trickling flow to go through. Since control valves take some time to open or close, its dynamics are modeled as

$$v(t) = v_f - e^{-t/\tau_V} (v_f - v_0), \quad (2.4)$$

where v_0 and v_f are the initial and final closing fractions, and τ_V is the time constant of the valve taken to be 1 s.

The performance of a pump, which is the prime mover that increases the pressure of the water, is given by empirically-determined characteristic curves. This can be conveniently represented as a low order polynomial such as $H = a_1 + a_2q + a_3q^2$ for the primary loop, where H is the head and q the volume flow rate. Similarly, for the secondary loop $H = b_1 + b_2q + b_3q^2$. The values $a_1 = 21$ m, $a_2 = -0.499$ s/m², $a_3 = -0.018$ s²m⁵, $b_1 = 14.5$ m, $b_2 = -0.237$ s/m², and $b_3 = -0.035$ s²m⁵

are determined from a manufacturer's technical data (Hodge, 1990). The dynamic behavior of the pump is also taken to be

$$H(t) = H_f - e^{-t/\tau_P}(H_f - H_0), \quad (2.5)$$

where H_0 and H_f are the initial and final values of the head, and where the time constant of the pump is $\tau_P = 1$ s again.

2.2 Thermal balance

Pipes in hydronic systems are usually heavily insulated so that heat transfer can be assumed to take place only at the heat exchangers: cooling coils and the chiller. Chilled water flowing inside the tubes of a cooling coil removes heat from the air flowing over it. Heat transfer rates are modeled using the inside and outside coefficients of heat transfer and the temperature differences between each fluid and the body of the heat exchanger. The correlations below are taken from an experimental study of a single-row heat exchanger (Zhao, 1995):

$$\text{Air side} \quad \zeta Nu_a = 0.074 Re_a^{0.59} Pr_a^{1/3}, \quad \text{for } 180 < Re_a < 700, \quad (2.6)$$

$$\text{Water side} \quad Nu_w = 0.03 Re_w^{0.79} Pr_w^{0.3}, \quad \text{for } 1200 < Re_w < 5.3 \times 10^4, \quad (2.7)$$

where the total efficiency of the air side surface, ζ , is taken to be unity. The Nusselt and Prandtl numbers are defined by $Nu = hl/\kappa$ and $Pr = \nu/\alpha$, respectively. h , κ and α are respectively the heat transfer coefficient, thermal conductivity and thermal diffusivity. $Pr_w = 12.22$, $Pr_a = 0.707$, $\kappa_w = 0.574$ W/mK and $\kappa_a = 0.0263$ W/mK (Incropera and DeWitt, 1996).

A lumped parameter equation is used for the heat exchangers. A distributed model based on partial differential equations would be more accurate but would be computationally time-consuming to solve, require larger computational resources,

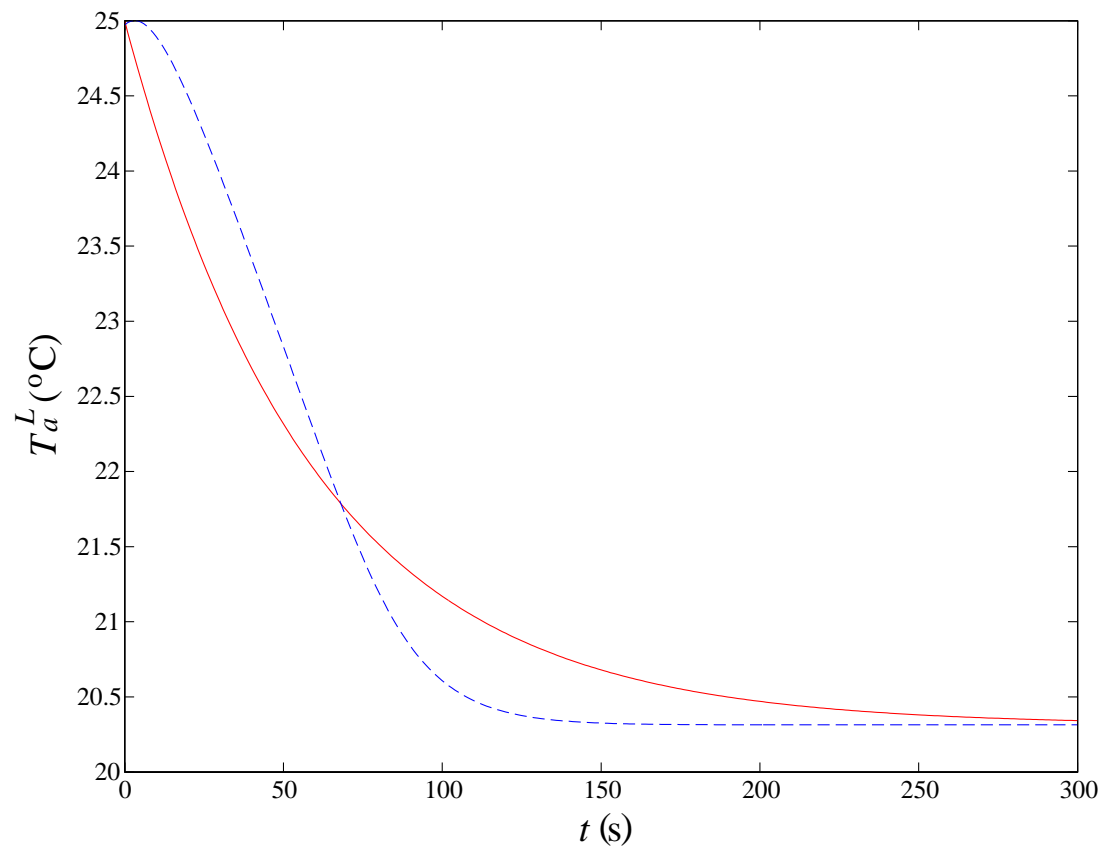


Figure 2.1. Coil leaving air temperature using -- distributed and — lumped parameter models.

and take away the flexibility needed to carry out control and optimization for networks. Figure 2.1 shows the dynamics of the leaving air temperature of a heat exchanger to a change in the water inlet temperature. The finite-difference results obtained by Alotaibi *et al.* (2002) using a distributed model are compared to those of a lumped parameter calculation where the parameters correspond to those which give zero average difference between them over the period of time shown. There is fairly good agreement between the time-dependent response of the two methods. Thus the lumped-parameter approach leads us to the following equation for the temperature of the cooling coil T_{cc} :

$$M_{cc}c_{cc}\frac{dT_{cc}}{dt} = h_a A_a (T_a - T_{cc}) - h_w A_w (T_{cc} - T_w), \quad (2.8)$$

where A is the heat transfer area, M the cooling coil mass and c the coil specific heat. The heat transfer coefficients are found using correlations (2.6) and (2.7). The fluid temperatures are taken to be the averages between entrance and leaving sections, so that

$$T_w = \frac{1}{2} (T_w^E + T_w^L), \quad (2.9)$$

$$T_a = \frac{1}{2} (T_a^E + T_a^L). \quad (2.10)$$

The value used for $M_{cc}c_{cc}$ is 22.725 kJ/K.

The cooling water in a chiller is cooled by a refrigerant. The refrigerant saturation temperature, T_{sat} , is taken to be 0°C and the refrigerant-side coefficient of heat transfer is set at a typically high value of $h_{rf} = 50,000$ W/m²K (Incropera and DeWitt, 1996). On the water side of the chiller, Equation (2.7) is used. Again, using a lumped approach the dynamics of the chiller are governed by

$$M_{ch}c_{ch}\frac{dT_{ch}}{dt} = h_w A_w (T_w - T_{ch}) - h_{rf} A_{rf} (T_{ch} - T_{sat}). \quad (2.11)$$

$M_{ch}c_{ch} = 22.725$ kJ/K, which is a typical value, is used for the computations. The heat exchanger geometries correspond to the one used by Zhao (1995).

2.3 Network principles

The equations for the components are combined into equations for the network.

- The sum of the mass flow rate at every junction is zero, symbolically represented as

$$\sum_{in} \dot{m} = \sum_{out} \dot{m}, \quad (2.12)$$

where \dot{m} is the mass flow rate in each pipe coming into and going out of the junction. The advective heat flow to each junction is also zero, giving

$$\sum_{in} \dot{m} T_{in} = \sum_{out} \dot{m} T_j, \quad (2.13)$$

where T_{in} is the temperature of the water coming into the junction and T_j is the water temperature there after complete mixing.

- Furthermore, the sum of the pressure drops in each branch of every closed loop must be zero, so that

$$\sum_{loop} \Delta p = 0, \quad (2.14)$$

symbolically.

Applying these equations to all the junctions and loops in a network gives a dynamic thermal-hydraulic mathematical model consisting of a set of nonlinear DAE that can be numerically integrated. In the present study equations are integrated by using an implicit Euler scheme and solving the resulting set of nonlinear algebraic equations at each time step using an *IMSL* library program (*zeros_sys_eqn*) based on a modified Powell hybrid algorithm.

2.4 Open-circuit fluid networks

In open circuits the fluid enters and leaves the network at one or several nodes. The flow is driven by nodal pressure differences between the inlet and outlet or by

pumps placed along the system or by the combination of both. In Figure 2.2 fluid enters at node a and leaves at e provided that $p_{in} - p_{out} > 0$. The arrows indicate the flow direction. The hydrodynamics are modeled by the momentum equation in each pipe and the mass conservation at each node. That is

$$\dot{U}_1 = -\frac{f_1}{2d_1}U_1|U_1| + \frac{1}{\rho l_1}(p_{in} - p_b), \quad (2.15)$$

$$\dot{U}_2 = -\frac{f_2}{2d_2}U_2|U_2| + \frac{1}{\rho l_2}(p_b - p_c), \quad (2.16)$$

$$\dot{U}_3 = -\frac{f_3}{2d_3}U_3|U_3| + \frac{1}{\rho l_3}(p_c - p_d), \quad (2.17)$$

$$\dot{U}_4 = -\frac{f_4}{2d_4}U_4|U_4| + \frac{1}{\rho l_4}(p_d - p_{out}), \quad (2.18)$$

$$\dot{U}_5 = -\frac{f_5}{2d_5}U_5|U_5| + \frac{1}{\rho l_5}(p_b - p_d), \quad (2.19)$$

$$0 = d_1^2 U_1 - d_2^2 U_2 - d_5^2 U_5, \quad (2.20)$$

$$0 = d_2^2 U_2 - d_3^2 U_3, \quad (2.21)$$

$$0 = d_3^2 U_3 + d_5^2 U_5 - d_4^2 U_4, \quad (2.22)$$

where the five fluid velocities and the pressures at b , c and d are determined by the pressure difference between a and e , the geometry of the branches and the friction factor. The mathematical model is a nonlinear DAE system of index 2. The model becomes a dynamical system by differentiating the three algebraic equations, substituting the differential equations in these three new equations and differentiating them again. This new set of differential equations is known as the underlying ODE.

2.5 Closed-circuit fluid networks

In closed circuits the fluid remains in the branching network. The flow is driven by one or several pumps. In Figure 2.3 fluid is circulated by a pump that produces a pressure increment \mathcal{P} . The arrows indicate the flow direction. As in open circuits,

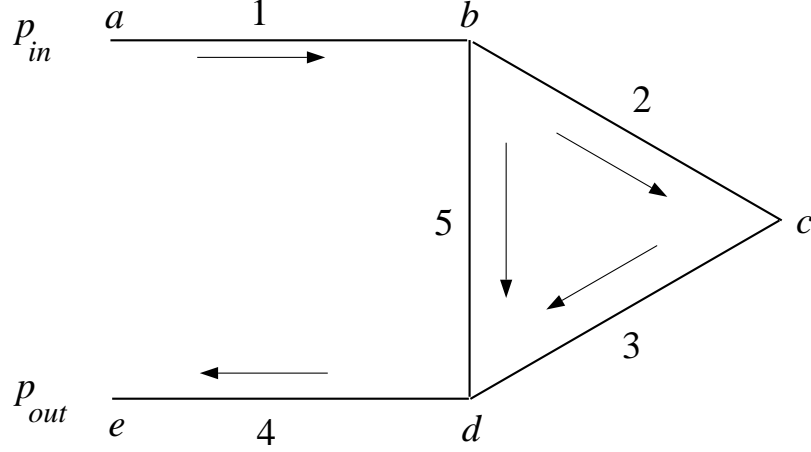


Figure 2.2. Open loop flow circuit.

the hydrodynamics are modeled by the momentum equation in each pipe and the mass conservation at each node. That is

$$\dot{U}_1 = -\frac{f_1}{2d_1}U_1|U_1| + \frac{1}{\rho l_1}(p_a - p_b + \mathcal{P}), \quad (2.23)$$

$$\dot{U}_2 = -\frac{f_2}{2d_2}U_2|U_2| + \frac{1}{\rho l_2}(p_b - p_c), \quad (2.24)$$

$$\dot{U}_3 = -\frac{f_3}{2d_3}U_3|U_3| + \frac{1}{\rho l_3}(p_c - p_d), \quad (2.25)$$

$$\dot{U}_4 = -\frac{f_4}{2d_4}U_4|U_4| + \frac{1}{\rho l_4}(p_d - p_a), \quad (2.26)$$

$$\dot{U}_5 = -\frac{f_5}{2d_5}U_5|U_5| + \frac{1}{\rho l_5}(p_b - p_d), \quad (2.27)$$

$$0 = d_1^2 U_1 - d_2^2 U_2 - d_5^2 U_5, \quad (2.28)$$

$$0 = d_2^2 U_2 - d_3^2 U_3, \quad (2.29)$$

$$0 = d_3^2 U_3 + d_5^2 U_5 - d_4^2 U_4, \quad (2.30)$$

$$0 = d_4^2 U_4 - d_1^2 U_1, \quad (2.31)$$

where the five fluid velocities and the pressures at a , b , c and d are determined by the pump head, the geometry of the branches and the friction factor. The model becomes a dynamical system by manipulating the algebraic equations as outlined

for the open-circuit analysis in Section 2.4. The mathematical model is a nonlinear DAE system of index 2. There are 9 unknown variables in 9 equations. However the equations of mass conservation are linearly dependent; equation (2.31) is obtained by adding (2.28), (2.29) and (2.30). To integrate the DAE an algebraic relation must be eliminated and a nodal pressure should be fixed.

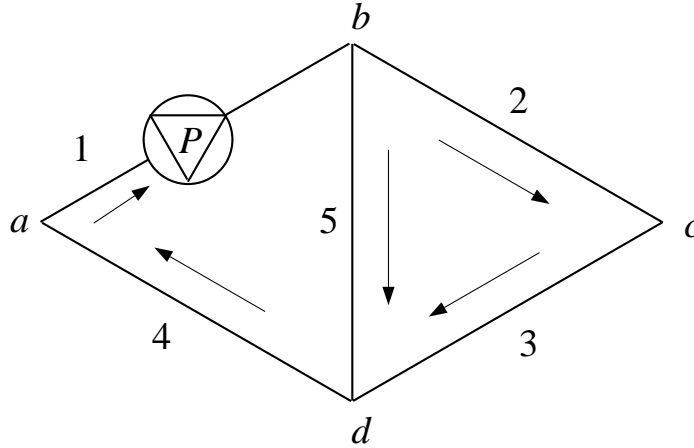


Figure 2.3. Closed loop flow circuit.

CHAPTER 3

HEATING AND COOLING OF BUILDINGS

This Chapter describes three common thermal control techniques used by the *HVAC* community for cooling and heating of buildings. The strategies, defined by the piping arrangement and hardware elements used to achieve control, will be analyzed in following chapters using the mathematical models presented in Chapter 2. In complex heating and cooling systems of buildings is customary to use primary and secondary loop design. The reason is the different requirements in the circuit. In a cooling system the chiller may be designed to operate at a 10°C temperature change, but the change in the cooling coils may be 15°C. The heating or cooling is produced by the primary system and distributed by the secondary. The secondary or user system meets the heating and cooling needs of specific zones. To meet these thermal needs there are several control techniques based on the selection of piping arrangement, hardware and the variable to be controlled. In this manuscript two of the most common used in *HVAC* systems are considered along with a relatively new technique that is also popular. Heating and cooling processes are very similar to each other. Indeed the user loop configuration is the same for both processes. The difference is in the primary loop where heaters are replaced by chillers. In the present study cooling systems are considered.

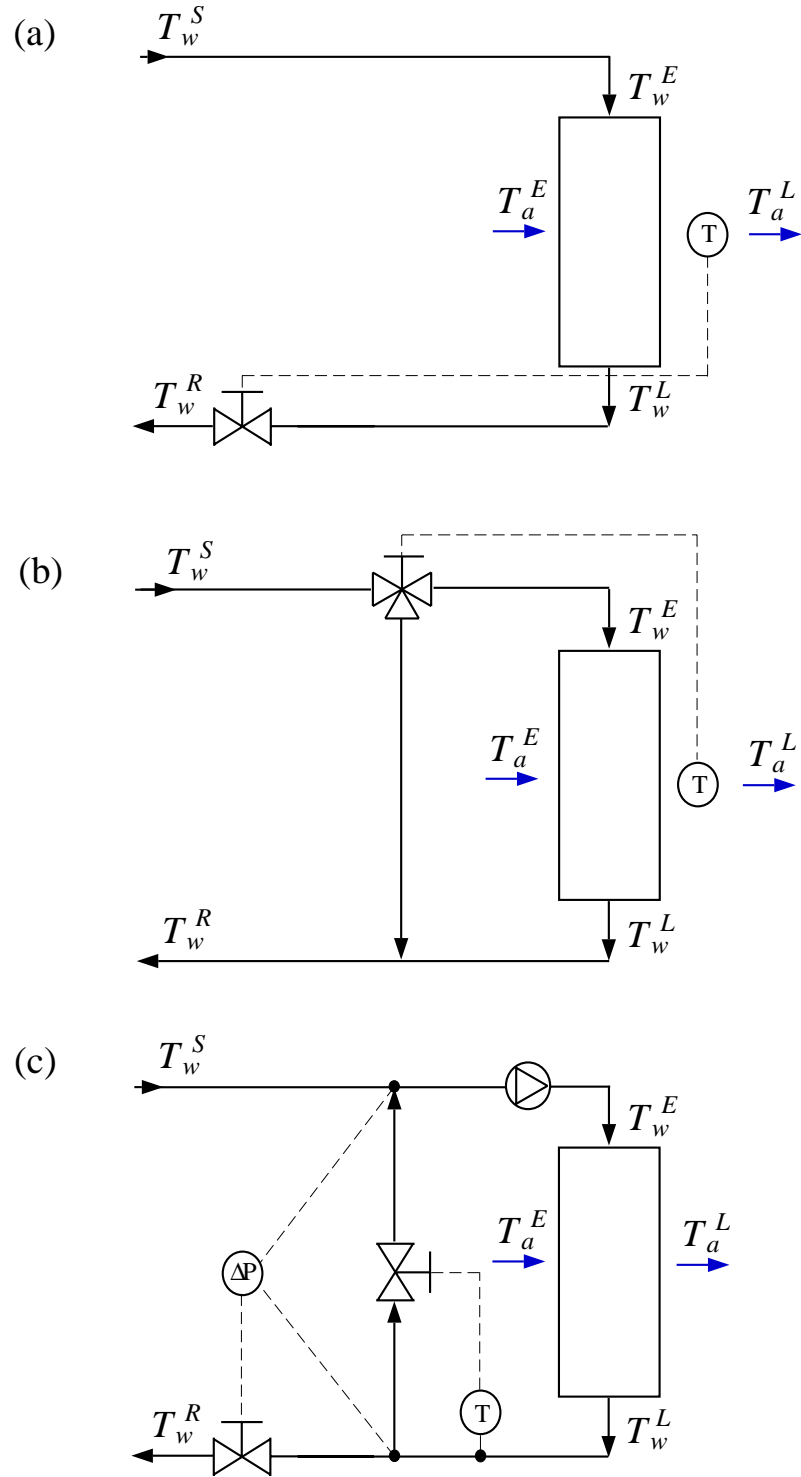


Figure 3.1. (a) Variable flow, *VF*. (b) Constant flow, *CF*. (c) BRDG-TNDR, *BT*. Broken lines represent control signals.

3.1 Thermal control strategies

Figure 3.1 illustrates three different control methodologies commonly used in *HVAC* design. Only the user loops are shown. Chilled-water is supplied at temperature T_w^S to the user loop and enters the cooling coil at temperature T_w^E . Hot air at T_a^E enters the coil and leaves at a lower temperature T_a^L after heat has been transferred. The water leaves the coil at a higher temperature T_w^L and is returned at a temperature T_w^R . Thermal control is achieved by modifying the water flow rate which is controlled by adjustable valves.

3.1.1 Variable flow

Figure 3.1(a) shows a variable flow technique in which the chilled-water flow to the cooling coil is modulated by a two-way valve to control T_a^L . The flow to the user loop and to the coil varies as a function of the thermal load. This is a single-input single-output (*SISO*) control system. The technique will be referred as *VF*.

3.1.2 Constant flow

Figure 3.1(b) shows a commonly-used constant flow technique with a bypass and a three-way valve to control T_a^L . Chilled-water is either bypassed or sent to the coil. The supplied flow is constant to the secondary but variable to the coil. This is also a *SISO* control system. The technique will be referred as *CF*.

3.1.3 Constant temperature difference

The third technique, Figure 3.1(c), is a double-input double-output (*DIDO*) control system, to be called BRDG-TNDR and referred as *BT*, which is the subject of several patents (Mannion and Mannion, 1994; Dorini *et al.*, 1994; Krist, 1994). In this technique, the valve on the bypass is modulated as a function of the water temperature leaving the cooling coil, T_w^L , and the valve on the returning pipe as a

function of the pressure drop across the bypass, Δp_{bp} . The aim of the *BT* method is to maintain a constant flow rate to the cooling coil by modifying the pressure drop in the bypass, and a constant leaving water temperature by modifying the water temperature entering the cooling coil.

CHAPTER 4

EXPERIMENTAL HYDRONIC NETWORK

This Chapter contains a detailed description of the experimental facility operation and equipment. The Hydronics Laboratory is provided with an experimental network of heat exchanger that features the control techniques described in Chapter 3, that is *VF*, *CF* and *BT*. A picture of the facility is shown in Figure 4.1. The picture shows that the experiment is mounted on a wall covering an approximate area of 4 m by 2 m. It has two different closed water circuits: a heating loop which produces the thermal load and a cooling loop where the control strategies take place. The purpose of the experiment is to provide different operational scenarios that allow to study hydraulic, thermal and control aspects of commonly used *HVAC* elements and methodologies, for instance to look at component and system dynamics such as physical coupling, thermal delays, hysteresis; to extract hardware information for modeling like time constants and power consumption; to establish control properties as stability and reachability; to implement different type of controllers like *PID*, Artificial Neural Networks, Fuzzy Logic; to explore different protocols of control like for example distributed, integral and remote.

4.1 Heating circuit

The diagram of the thermal-hydraulic network is shown in Figure 4.2. In the heating loop the hot water is generated by heaters HT_1 (6 kW), shown in Figure 4.3,



Figure 4.1. Experimental hydronic network.

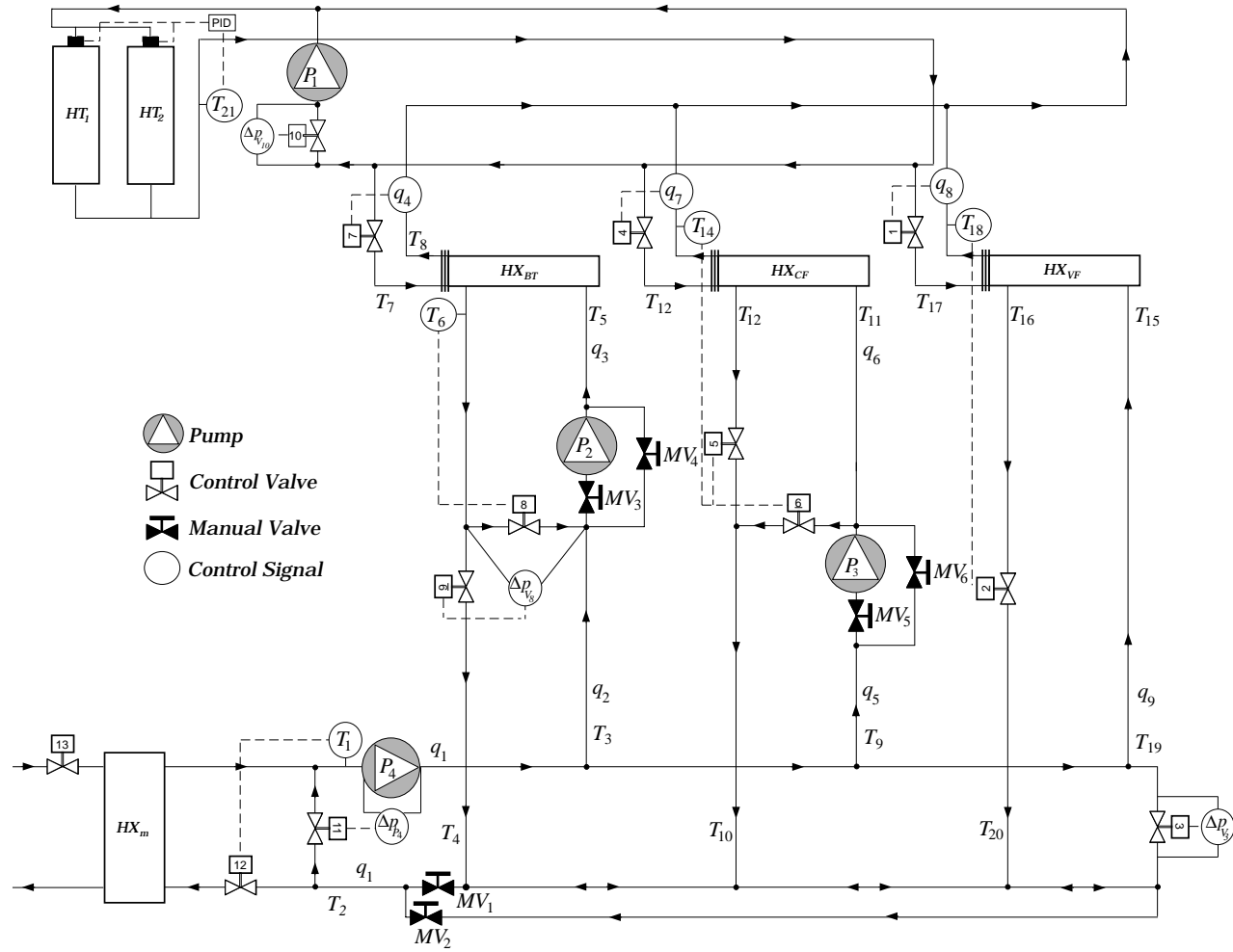


Figure 4.2. Experimental network layout.

and HT_2 (15 kW) that feed the four-pass water-water shell-tube heat exchangers (Bell & Gossett 308-4S) HX_{BT} , HX_{CF} and HX_{VF} with flow modulated by valves V_7 , V_4 and V_1 respectively. These are normally-closed valves; that is they open as they are energized. The control valves are of the globe type and pneumatically actuated. The actuators operate at 137.9 kPa (20 psi). The heat exchanger HX_{VF} is presented in Figure 4.4. Water is driven by a 3/4 HP pump (TEEL 1P833) P_1 located in the main or primary heating loop. V_{10} controls its own pressure drop to maintain a constant flow on the primary. The water on the heating loop covers approximately 14 m of pipes circulating through the primary and one secondary loop before returning to its starting point. The objective of the heating loop is to provide a controlled thermal load to the secondary cooling loops. The temperature of the supplied water is controlled by a built in *PID* (REX-F400 from RKC Instruments).

4.2 Cooling circuit

In the cooling side a compact plate-fin heat exchanger (Bell & Gossett BP415-50) HX_m placed at the main loop and shown in Figure 4.5 cools down the returning water from the secondaries using chilled water provided by the building services; a normally-closed valve V_{13} controls the flow from the building system to HX_m . A 1.5 HP variable speed pump (Bell & Gossett series 90, 15 gpm @ 60 ft) P_4 at the main loop drives the cooling water to the secondaries. Figure 4.6 shows the pump. V_{11} and V_{12} are modulated to supply a constant water flow at a fixed temperature, these are normally closed and open valves respectively. V_3 , normally open, may be modulated to change the total pressure loss in the primary loop; this is to emulate system losses that would exist with a longer primary run to other secondary loops.

The primary loop allows either direct or reverse water return by means of closing and opening manual valves: by closing MV_2 and opening MV_1 direct return is



Figure 4.3. Water heater.



Figure 4.4. Water-water shell-tube heat exchanger.



Figure 4.5. Water-water compact heat exchanger.



Figure 4.6. Variable speed pump.

implemented; reverse return takes place if it is the other way around. In direct return the water travels through less piping than in the other, but the flow is unbalanced since the flow resistance through the closest secondary to the pump is much less than that through the next secondary. In large systems balancing valves are used to equalize the resistance between secondaries. In reverse return the water travels approximately equal distances for each heat exchanger at the secondary. As a result the flow is balanced.

The secondary loop closest to the main pump P_4 has a 1/5 HP booster pump (Bell & Gossett PL-30B) P_2 , a bypass, a normally-closed control valve V_8 and a normally-open control valve V_9 ; this is the *BT* configuration. Figure 4.7 and 4.8 show P_2 and V_8 , respectively. The next secondary has a booster pump P_3 , a bypass, a normally-open control valve V_5 and a normally-closed control valve V_6 ; this is the *CF* configuration. The three-way valve is emulated by coupling the two-way valves. The third secondary, the farthest from P_4 , has the normally-open control valve V_2 ; this is the *VF* configuration. The water on the cooling circuit covers approximately 18 m of pipes circulating through the primary and one secondary loop before returning to its starting point.

4.3 Data acquisition and processing

The data acquisition from instruments and the signal output to the valves is carried out through National Instruments boards (PCI-6033E, PCI-6704 and PCI-MIO-16E-4) and LabVIEW software running on a Windows 95 platform. There are 23 thermocouples, 9 flow meters and 8 pressure transducers that occupy 40 input channels. 13 valves and 9 flow meter signal conditioners need 22 output channels. LabVIEW interacts with a controller written in standard C language. The controller

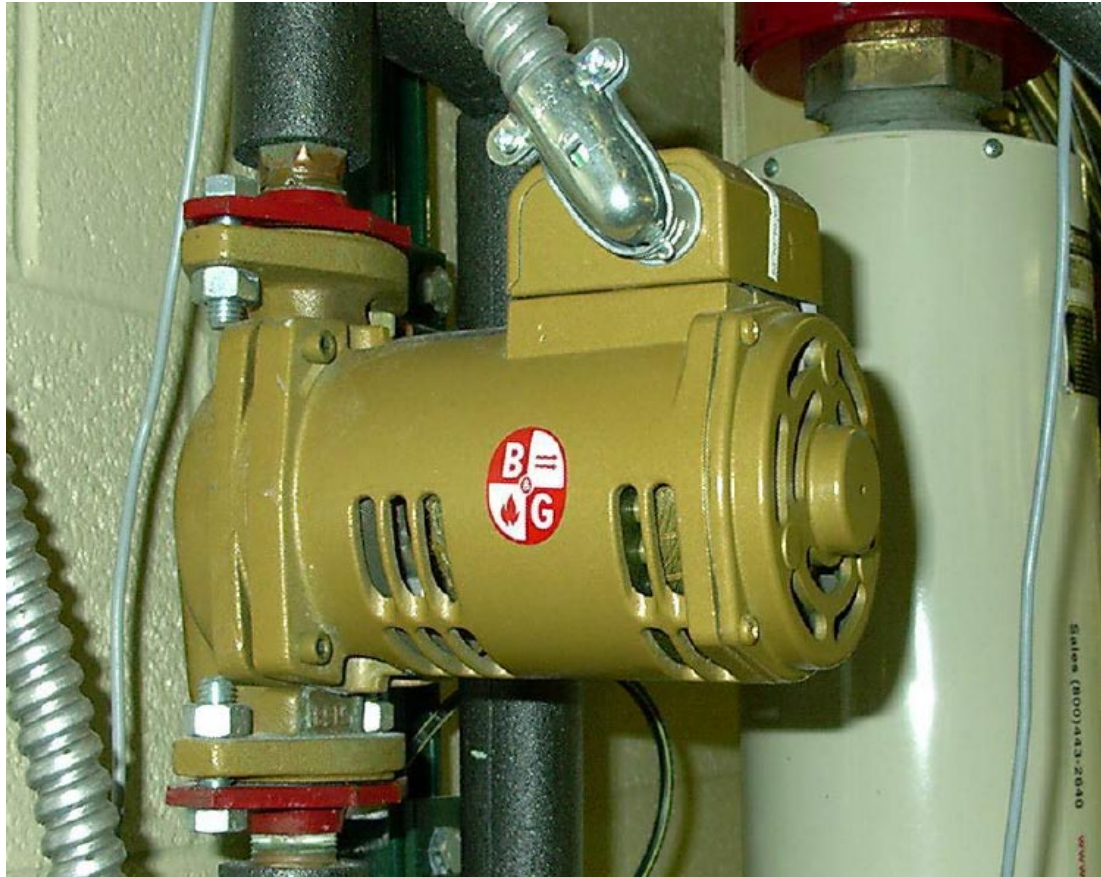


Figure 4.7. Booster pump.

receives measurements and set points and calculates the signals for the valves using a *PID* algorithm.

The temperature of the water is measured by type J thermocouples and an ice point cell. Water flows are measured by Omega turbine meters (FTB-4607 on the main cooling loop and FTB-4605 everywhere else). Flow signal conditioners convert the meters frequency output to analog input for the board. Pressure differences are measured through Omega pressure transducers (PX26-030DV). Valve size is 1 in if located on a main loop and 1/2 in if located on a secondary. An electro-pneumatic transducer (Johnson Controls EP-8000) sends the signal from the board to the actuator (Johnson Controls V-3000-8011).

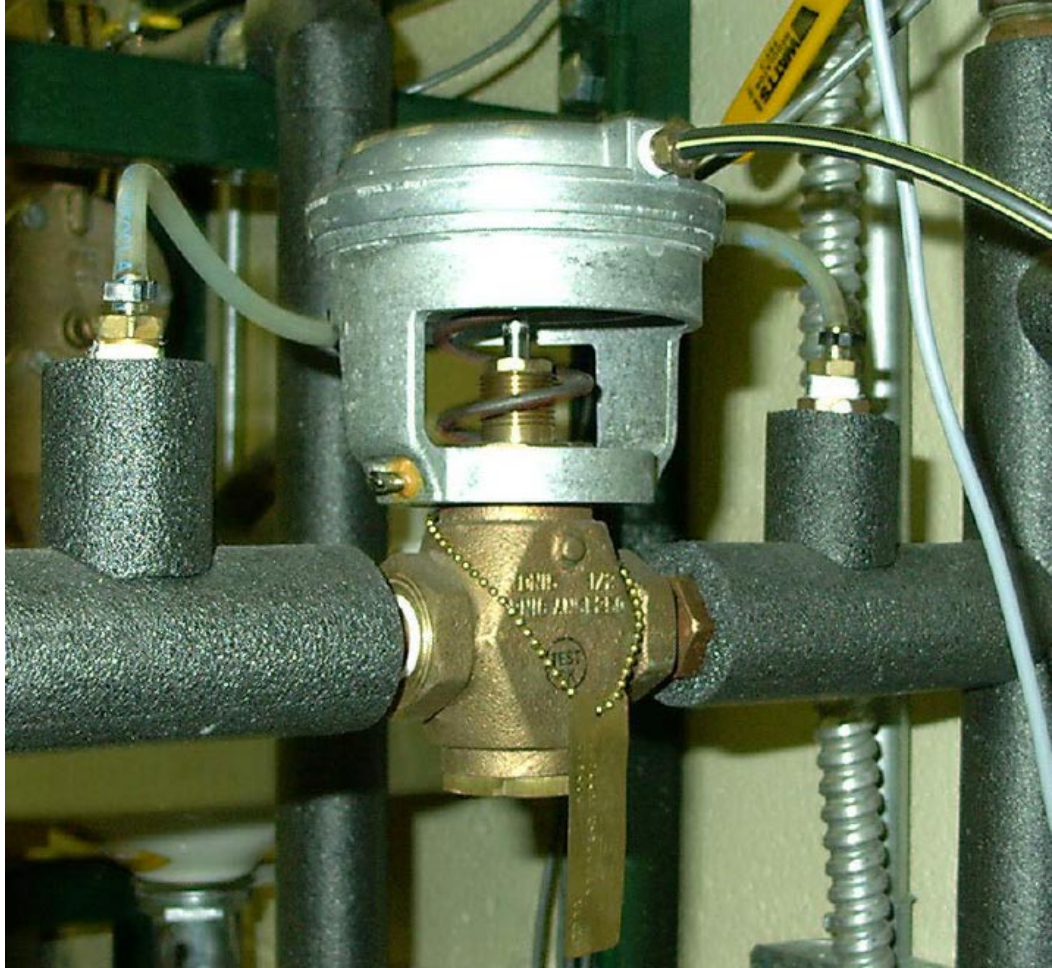


Figure 4.8. Pneumatic control valve.

CHAPTER 5

NUMERICAL STUDY OF THERMAL CONTROL STRATEGIES

The purpose of this Chapter is to present a quantitative study of the control methodologies described in Chapter 3 in order to evaluate their dynamic behavior and relative merits with respect to specific criteria. The analytical study is carried out using the models presented in Chapter 2. Thermal and fluid networks of piping and heat exchangers play an essential role in the performance of distributed heating and cooling systems in high rises and building complexes. While many steady-state studies and mathematical models of these networks are available, there are very few detailed analyses or comparisons of the control methodologies. The results included in this Chapter have been published in proceedings (Franco *et al.*, 2002) and a journal article (Franco *et al.*, 2003b).

A dynamic thermal-hydraulic analysis of the *VF*, *CF* and *BT* strategies used for the control of hydronic piping and heat exchanger networks is carried out next. The three control methods are analyzed and compared using the mathematical model early developed. For this purpose a general thermal network with a primary loop, a secondary loop and a bypass that has the three control systems as special cases is proposed. The primary loop includes a chiller, while the secondary has a water-air cooling coil which serves as a thermal load. For each the response to integral controllers as a function of the thermal load is determined. The behavior of each

of the three control schemes is then compared to assess their relative merits with respect to their effect on the temperature drop in the chiller.

5.1 Generalized network configuration

A central plant usually involves several chillers, pumps, cooling load units, etc., which together as a network constitutes a formidable problem. In this study a simple network is used for analysis which is general enough to include the most common hydronic control strategies. Since it is difficult to have a balanced comparison between three different networks, they have all been made special cases of a single configuration. The network includes a constant primary flow system with one chiller and a secondary loop with one cooling coil.

The proposed network in Figure 5.1 can be reduced in special cases to those in Figure 3.1. The distribution pump P_1 in the primary loop supplies chilled water from the chiller ch to the secondary loop at b , which returns to the primary at a higher temperature at g . The secondary loop has a water-to-air cooling coil cc , two pumps P_2 and P_3 , a bypass branch cf , and three valves to implement the control. The valves V_1 , V_2 and V_3 are regulated by the closing parameters v_1 , v_2 and v_3 , respectively. Pumping action in the secondary depends on the value of B which can be seen as a partition parameter: when $B = 1$, P_2 is active and P_3 is inactive; when $B = 0$, P_3 is active and P_2 is not. Thus switching B between 0 and 1 is equivalent to changing the pump location. For the cooling coil the entering and leaving air temperatures are T_a^E and T_a^L , while the water enters at T_w^E and leaves at T_w^L . The numerical values of the pipe length and diameters selected for the network are given in Table 5.1.

For VF , the parameters must be kept at $B = 1$, $v_3 = 0$ and $v_1 = 1$, while a variable v_2 is used to regulate the chilled water flow rate to the cooling coil. There

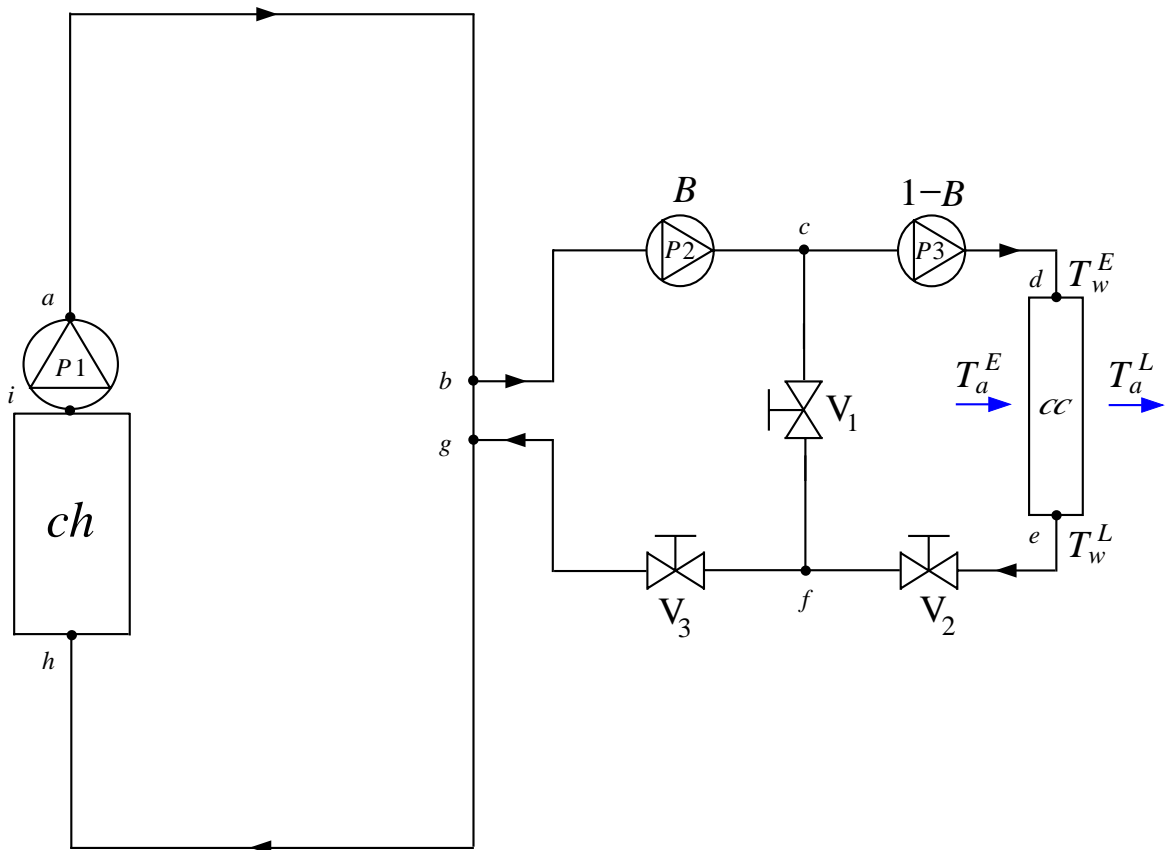


Figure 5.1. Generalized network layout.

is no flow through the bypass. T_a^L is the variable to be controlled. The *CF* method is obtained when $B = 1$, $v_3 = 0$ and $v_1 = 1 - v_2$ simulating a three way valve. The three-way valve directs the chilled water flow either to the bypass or the cooling coil; the flow in the bypass is from c to f . The control variable is also T_a^L and the manipulated variable is the closing parameter v_2 . The *BT* technique corresponds to $B = 0$ and $v_2 = 0$, while v_1 and v_3 are free and independently varied to carry out the task of controlling T_w^L as well as Δp_{bp} . The two-way valves V_1 and V_3 are thus the control elements through the manipulated variables v_1 and v_3 , respectively. Flow in the bypass is now from f to c and the two streams, one of chilled water directly from the chiller and the other of warmer water from the cooling coil, blend at c .

It must be noted that, as a consequence of using the same network for all three control strategies, each works in a configuration that may have extra hardware elements (pumps, valves and bypass *cf*), and may be connected to the primary (bypass *bg*) in a way that is different if it alone were being tested. Having extra hardware elements is not a problem in the comparison if the parameters are kept constant. However, the connection with the primary does make a difference; this must be kept in mind in evaluating the results.

5.2 Integral control

For feedback control, the valves respond to a signal from the controller which is based on the difference between the system output and the set point. In each control strategy a *PID* controller set in the integral mode is used to modify the valve closings. Since *VF* and *CF* are *SISO* systems with the same manipulated variable, they use the same control equations. The error

$$e(t) = \frac{1}{T_{ref}} (\bar{T}_a^L(t) - T_a^L(t)), \quad (5.1)$$

Table 5.1. DIMENSION OF PIPES IN GENERALIZED NETWORK.

<i>Between</i>		<i>l (m)</i>	<i>d (m)</i>
<i>a</i>	<i>b</i>	6.0	0.03
<i>b</i>	<i>c</i>	3.0	0.03
<i>b</i>	<i>g</i>	0.1	0.10
<i>c</i>	<i>f</i>	1.0	0.03
<i>c</i>	<i>d</i>	1.0	0.03
<i>d</i>	<i>e</i>	7.37	0.0149
<i>e</i>	<i>f</i>	1.0	0.03
<i>f</i>	<i>g</i>	3.0	0.03
<i>g</i>	<i>h</i>	6.0	0.03
<i>h</i>	<i>i</i>	7.37	0.0149

where the bar indicates the set value that is the target and $T_{ref} = 40^\circ\text{C}$. The control action on the valve is determined by

$$v_2(t + \delta t) = v_2(t) + k_{I,2} e(t), \quad (5.2)$$

where δt is a time interval taken to be 0.1 s. The *BT* is a *DIDO* system that manipulates valves V_1 and V_3 . For V_1 , we have

$$e_T(t) = \frac{1}{T_{ref}} (\bar{T}_w^L(t) - T_w^L(t)), \quad (5.3)$$

$$v_1(t + \delta t) = v_1(t) + k_{I,1} e_T(t), \quad (5.4)$$

$$(5.5)$$

while for V_3 , we write

$$e_{\Delta p}(t) = \frac{1}{\Delta p_{ref}} (\Delta \bar{p}_{bp}(t) - \Delta p_{bp}(t)), \quad (5.6)$$

$$v_3(t + \delta) = v_3(t) + k_{I,3} e_{\Delta p}(t), \quad (5.7)$$

where $\Delta p_{ref} = 100000$ (N/m²). In the above the controller gains, $k_{I,1}$, $k_{I,2}$ and $k_{I,3}$ are taken to be -0.1 .

5.3 Open-loop control

The first step in analyzing the network is to find out how much the control variables are changed on varying the manipulated variables without feedback control. This will give an idea of the states that can be reached for purposes of control. For the *VF* and *CF* methodologies the concern is with T_a^L , and for *BT* it is T_w^L and Δp_{bp} .

Figure 5.2 shows T_a^L for *VF* and *CF* as a function of v_2 for three different U_a . T_a^E is kept constant at 30°C. For *VF*, T_a^L increases as V_2 closes and decreases the water flow to the cooling coil. For *CF*, T_a^L also increases as the three-way valve shuts off flow to the cooling coil; V_1 and V_2 are inversely coupled so that as v_2 increases V_2 closes allowing less flow to the cooling coil, and V_1 opens to let more flow through the bypass. The figure shows that not all operational states can be achieved. It is simply not possible for the system to cool down air coming at 10 m/s and 30°C to 25°C (say). Even when the desired conditions can be reached, the system may be too sensitive to changes in the manipulated variable for stable control. Near $v_2 = 1$, the volume flow rate is very small and T_a^L becomes very sensitive to changes in v_2 making control difficult on that region. Among the two methods *CF* seems to have less of a problem. A similar behavior is observed for different T_a^E . This is shown in Figure 5.3 where U_a is kept constant.

Figure 5.4 shows the network performance for *BT*. Variation of Δp_{bp} and T_w^L is shown in Figure 5.4(a) as contour lines in a v_1 - v_3 plane. As v_1 increases the flow through the bypass is decreased, and as a consequence there is less warm water coming from the cooling coil to blend with the chilled water supply at c . When v_3 increases, the water flow to the secondary loop is restricted. The lowest T_w^L is achieved when the highest chilled water flow rate with no mixing is circulated to the cooling coil, i.e. when v_1 is the highest and v_3 the lowest at the lower right corner in the figure. Figure 5.4(b) is the contour plot of T_a^L . The sensitivity of T_w^L to v_3

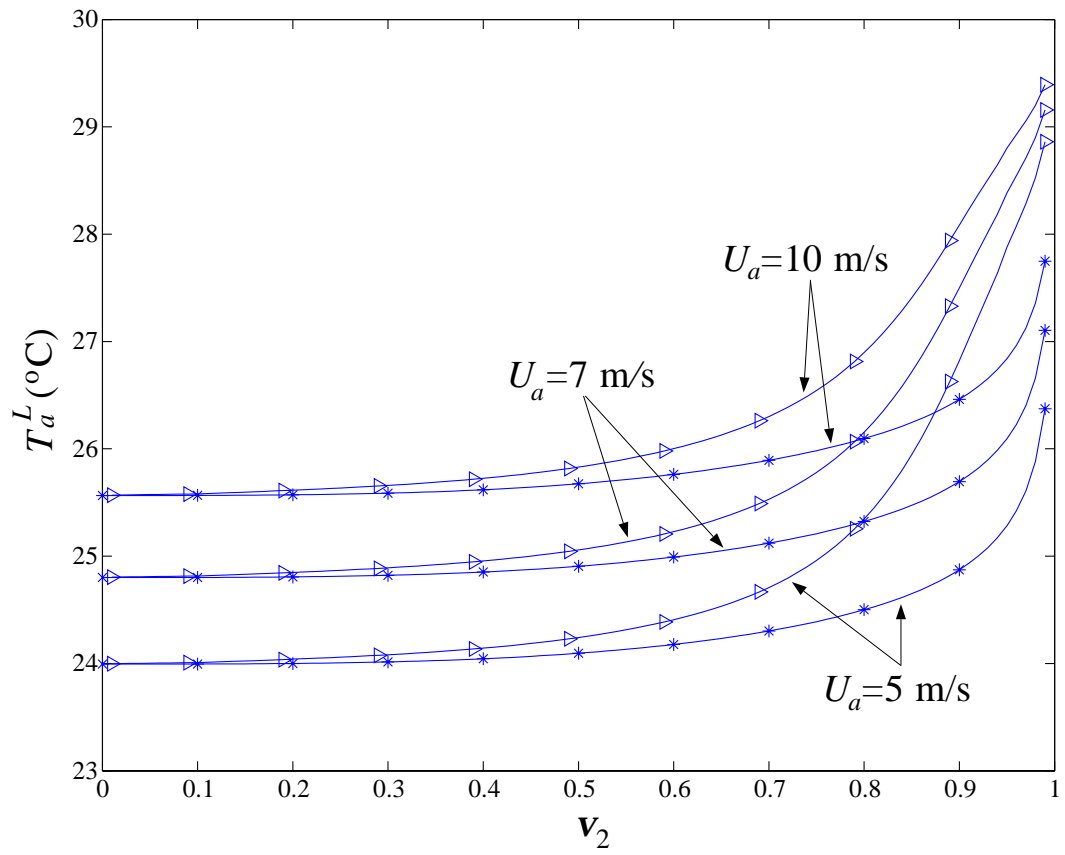


Figure 5.2. Leaving air temperature as function of valve closing parameter for three different air velocities; $-*$ $-VF$ and $-▷$ $-CF$; $T_a^E = 30^\circ\text{C}$.

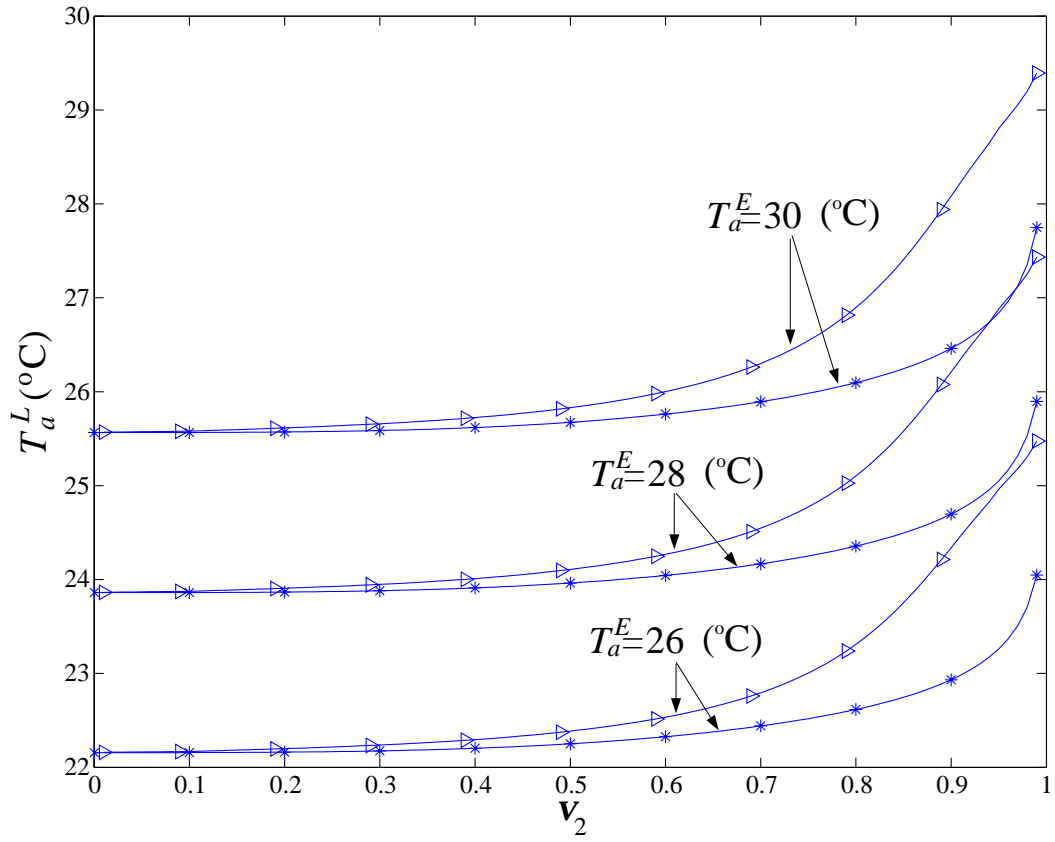


Figure 5.3. Leaving air temperature as function of valve closing parameter for three different entrance air temperatures; $- * - VF$ and $- \triangleright - CF$; $U_a = 10$ m/s.

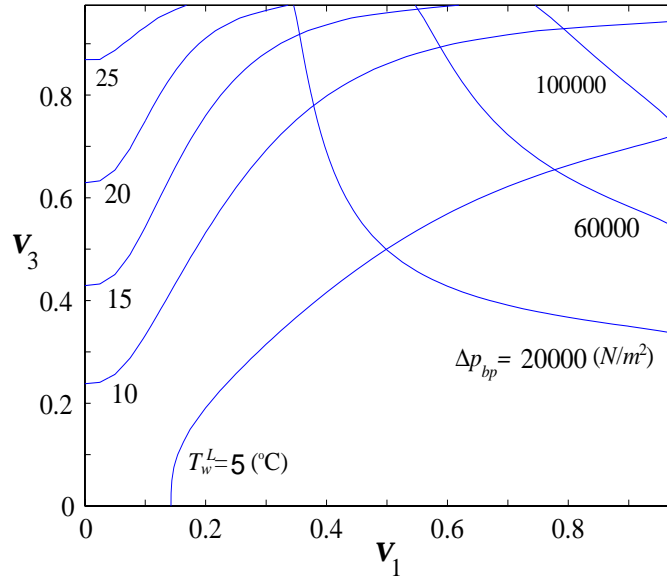
is also a problem near $v_3 = 1$. Extreme sensitivity of Δp_{bp} to v_1 may occur with V_1 partially open.

All three methods have a certain range of T_a^L that can be reached; for example, for $U_a = 10$ m/s and $T_a^E = 30^\circ\text{C}$, the range is $T_a^L = 25.57\text{--}30^\circ\text{C}$; the thermal load requirements can be satisfied with any one of the three strategies. However, each method takes the system to a different set of velocities, pressures and temperatures (except for the control variables).

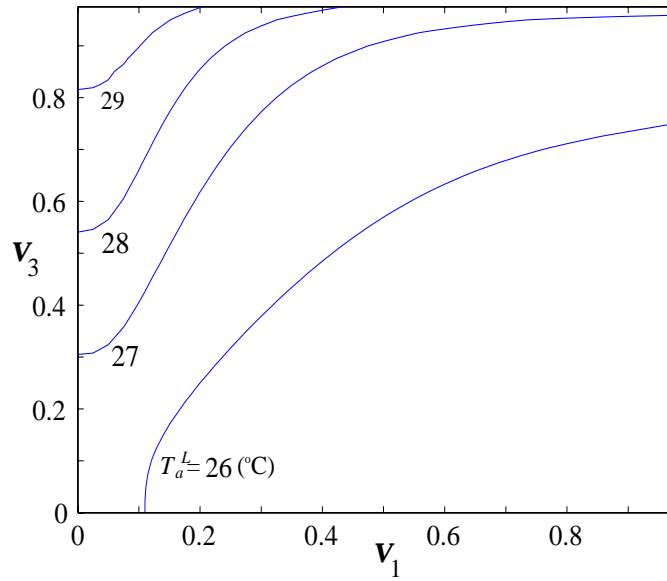
5.4 Dynamics and feedback control

Control is a dynamic process so that the time-dependent response of the network and its components in open loop is very important. The transient starting response of the network is presented in Figure 5.5 for *VF* and *CF*. Figure 5.5(a) shows the flow rates at the chiller and cooling coil where the heat transfers take place. Once the pump P_1 is started the water flow rate in the primary loop remains constant since it is decoupled from the secondary. The mass flow adjusts fairly quickly though there is a large overshoot for the cooling coil flow rate for *VF*. Figure 5.5(b) shows that T_a^L takes longer, up to about 20 s, to adjust. Of the two methods, *CF* takes more time. Figure 5.6 presents the corresponding dynamics for *BT*. Once again, the temperatures take longer than the flow rates and pressure drop to adjust to the change. There is less oscillation for *BT* than for *VF*.

Next, integral control is applied to analyze the response of the system to a disturbance in the air entrance conditions for the three control strategies. For each the network is started and taken to a certain operational point which can be regarded as the design condition. The task of the *VF* and *CF* methods is to keep a desired T_a^L , while that of the *BT* is to keep T_w^L and Δp_{bp} at desired values. A step-change

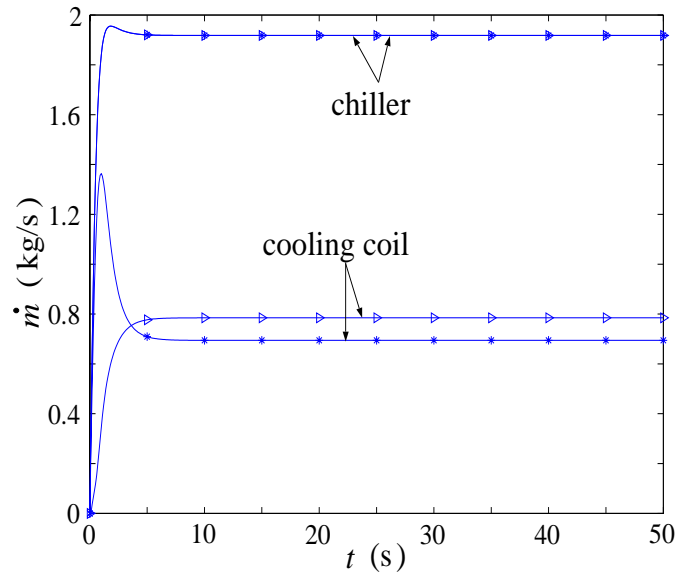


(a)

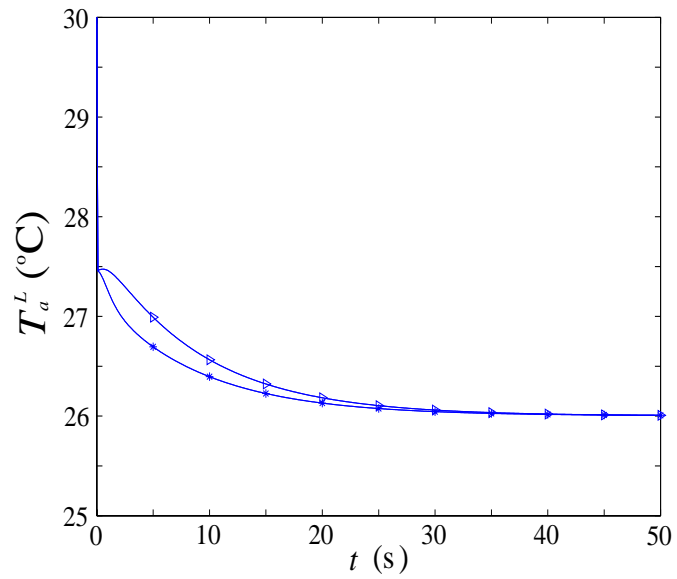


(b)

Figure 5.4. Network behavior, *BT* method: (a) Δp_{bp} and T_w^L ; (b) T_a^L ; $T_a^E = 30^\circ\text{C}$, $U_a = 10$ m/s.

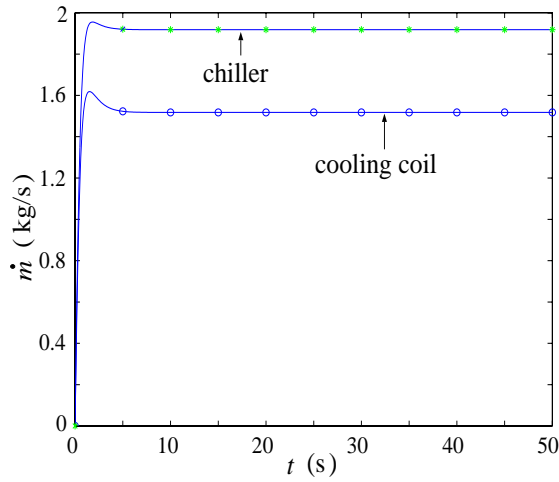


(a)

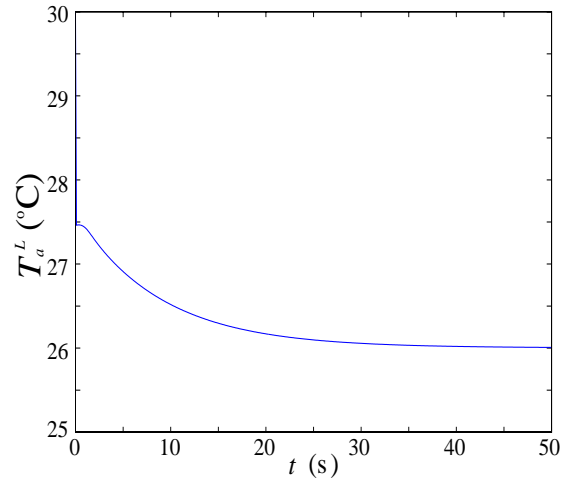


(b)

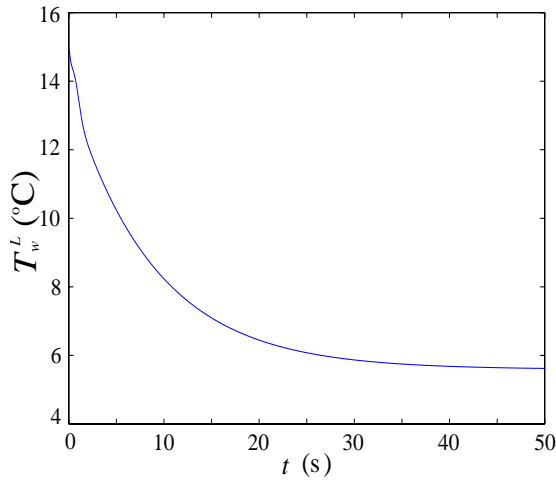
Figure 5.5. Method $- * -VF$ and $- \triangleright -CF$: (a) mass flow rates, (b) leaving air temperature; $T_a^E = 30^\circ\text{C}$, $U_a = 10$ m/s, $v_2 = 0.76$.



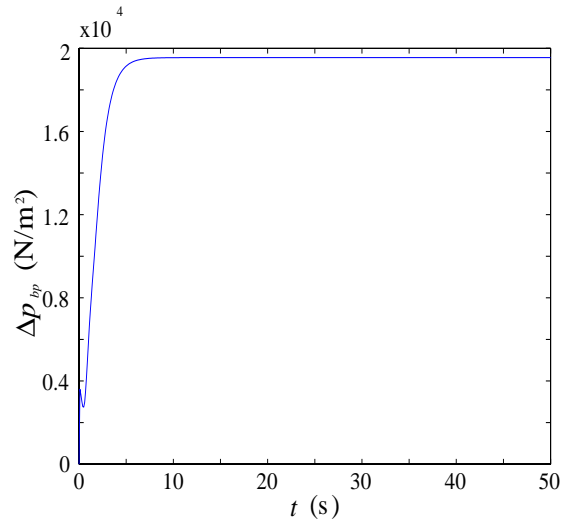
(a)



(b)



(c)



(d)

Figure 5.6. Method *BT*: (a) mass flow rates, (b) leaving air temperature, (c) leaving water temperature, (d) pressure drop in bypass; $T_a^E = 30^\circ\text{C}$, $U_a = 10 \text{ m/s}$, $v_1 = 0.46$, $v_3 = 0.54$.

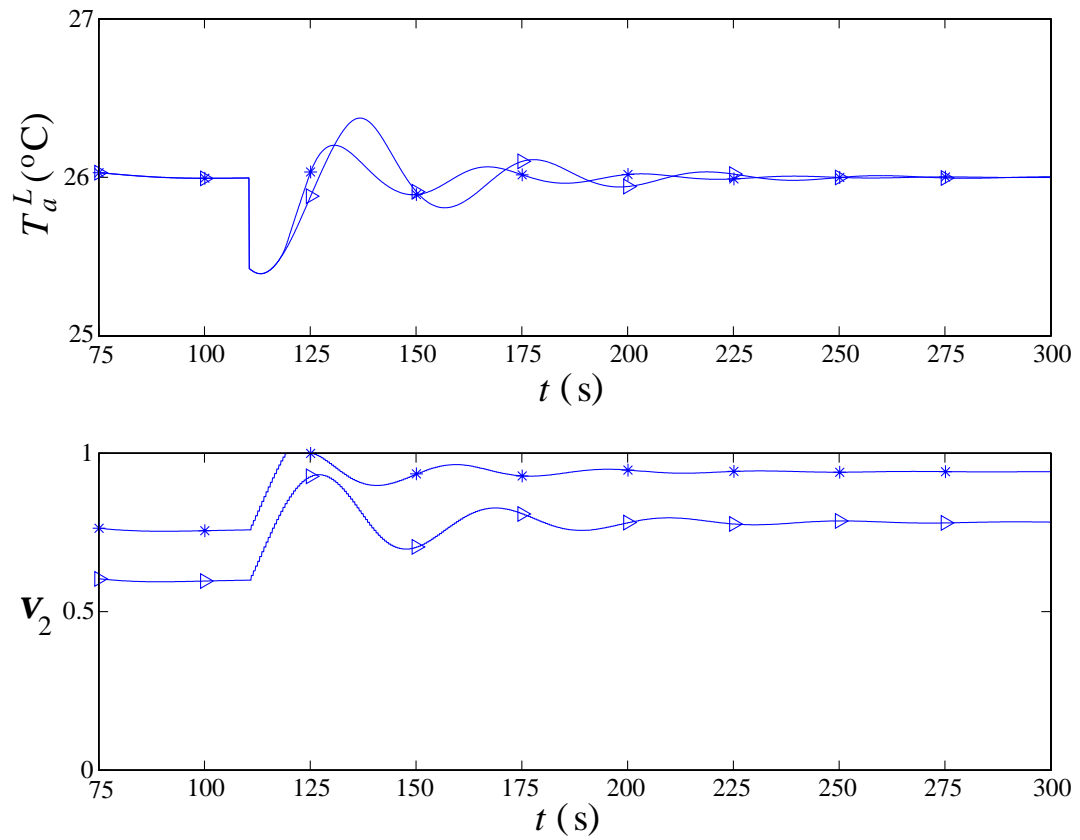


Figure 5.7. Dynamic response of control system to drop in air velocity, method $- * -VF$ and $- \triangleright -CF$; $\bar{T}_a^L = 26^\circ\text{C}$, $T_a^E = 30^\circ\text{C}$.

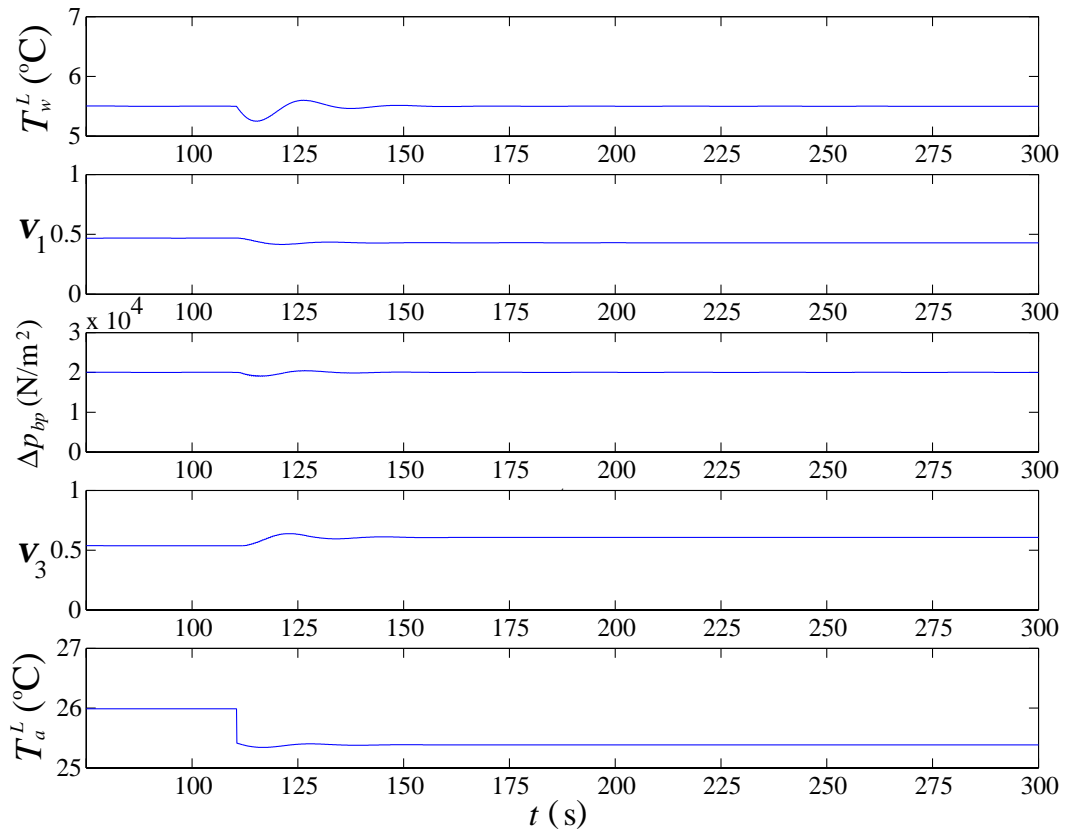


Figure 5.8. Dynamic response of control system to drop in air velocity, *BT* method;
 $\bar{T}_w^L = 5.5^\circ\text{C}$, $\Delta\bar{p}_{bp} = 20000 \text{ N/m}^2$; $T_a^E = 30^\circ\text{C}$.

disturbance is then introduced in the air side: U_a is reduced from 10 m/s to 7 m/s with a consequent reduction in the thermal load.

Each of the three methods is able to overcome the disturbance as shown in Figures 5.7 and 5.8. As U_a is reduced, the cooling coil requires less chilled water, a warmer water flow, or a combination of both to avoid overcooling the air. The *VF* and *CF* strategies are to restrict the chilled water flow rate. Figure 5.7 shows the oscillations in temperature and valve positions that result. The *BT* strategy is to maintain a constant water flow rate to the cooling coil with constant return water to the primary loop by blending the water from the chiller with that from the bypass. Figure 5.8 shows that T_a^L drops as a consequence of maintaining the set values.

Comparing the valve dynamics in Figures 5.7 and 5.8, it is observed that the control and manipulated variables and T_a^L oscillate much less for *BT* than for *VF* or *CF*. The smallest valve displacement is also for *BT*.

5.5 Comparison of strategies

The effect on the primary loop during the disturbance can also be computed. ΔT_{ch} (left y axis) and T_a^L (right y axis) are shown in Figures 5.9 and 5.10 as a function of U_a and T_a^E , respectively. In Figure 5.9, ΔT_{ch} decreases as U_a is decreased from the design value of 10 m/s. The *VF* and *CF* methods undergo a change in ΔT_{ch} that is almost twice as large as *BT*. In Figure 5.10, ΔT_{ch} also decreases as T_a^E is decreased from 30°C, but for *VF* and *CF* the change is almost four times larger than *BT*. Figures 5.9 and 5.10 also show that *VF* and *CF* maintain T_a^L constant but *BT* lowers it.

Figure 5.11 shows the ΔT_{ch} dynamics for each control strategy. Before the disturbance is introduced, the ΔT_{ch} is at the same design condition. A drop in U_a implies a change in the thermal load and therefore the design conditions are

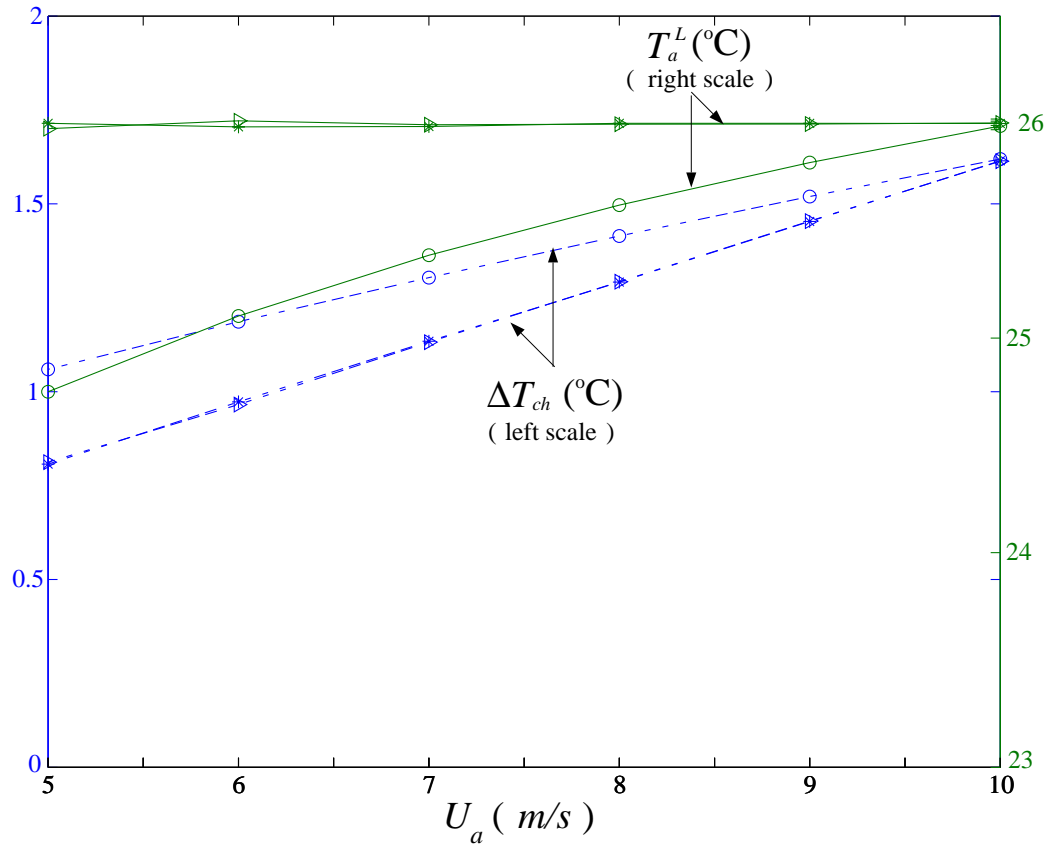


Figure 5.9. Temperature drop in chiller as function of air velocity; $- \circ -$ BT , $- \triangleright$ CF , $- * -$ VF .

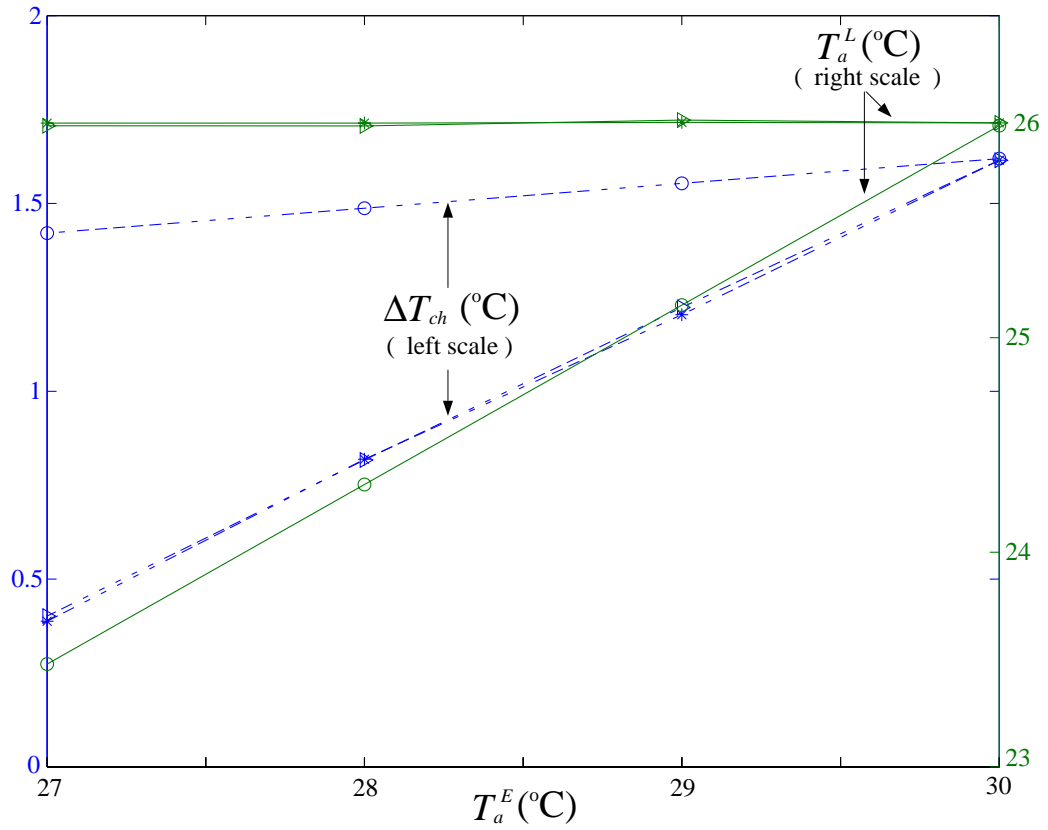


Figure 5.10. Temperature drop in chiller as function of air entering temperature;
 $- \circ - BT$, $- \triangleright - CF$, $- * - VF$.

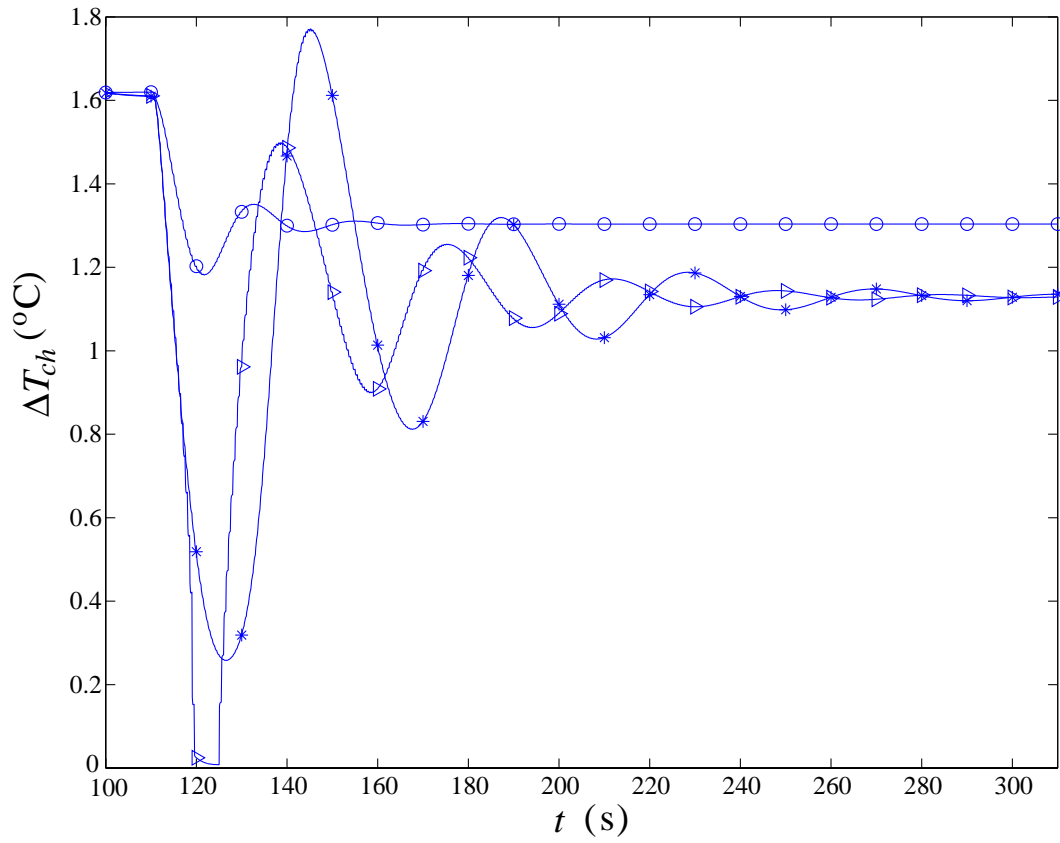


Figure 5.11. ΔT_{ch} dynamics; $- \circ -$ BT , $- \triangleright -$ CF , $- * -$ VF .

no longer valid. As each method overcomes the disturbance, ΔT_{ch} is set to a new equilibrium state. It can be seen that *BT* produces the smallest oscillation in ΔT_{ch} as well as the smallest change between initial and final values.

5.6 Discussion

It has been shown that there is no significant difference between the three control strategies studied if the network is operated at design conditions. When a disturbance in either the velocity or the temperature of the air is introduced, each control technique is able to overcome it by manipulating the control valves. As the air velocity decreases, the thermal load is decreased calling for a reduction in the heat transfer at the cooling coil; *VF* and *CF* diminish the chilled water flow while *BT* keeps a constant flow rate to the cooling coil but at a higher temperature. The response is similar when the inlet air temperature is decreased. For low flow rates, *VF* and *CF* become more difficult to control. The temperature difference across the chiller in the primary loop, ΔT_{ch} , changes to a new value because of the change in load in the secondary loop. *VF* and *CF* strategies present larger changes than *BT*. The air leaving the heat exchanger, T_a^L , keeps its value in *VF* and *CF*, but drops for *BT*. The *BT* method also produces smaller time-dependent oscillations in ΔT_{ch} than *VF* and *CF* during the control operation.

The existence of practical bounds in the manipulated variables leads to some limits in the control that is possible. If the magnitude of the thermal load continues to decrease, for instance, a point will be reached when *VF* or *CF* will find it difficult to achieve control because the valve is nearly closed. In practice what is usually done in this case is to diminish the central cooling capacity by shutting down one chiller or by reducing the flow rate in the main loop in such a way that the operational range of the control valve is shifted. However, it is possible that the chillers that are

left online do not have the capacity to cope with the thermal load. Furthermore, reducing the flow in the main loop may affect delivery to other secondary loops that may be in parallel. *BT* works in a different way by keeping the flow to the coil constant. However, as the thermal load decreases, at some point the set value of the leaving water temperature cannot be maintained since the thermal load at the coil is not enough to extract the required heat.

It has been pointed out that the general network studied here is slightly different from those that would be used if each one of the control strategies were studied separately, especially with respect to the connection to the primary. However, the conclusion that one strategy has the lowest change in ΔT_{ch} holds even if three different networks were studied. In a piping network in which only *BT* is implemented, the secondary bypass *bg* in Figure 5.1 does not exist and there is no mixing between the supply and return chilled water. Therefore, the water return temperature to the chiller is constant. In the present study there is no control on the chiller; with control the water supply temperature at *b* would be constant making the ΔT_{ch} constant at different thermal loads. In fact, even without chiller control, ΔT_{ch} would still be constant since the returning water temperature at *g* would not be changing. For *VF* and *CF* the ΔT_{ch} is not constant since the returning chilled water temperature changes as the thermal load at the heat exchanger changes. Thus, of the three control strategies studied here *BT* would still produce the lowest change in ΔT_{ch} even if they were in different but similar networks.

CHAPTER 6

EXPERIMENTAL STUDY OF THERMAL CONTROL STRATEGIES

An experimental study of the hydronic methodologies for temperature control VF , CF and BT is presented in this Chapter. The strategies are defined by the piping arrangement, the hardware used to achieve control and the variables to be controlled. This work complements the theoretical study presented in Chapter 5 by including all the complexity of the problem that is difficult to take into account in numerical experiments. This is due to the lack of accurate, reliable and validated models for the different components that are part of a thermal-fluid network and its control system, and the physical phenomena that take place. Complexity such as hysteresis in the valves, thermal delays, dynamic time constants, imperfect actuators, and imperfect sensors is inherent to *HVAC* systems. The flow and heat transfer are usually under turbulent conditions and thus not easily computable. The results presented in this Chapter are included in a journal article submitted for review (Franco *et al.*, 2003c).

The experimental facility, described in Chapter 4, is a cooling-water closed loop with a heat exchanger on the primary and three heat exchangers on the secondaries. The heat exchanger on the primary cools down the returning water from the secondaries using chilled water provided by the building services. A different control method is applied to each secondary. Two water heaters in a closed heating loop provide the thermal load to the heat exchangers at the secondaries. *PID* controllers are used to respond to changes in the thermal load. The temperature difference at

the primary loop heat exchanger is used as a criterion for comparison to assess the control strategies relative advantages or disadvantages. This criterion is equivalent to the ΔT_{ch} used in the theoretical study. As a consequence of changing the load, the stability and reachability of the thermal control system become key factors for the operation of the cooling network. The experimental set up is schematically shown in Figure 4.2.

The chilled-water cooling system used in the current experimental facility is an example of the ΔT variation that was discussed in Section 1.5.1. The water is supplied by the chillers in the building in which the laboratory is housed. Though the temperature of the water is meant to be constant, there are variations of up to 5°C in three hours and about 10°C degrees from one day to the other. This is due to several factors: different user demands, changes in the outdoor temperature, changes in set points by the operator. This implies that the system is not always working at design conditions, and terminal users may not receive water at the design temperatures. The experiments were performed early in the morning during holidays in order to eliminate uncontrolled disturbances in the temperature of the chilled water supplied by the building.

6.1 Proportional-integral-derivative control

PID controllers are among the most popular controls because of their simplicity, compactness, flexibility, low cost and good response. The proportional action adjusts the controller output according to the size of the error, the integral action eliminates steady-state offset, and the derivative action anticipates the future trend.

For feedback control the valves respond to a signal from the controller which is based on the difference between the system output and the set point. In every

Table 6.1. *PID* CONTROLLERS GAINS.

j	$k_{P,j}(\text{Volts})$	$k_{I,j}(\text{Volts/s})$	$k_{D,j}(\text{Volts s})$
1	5.0	0.10	1.0
2	8.0	0.67	24.0
3	1.0	0.5	0.5
4	5.0	0.10	1.0
5	8.0	0.67	24.0
7	5.0	0.10	1.0
8	2.0	0.20	1.0
9	5.0	0.10	1.0
11	-1.0	-0.50	-0.5
12	3.0	0.67	1.0

control valve a *PID* controller is used to modify the valve closings or openings. The control action is explicitly determined by

$$v_j(t + \delta t) = k_{P,j}e_j(t) + k_{I,j} \int_{t_0}^t e_j(s)ds + k_{D,j} \frac{de_j(t)}{dt}, \quad (6.1)$$

where v_j is the input voltage to valve j that takes place at a time δt after the right side of the equation is evaluated. k_P , k_I and k_D are the proportional, integral and derivative controller gains respectively. The gains used are shown in Table 6.1. The time step for data acquisition and processing is $\delta t = 1$ s. The tuning was based on the relay feedback method (Åström and Hägglund, 1984). Because just one secondary at a time is tested it is not necessary to use V_{10} , which remains completely open. V_6 , which is a normally-closed valve, is directly coupled to V_5 , a normally-opened valve so that $v_6 = v_5$.

To calculate the error the variables are scaled by $T_{ref} = 100^\circ\text{C}$ (212°F), $q_{ref} = 12.62 \times 10^{-4} \text{ m}^3/\text{s}$ (20 gpm) and $\Delta p_{ref} = 137.90 \text{ kPa}$ (20 psi) respectively. Since VF and CF are *SISO* systems with the same manipulated variable, they use the same error

$$e_2(t) = \frac{1}{T_{ref}} (\bar{T}_{18}(t) - T_{18}(t)), \quad (6.2)$$

$$e_5(t) = \frac{1}{T_{ref}} (\bar{T}_{14}(t) - T_{14}(t)), \quad (6.3)$$

to manipulate respectively V_2 and V_5 . T_{18} and T_{14} are the temperatures of the water at the heat exchanger outlets on the heating side. The bar indicates the set value that is the target. The *BT* is a *DIDO* system that manipulates valves V_8 and V_9 , where the error is defined as

$$e_8(t) = \frac{1}{T_{ref}} (\bar{T}_6(t) - T_6(t)), \quad (6.4)$$

$$e_9(t) = \frac{1}{\Delta p_{ref}} (\Delta \bar{p}_{V_8}(t) - \Delta p_{V_8}(t)), \quad (6.5)$$

respectively. T_6 is the temperature of the water at the heat exchanger outlet on the cooling side and Δp_{V_8} is the pressure drop across V_8 . On the heating side V_1 , V_4 and V_7 control the secondary hot water flow rates q_8 , q_7 and q_4 to the heat exchangers, respectively. Thus

$$e_1(t) = \frac{1}{q_{ref}} (\bar{q}_8(t) - q_8(t)), \quad (6.6)$$

$$e_4(t) = \frac{1}{q_{ref}} (\bar{q}_7(t) - q_7(t)), \quad (6.7)$$

$$e_7(t) = \frac{1}{q_{ref}} (\bar{q}_4(t) - q_4(t)). \quad (6.8)$$

The valves V_{12} , V_{11} and V_3 in the primary cooling loop control respectively the supply water temperature T_1 , the pressure drop Δp_{P_4} across the pump and the pressure drop Δp_{V_3} across the valve V_3 , so that

$$e_{12}(t) = \frac{1}{T_{ref}} (\bar{T}_1(t) - T_1(t)), \quad (6.9)$$

$$e_{11}(t) = \frac{1}{\Delta p_{ref}} (\Delta \bar{p}_{P_4}(t) - \Delta p_{P_4}(t)), \quad (6.10)$$

$$e_3(t) = \frac{1}{\Delta p_{ref}} (\Delta \bar{p}_{V_3}(t) - \Delta p_{V_3}(t)). \quad (6.11)$$

The hot water supply temperature is controlled by the water heater built-in *PID*.

6.2 Experimental methodology

The experimental facility is used to compare the advantages and disadvantages of three different control methodologies. For this purpose each control strategy was individually tested under similar conditions: the entire network was set to run at certain flow and temperature values, and later one of these flow values was modified to let the controllers cope with the change in conditions. While testing control in one secondary, the others remain shut down with no water running through. In the presentation of the results, the noise is filtered out by taking an average of the next and previous 10 measurements.

6.3 Steady state and dynamics of control valves

Before showing the performance, merits and drawbacks of each control strategy, the steady state and dynamic response of valves is presented to illustrate some inherent difficulties in the control task.

Figure 6.1 shows the steady state pressure drop $\Delta p_{V_{10}}$ across V_{10} as a function of the signal input v_{10} to valve V_{10} . This is a normally open valve which closes as it is energized. The pressure drop values when closing are different than those when opening at the same voltage input. Figure 6.2 shows the steady state and dynamic flow rate q_4 as a function of the input signal v_7 to valve V_7 which is normally closed. The valve opens and closes as the voltage increases and decreases, respectively. The flow is measured by turbine meters that send pulses to frequency-to-analog signal conditioners. Thus the number of pulses in a fixed time interval Δt determine the flow. At low flow rates there are few pulses, hence the readings are more erratic. This is illustrated by the steady state curve in Figure 6.2 for $q_4 < 1.5 \times 10^{-4} \text{ m}^3/\text{s}$ (2.4 gpm). The dynamic flow corresponds to the valve operation during *BT* test. The arrows indicate the followed path as time went by. The control valve drives the

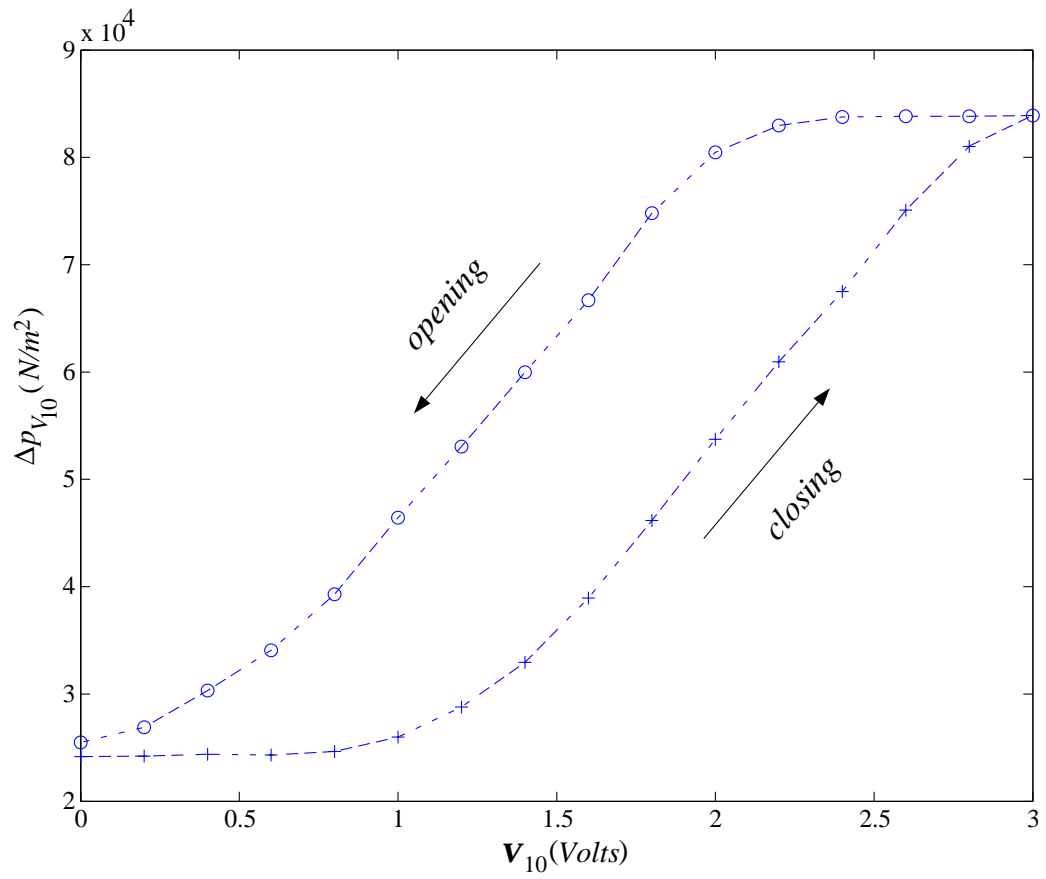


Figure 6.1. Steady state pressure drop $\Delta p_{V_{10}}$ as function of input signal v_{10} ; $- \circ -$ opening, $- + -$ closing.

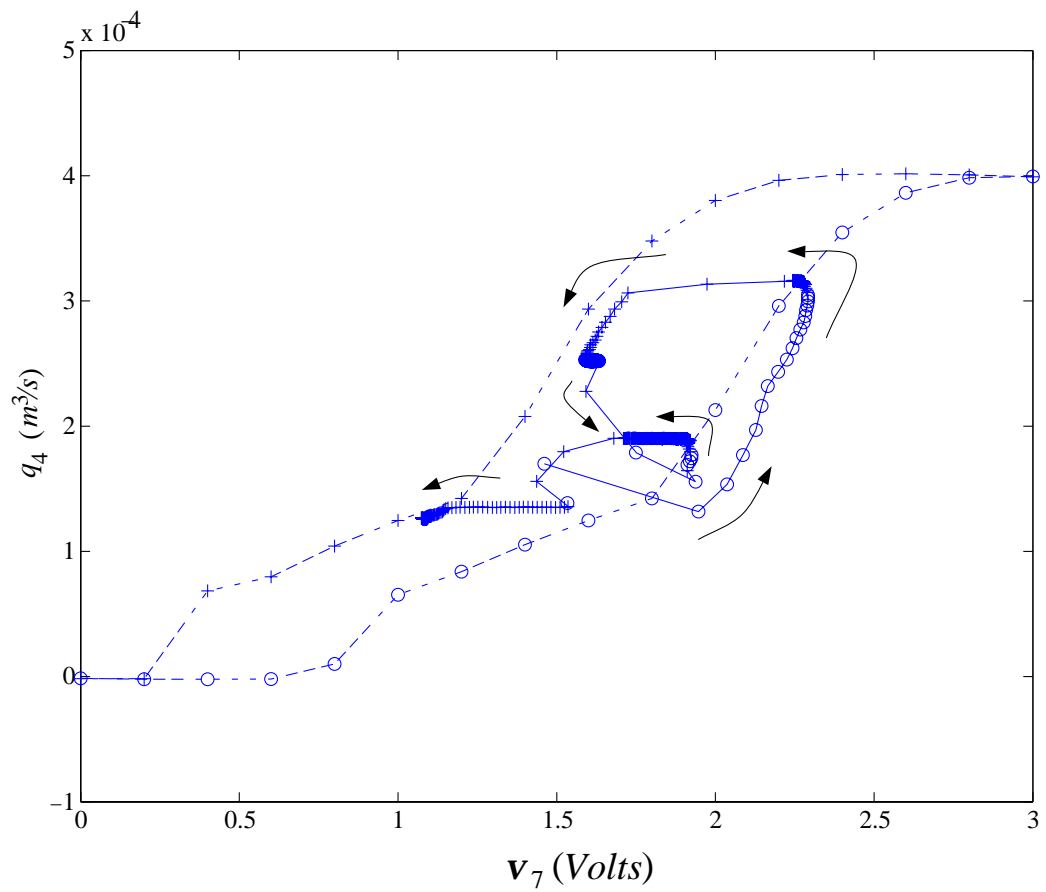


Figure 6.2. Steady and dynamic flow rate q_4 as function of input signal v_7 ; $- \circ -$ opening, $- + -$ closing. Arrows indicate direction of dynamic path.

water flow from an initial value to its set point value of $3.16 \times 10^{-4} \text{ m}^3/\text{s}$ (5 gpm). Later the controller set point is changed to 2.53, 1.89 and $1.26 \times 10^{-4} \text{ m}^3/\text{s}$ (4, 3 and 2 gpm) at $t = 900, 2700$ and 4500 s respectively. As seen in the figure the valve achieves control at every change. The figure also shows that the dynamic path does not coincide with the static. Furthermore, at some instants the flow decreases as the voltage increases; i.e. as the valve opens. Analytical valve models based on the static performance cannot fully predict valve dynamics.

The hysteresis and nonlinearity of valves are phenomena frequently overlooked in simulations and control design. The response and stability of the control system may be seriously affected by this phenomenon. A similar steady state response was found in the rest of the valves controlling flow rate and pressure drop. It is always desirable that the valve operates away from its maximum and minimum opening, specially in control situations where the system may be too sensitive to changes in the manipulated variable for stable control.

6.4 Dynamics of feedback control response

From initial operational conditions the controllers take the network to its design operational values. A change in the set point of the hot water flow rate is then introduced and the network goes to new operational conditions. The control strategies are expected to reject disturbances in the thermal load.

6.4.1 Primary heating and cooling loops

The heating loop provides water at $3.16 \times 10^{-4} \text{ m}^3/\text{s}$ (5 gpm) and 37.8°C (100°F). The hot water flow is then diminished by changing its controller set point. As a consequence, the controllers on the cooling side adjust their valve setting to maintain their set point values. Figure 6.3 shows the secondary hot water flow rates q_8 , q_7 and q_4 to the heat exchangers for the three different experiments. Each curve represents

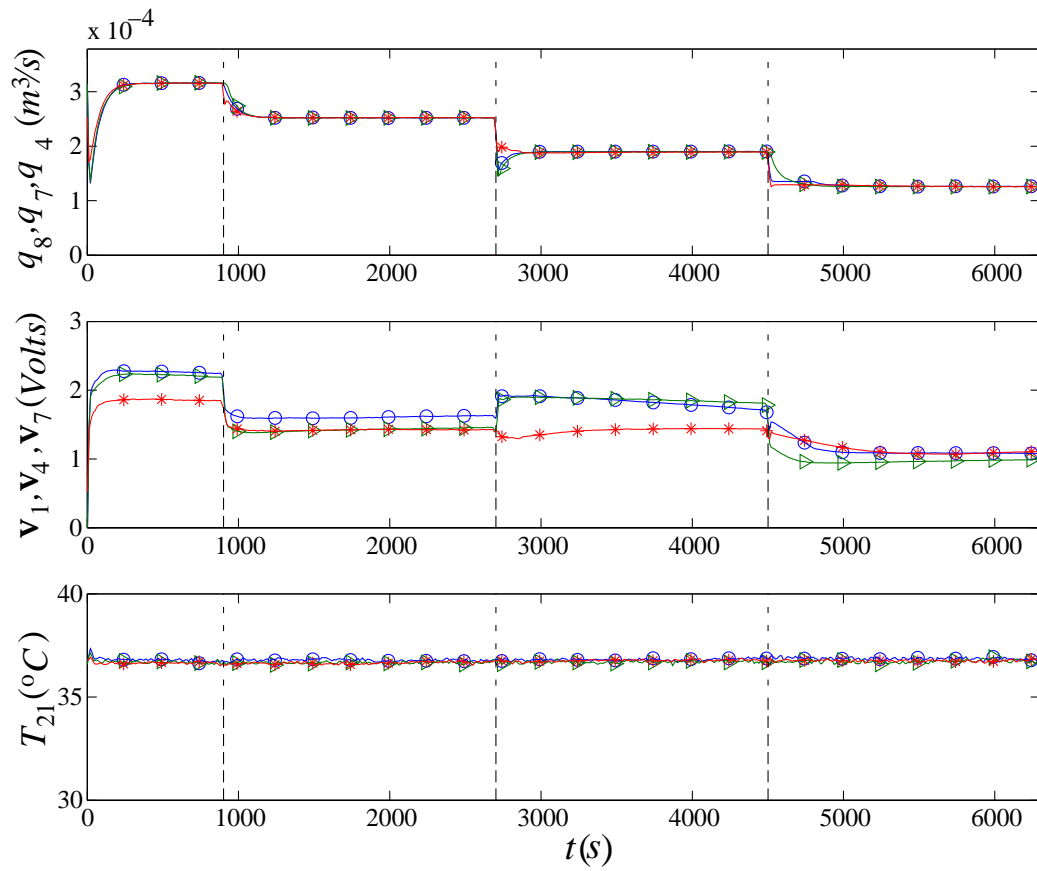


Figure 6.3. Secondary water flows and heat exchanger inlet temperature T_{21} on heating loop: $-\circ-$ BT , $-\triangleright-$ CF , $-\ast-$ VF . Dashed vertical lines are instants at which thermal load is changed.

one independent run; that is, water flow to HX_{BT} and HX_{CF} is zero when testing VF , and so on. The vertical lines mark the time when the hot water flow set point was changed. Thus there are four control scenarios. During the first 900 s the system is taken to what is called design conditions: the set of nominal values for which the network is intended to operate. In the next 5400 s the hot water flow is decreased $6.31 \times 10^{-4} \text{ m}^3/\text{s}$ (1 gpm) every 1800 s, and the control strategies drive the system to different operational points while coping with the changes. The flows reach steady state in 240 s. The input signals v_7 , v_4 and v_1 that control flow and the hot water temperature at the heat exchanger inlet T_{21} are also shown in Figure 6.3 for the three cases. T_{21} is controlled by the heater built-in PID . The signal inputs illustrate the hysteresis effect. As the flow is decreased the valves must close and the voltage should decrease, which is not the case for $2700 \text{ s} < t < 4500 \text{ s}$.

Chilled water to the secondaries is provided simultaneously by the compact heat exchanger HX_m and the variable speed pump P_4 that are located on the main loop on the cooling side. As shown in Figure 4.2 the task of control valves V_{11} and V_{12} is to maintain a constant pressure drop Δp_{P_4} across the pump and to supply water at a constant temperature T_1 , respectively. The control response of these valves to the described changes in the hot water side are presented in Figure 6.4, along with their respective signal inputs v_{11} and v_{12} , for the three different runs. V_{11} and V_{12} are normally closed and open valves respectively. The first 900 s show that T_1 and Δp_{P_4} take 720 and 240 s respectively to reach their set point value. A fixed pressure drop across P_4 produces a constant primary flow q_1 as shown in Figure 6.5. The test set-up for VF is different from those for CF and BT since it is desirable to have approximately the same operational conditions for each strategy: in each test at the design conditions $9.15 \times 10^{-4} \text{ m}^3/\text{s}$ (14.5 gpm) of water at 15°C (59°F) are circulated by P_4 on the primary and $3.16 \times 10^{-4} \text{ m}^3/\text{s}$ (5 gpm) are fed to the heat exchanger

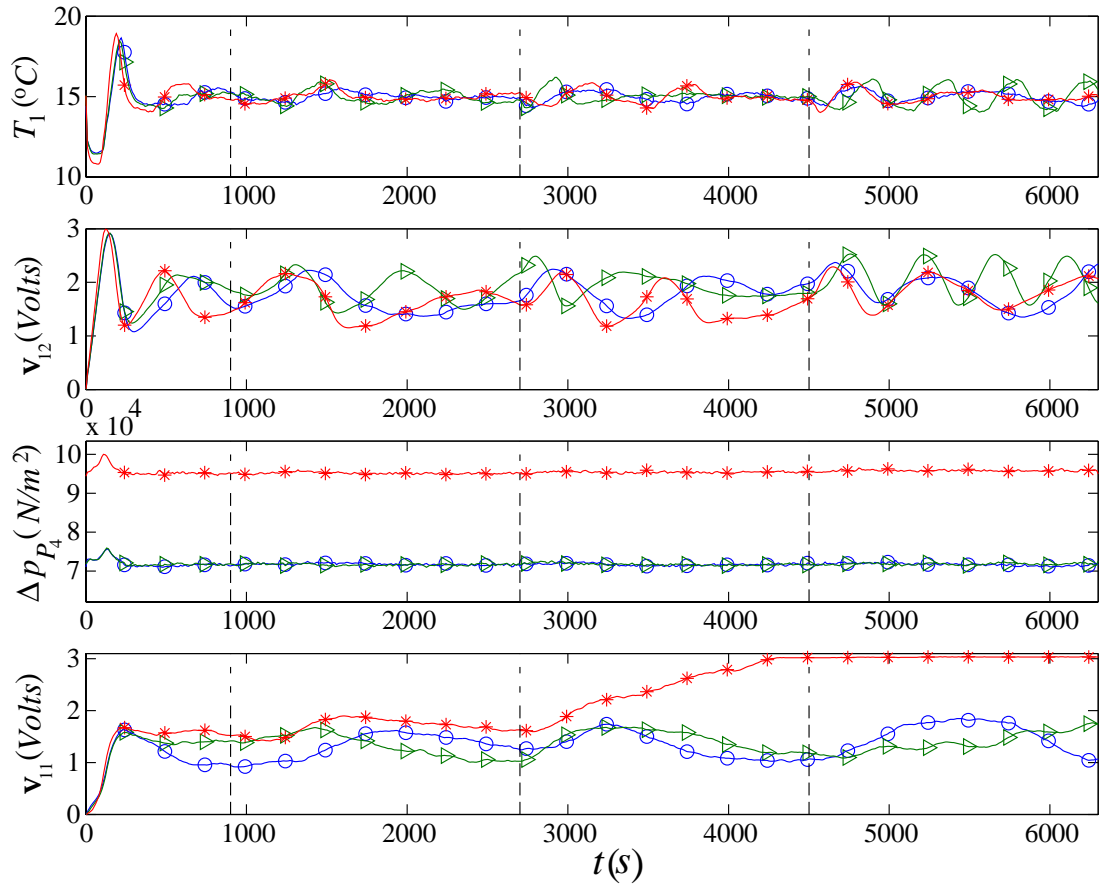


Figure 6.4. Supply temperature T_1 and pressure drop Δp_{P_4} across pump on primary cooling loop: $- \circ -$ BT , $- \triangleright -$ CF , $- * -$ VF . Dashed vertical lines are instants at which thermal load is changed.

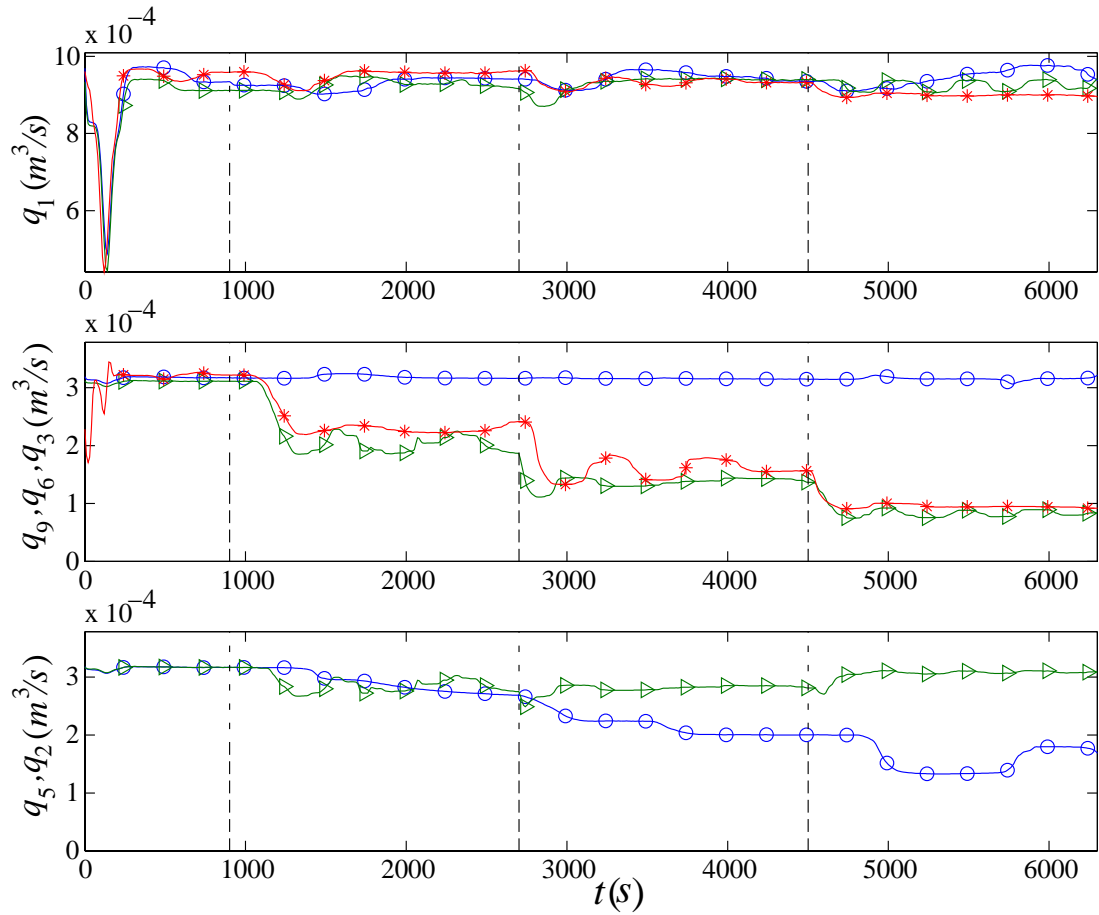


Figure 6.5. Main loop flow q_1 , heat exchanger inlet flows q_9 , q_6 and q_3 , and supply flows q_5 and q_2 to secondary on cooling loop: $-\circ-$ BT , $-\triangleright-$ CF , $-*$ VF . Dashed vertical lines are instants at which thermal load is changed.

at the secondary. To achieve these values the variable speed pump and the pressure drop $\Delta\bar{p}_{P_4}$ were set to 43.8 Hz and 95.15 kPa (13.8 psi), respectively, for *VF* and to 38.5 Hz and 95.15 kPa (13.8 psi) for *CF* and *BT*. Δp_{P_4} is shown in Figure 6.4. While testing *VF* the control valve V_3 is set to $\Delta\bar{p}_{V_3} = 28.06$ kPa (4.07 psi) during the first 900 s, then the V_3 controller is turned off and the valve opening remains constant. In the other cases V_3 remains open.

6.4.2 Secondary loops

VF controls the outlet hot water temperature T_{18} that is set to 30°C (86°F) by modifying the cooling water flow q_9 to the heat exchanger by means of the control valve V_2 . *CF* controls the outlet hot water temperature T_{14} that is also set to 30°C (86°F) by modifying the cooling flow q_6 to the heat exchanger by means of the coupled control valves V_5 and V_6 . As mentioned, these two strategies are *SISO* control systems with the same control variable. Figure 6.6 shows the control variables T_{18} and T_{14} along with the input signals v_2 and v_5 as a function of time. The outlet hot water temperature T_8 is also shown for comparison purposes but there is no control on this variable, changes are due to the control on different variables. It is observed that during the first 900 s there is no control on the secondary; the network is performing at certain values at $t < 0$ and at $t = 0$ the network is driven to its design operational values, hence little or no control effort is needed. When the flow rate on the hot water side decreases at $t = 900$ s the controller reacts by decreasing the cooling water to the heat exchanger to avoid overcooling the water at the heat exchanger outlet on the heating side. This is true for *VF* and *CF*. Figure 6.5 shows flows q_9 and q_6 to the heat exchangers and q_5 to the secondary *CF*. Notice that q_5 is practically constant. In Figure 6.6 the signal inputs v_2 and v_5 increase since V_2 and V_5 are normally opened. V_6 is normally closed, thus $v_6 = v_5$. Regarding

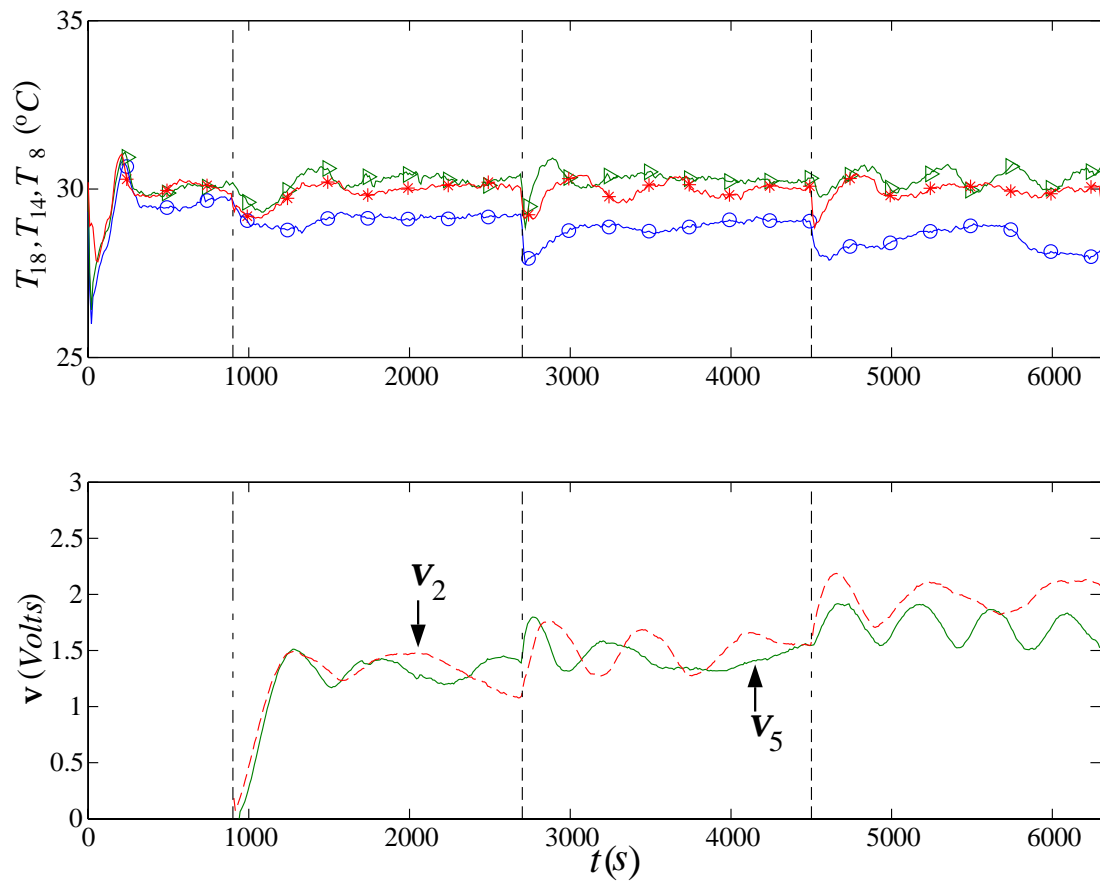


Figure 6.6. Heat exchangers outlet temperatures on heating loop: $-\circ-$ BT , $-\triangleright$ CF , $-*$ VF . Dashed vertical lines are instants at which thermal load is changed.

the control task both strategies overcome the decrease in the hot water flow rate to 2.53 and 1.89×10^{-4} m^3/s (4 and 3 gpm) maintaining the desired hot water outlet temperature. However when the flow decreases to 1.26×10^{-4} m^3/s (2 gpm) *CF* becomes unstable and *VF* achieves control: for $t > 4500$, T_{14} oscillates and T_{18} goes to the set point value.

BT controls the cooling water temperature at the heat exchanger outlet T_6 that is set to 21.5°C (70.7°F), and the pressure drop Δp_{V_8} across the valve at the bypass that is set to 18.96 kPa (2.75 psi), by means of manipulating V_8 and V_9 , respectively. The control variables and signal inputs to the valves are shown in Figure 6.7. For comparison purposes the cooling water return temperatures T_{10} and T_{20} are also shown; there is no control action on these variables. Note that $T_4 = T_6$. During the first 900 s there is no control in the secondary since the network is operating at nominal values. When the hot water flow rate is decreased the controllers react to the change. V_8 and V_9 are normally-closed and open valves respectively. V_9 restricts the cooling water supply flow to the secondary while V_8 allows mixing the cooling water from the heat exchanger outlet with the supply flow. Thus the heat exchanger inlet receives the same cooling flow but at a higher temperature. The valves have independent controllers however they are physically coupled in order to provide the proper cooling flow. Note the correspondence between signal v_8 and v_9 . It is observed that *BT* overcomes the hot water flow decrement to 2.53 and 1.89×10^{-4} m^3/s (4 and 3 gpm); however at 1.26×10^{-4} m^3/s (2 gpm) control is not achieved. Figure 6.5 shows the constant flow q_3 to the heat exchanger and the variable flow q_2 to the secondary *BT*.

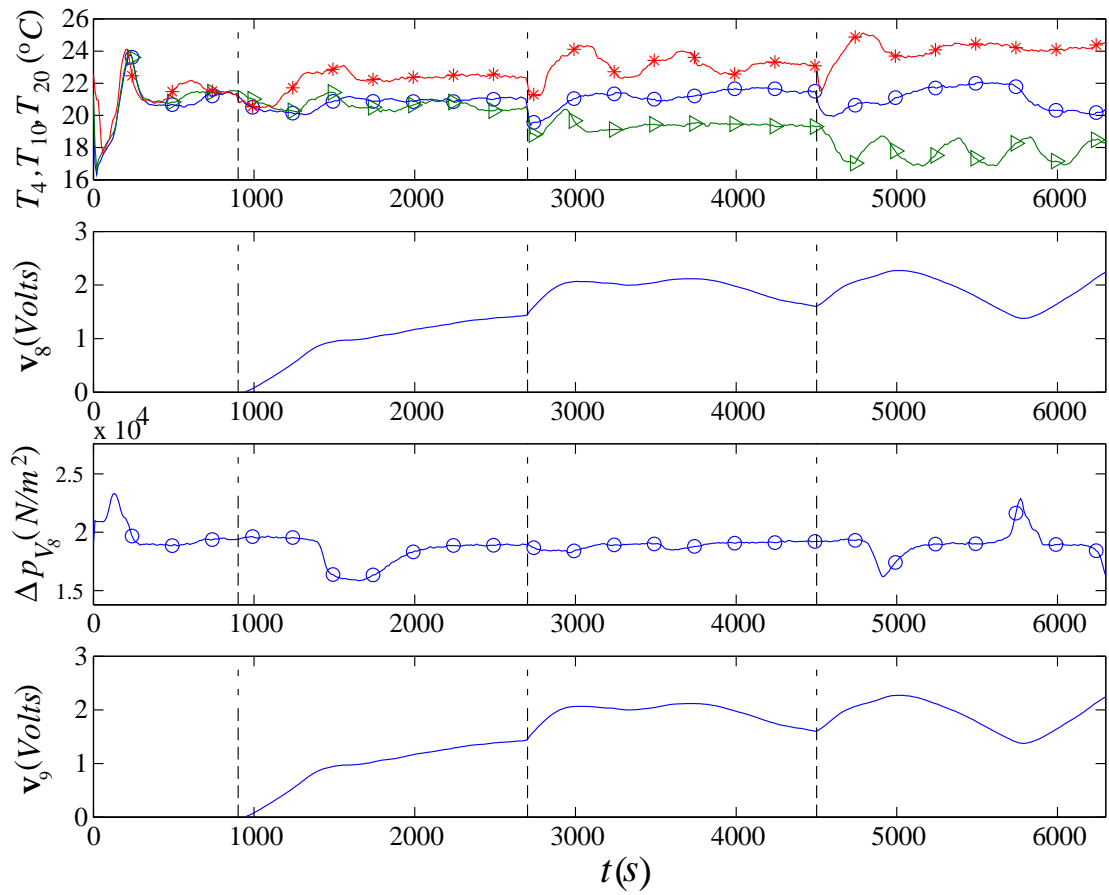


Figure 6.7. Secondary return temperatures and pressure drop Δp_{V_8} across V_8 on cooling loop: $-o-$ $-BT$, $-▷$ $-CF$, $-*$ $-VF$. Dashed vertical lines are instants at which thermal load is changed.

6.4.3 Stable and unstable control

The *PID* controllers are tuned for the network to perform at the design conditions. The gains in Table 6.1 set the dynamics of the experiments. Different gains would change the dynamics and the stability of the control system. A stable controller maintains the manipulated variable at the set point value. If it is unstable the manipulated variable oscillates around the set point. The temperatures of *CF* and *BT* are unstable for $t > 4500$ s, as presented in Figures 6.4, 6.6 and 6.7. The time interval corresponds to low hot water flows. For this interval Figure 6.8 illustrates the T_1 and v_{12} plane in *CF*. A limit cycle takes place. The controller of V_{12} on the primary is not able to deliver cooling water at the specified 15 °C to the secondary, instead T_1 fluctuates between 14 and 16 °C. Figure 6.7 shows that the pressure drop ΔP_{V_8} is also unstable for the same time interval. Figure 6.9 presents the ΔP_{V_8} and v_9 plane in *BT*. V_9 cannot maintain a fixed pressure drop across V_8 , hence the cooling water flow to HX_{BT} varies. It is not easy to assess why the network becomes unstable at lower flows since all individual controllers in the experiment are physically coupled to each other. Figures 6.3, 6.4 and 6.6 show that valves are operating away from its maximum and minimum opening even when instabilities arise. The controller gains can be adjusted to stabilize the control process at low flows. However there is no certainty that the process will be stable at higher flows. This illustrates the main disadvantage of simple *PID* controllers and a common situation during operation of cooling and heating systems in buildings.

6.4.4 System reachability

The existence of physical bounds in the network and its components leads to some limits in the control that is possible. *VF* control is stable at low flows but has reachability problems. Figure 6.4 shows that for $t > 4500$ s the signal $v_{11} = 3$

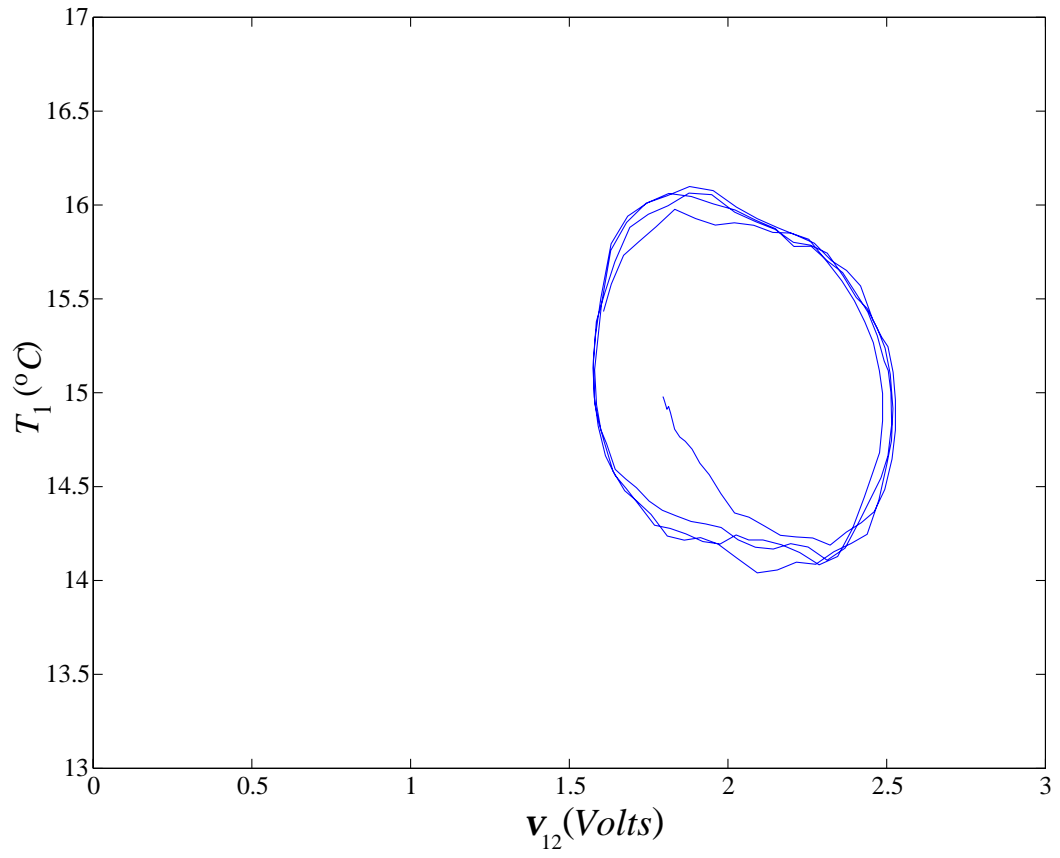


Figure 6.8. V_{12} phase space for VF when $t > 4500$ s.

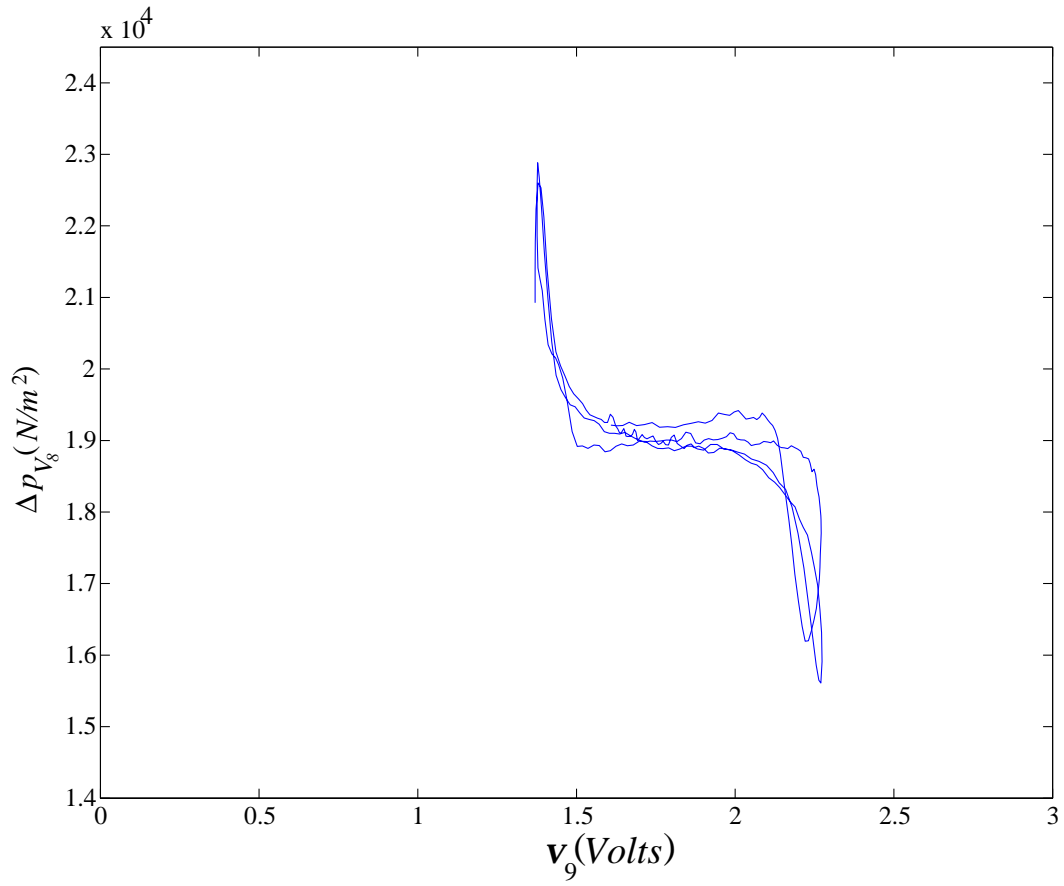


Figure 6.9. V_9 phase space for CF when $t > 4500$ s.

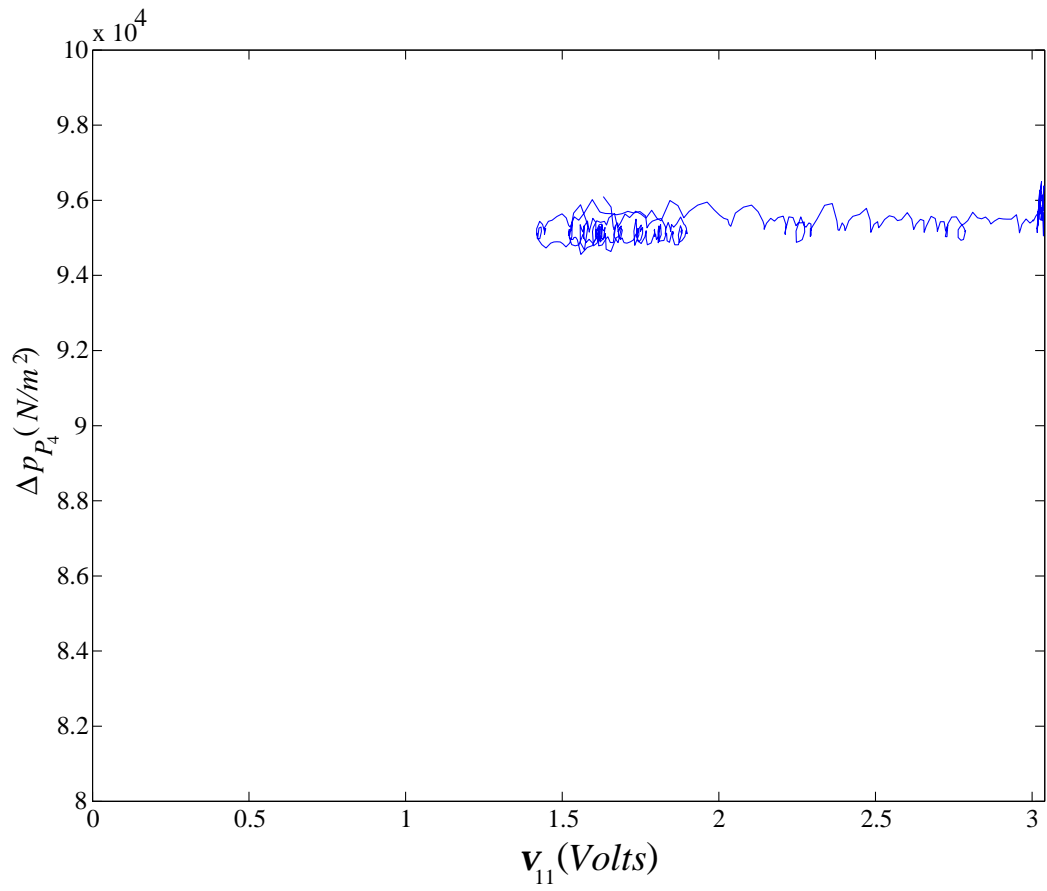


Figure 6.10. V_{11} during operation for VF .

Volts in the VF case. If a new hot water flow decrement is introduced V_{11} will not be able to maintain a fixed pressure drop across P_4 since it has reached maximum opening. As a consequence the system will be unbalanced because the flow in the primary will no longer be constant. A potential problem of unbalanced systems is to change the chilled water delivery to distant secondary loops. Figure 6.10 illustrates V_{11} dynamics on the phase space for $t > 300$ s during VF test. For every change in the thermal load the controller maintains the specified pressure drop by opening the valve until the valve reaches its maximum opening.

6.5 Comparison of control strategies

Looking at the first 900 s of Figures 6.4, 6.6 and 6.7 it is seen that there is no significant difference between the strategies studied while performing at design values. In each case the network operates at similar conditions achieving the same temperatures on the heating and cooling sides. Furthermore, for a hot water flow reduction to 2.53 and 1.89×10^{-4} m³/s (4 and 3 gpm), during $900 \text{ s} < t < 4500 \text{ s}$, the strategies are able to overcome the change maintaining their set point values. For a reduction to 1.26×10^{-4} m³/s (2 gpm), during $t > 4500$, VF is the only one that maintains its set point value.

6.5.1 Temperature effect on chiller

As discussed in the introduction it is desirable to maintain the chiller temperature difference near its design value. However, there is no chiller in the experimental facility, so that ΔT_{ch} is defined here as the difference in temperature of the water supplied by and returned to the heat exchanger HX_m . Thus the supplying and returning water temperatures on the primary cooling loop of the facility are used to define $\Delta T_{ch} = T_1 - T_2$. Figure 6.11 shows the steady state effect that each strategy would have on a chiller as the hot water flow decreases. BT stays closer to its design

value at $3.16 \times 10^{-4} \text{ m}^3/\text{s}$ (5 gpm). This is not surprising since it is controlling the heat exchanger outlet temperature at the secondary. Notice that water returning from the secondary loop mixes with bypassed water that runs in the primary loop through V_3 . If BT alone were used in a large system there would not be a bypass through V_3 and the secondary returning water temperature would be the same as the primary returning temperature, and so ΔT_{ch} would be constant. This technique uses a bypass by the bank of chillers and staged pumps. Therefore the primary loop operates at variable flow rates and constant temperatures. To assure that every secondary will be fed booster pumps in parallel to each other are installed. Figure 6.12 shows the secondary returning temperatures as a function of the change in the hot water flow rate: in BT temperature T_4 remains constant because T_6 is controlled, in CF temperature T_{10} decreases because cooling water is bypassed and in VF temperature T_{20} increases because the heat exchanger flow decreases.

6.5.2 Pressure drop effect on primary loop

Figure 4.2 illustrates the location of pressure transducers 1, 2 and 3 which are used to measure the pressure drop across each secondary. The pressure drops are shown in Figure 6.13. VF pressure drop varies since flow q_9 decreases. In this strategy there are larger changes with respect to its design pressure drop than in the others. CF maintains an almost constant pressure drop because of the booster pump P_3 . BT pressure drop varies because the booster pump P_2 is after the bypass.

6.5.3 Temperature effect on hot loop side

So far BT seems to be better because it maintains the chiller temperature difference near its design value. However CF and VF were designed to satisfy the conditioned room space. Figure 6.12 shows the hot water temperature at the heat

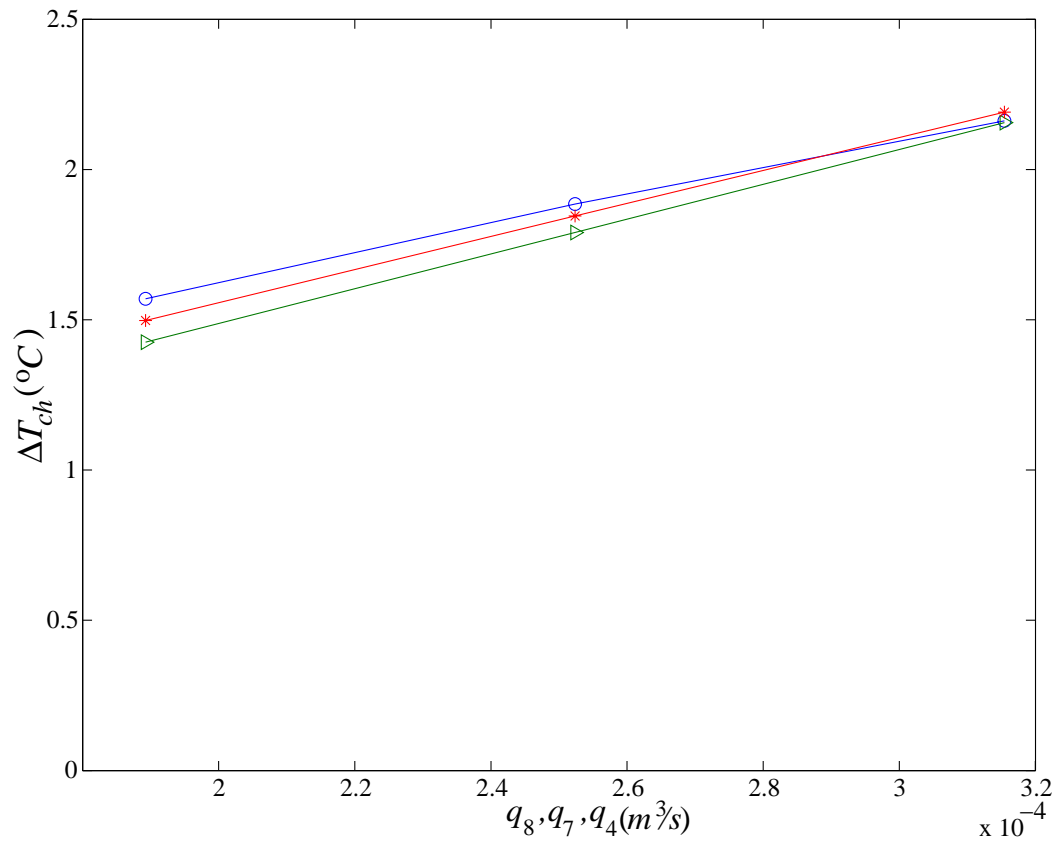


Figure 6.11. ΔT_{ch} as a function of hot water flow rates q_8 , q_7 and q_4 : $- \circ -$ BT ,
 $- \triangleright -$ CF , $- * -$ VF .

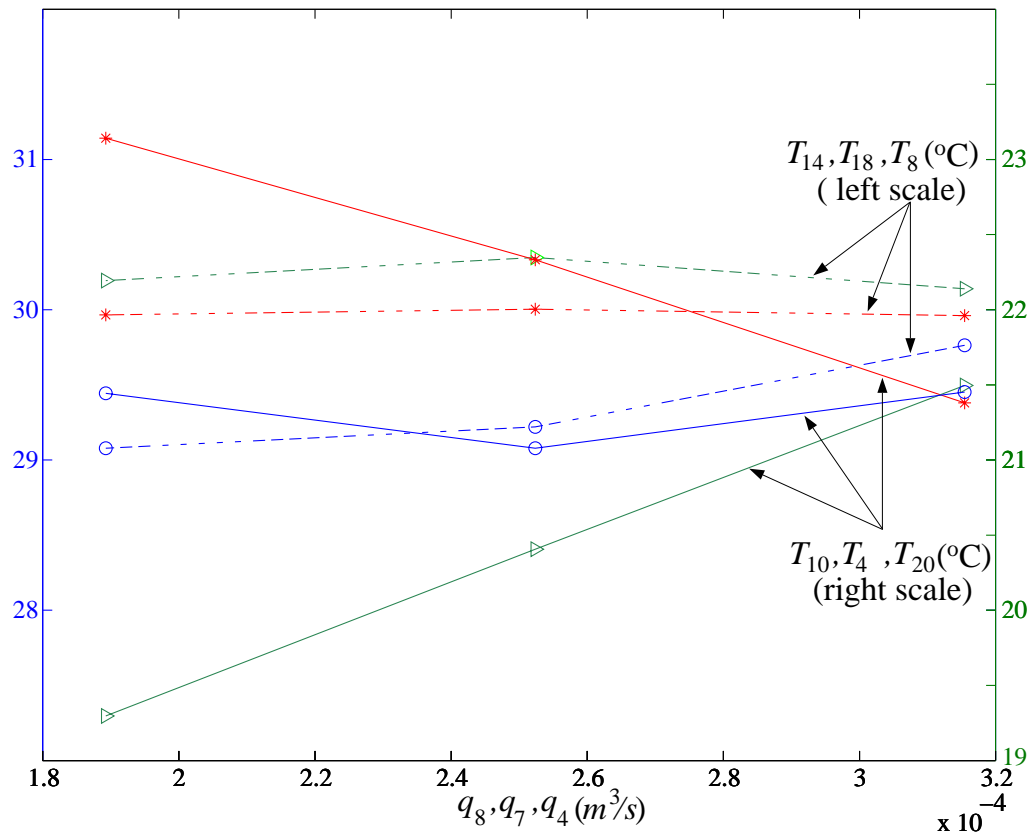


Figure 6.12. Return temperatures from secondaries on cooling side T_4 , T_{10} and T_{20} , and outlet temperatures on heating side T_8 , T_{14} and T_{18} as a function of hot water flow rates q_8 , q_7 and q_4 : $-o-$ $-BT$, $-▷$ $-CF$, $-*$ $-VF$.

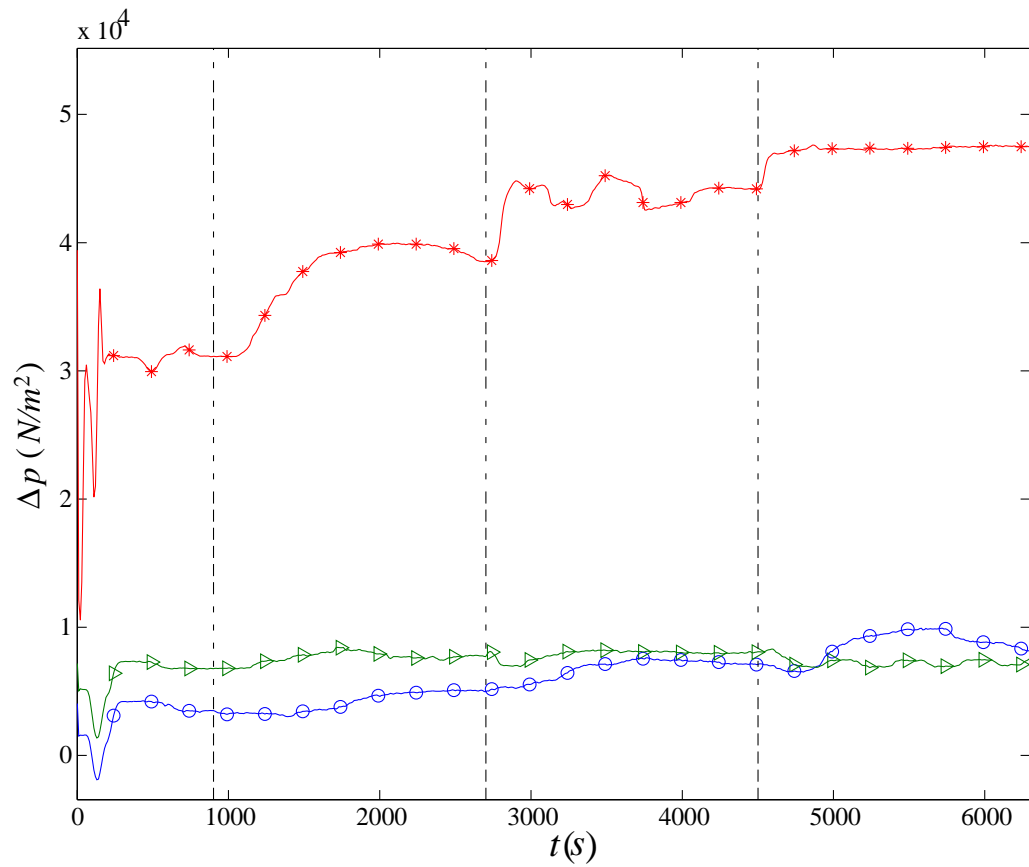


Figure 6.13. Pressure drop Δp at secondaries in cooling loop: $- \circ - BT$, $- \triangleright - CF$, $- * - VF$. Dashed vertical lines are instants at which thermal load is changed.

exchanger outlet as a function of the change in water flow rate. As expected *CF* and *VF* maintain the desired value for the conditioned space while *BT* does not.

In the theoretical study presented in Chapter 5 the leaving air temperature of the conditioned space remained constant for *CF* and *VF* but decreased for *BT* as the velocity of the hot air decreased. The effect on the chiller was also computed showing that the ΔT_{ch} decreased as the air velocity was decreased from the design value and that *BT* stayed closer to the design temperature difference. Results shown in Figures 6.11 and 6.12 are consistent with those observations.

6.6 Discussion

The objective of the experimental study presented in this chapter is to compare three common control strategies that are used for heating and cooling conditioned room space in buildings. The study incorporates the complexity of the problem that is impossible to consider in theoretical models. Hysteresis in the valves, dynamic time constants, imperfect actuators, imperfect instruments and thermal delays are inherent to this work. The temperature difference ΔT_{ch} at the heat exchanger on the primary loop is the criterion used for comparison. In addition the temperatures of the conditioned space are presented.

It has been found that there is no significant difference between the strategies studied if the hydronic network is operated at the design conditions. When a change in the thermal load is introduced each control technique is able to overcome it by manipulating control valves. The valves response is affected by imperfect actuators and imperfect instruments. Hysteresis is present in their static response. A highly nonlinear behavior was found during operation. *PID* controllers are used to manipulate the valves. The controller response is good until they loose stability at low thermal loads. As the hot water flow decreased, the thermal load decreased call-

ing for a reduction in the heat transfer at the heat exchangers. For low flow rates *BT* and *CF* become unstable and limit cycles arise; i.e. the manipulated variables oscillate as valves open and close. *VF* achieves control but the valve that manipulates the primary flow is saturated. If the hot water flow continues to decrease the flow in the primary will or will not change. As a consequence the system will be unbalanced.

The temperature difference across the heat exchanger in the primary loop changes to new values because of the changes in load in the secondary loop. *BT* is the control strategy that maintains the ΔT_{ch} closer to its design value as the thermal load changes. The drawback is that the conditioned room space temperature will change. *CF* and *VF* cannot maintain a constant ΔT_{ch} but they do maintain the conditioned room space temperature. In *CF* the changes in pressure drop at the secondary are the smallest while *VF* is the strategy that has the bigger changes. However *VF* is the least expensive to implement. From the cooling system point of view *BT* is a better option. Regarding the conditioned space *CF* and *VF* perform better than *BT*.

CHAPTER 7

SELECTION AND PLACEMENT OF HARDWARE

The results presented in Chapters 5 and 6 make evident the importance of the location of the hardware. The present Chapter explores the discrete space of possible hardware placements for a specific, but typical, user loop layout and seeks the optimum under some specified criterion. Valves and pumps are essential components of chilled water networks. A common thermal control practice is to use a valve as the control element and a fluid temperature as the control variable, while a booster pump drives the chilled water to a secondary loop with the cooling coil. In order to achieve the cooling task as a function of the variable thermal load, a control system adjusts the flow rate or the temperature of the chilled water. There are many possible places where the valves and pumps may be physically located to achieve a similar control effect. The results included in this Chapter have been published in proceedings (Franco *et al.*, 2003a).

The user or secondary loop chosen consists of a water-air cooling coil and five pipes: supply, bypass, coil inlet, coil outlet and return. Chilled water at a constant temperature is driven by a constant pressure drop. Hot air flows over the coil at a constant temperature and velocity. The hardware elements are a control valve and two booster pumps. Pumping action is divided among the two pumps to be able to look at possible combinations. A mathematical model of the thermal-hydraulic network is used as a basis for analysis. The change in operating conditions and

the output temperature reachabilities of the control system are used as criteria to compare the relative merits of different configurations. For any given configuration, open loop control is used to determine the range of operation of the system on the leaving air temperature at the coil, i.e. the temperature range achieved by opening and closing the control valve. This range varies from 0.1 to 3.5°C. The results show that the characteristics of the control system and that of the network are strongly influenced by the location of the hardware elements. The change in the returning water temperature is the operating condition used for comparison. The change is in the range of 0.2 to 18°C. Under the given layout constraints, an optimum valve and pump placement configuration has been found that minimizes the change in operating conditions from the design values and maximizes the temperature reachability of the control system.

7.1 Steady-state mathematical model

The model is based on the one described in Chapter 2. The assumptions on the fluid properties, velocity and temperature are the same. A lumped approach is also used for the cooling coil. In addition, longitudinal variations of the temperature along the coil are included in the thermal model.

7.1.1 Hydraulic components

Equation (2.1) in steady state is used for the flow in a pipe. The friction factor depends on the Reynolds number; for laminar flow ($Re_d < 2300$) it is $64/Re_d$, while for turbulent flow Equation (2.2) is used with a roughness of 4.6×10^{-5} m. The loss coefficient K for a valve is approximated by Equation (2.3). To avoid mathematical singularities the highest closing value used is $v = 0.9$, which allows a trickling flow to go through.

Booster pumps are installed when the pressure head at the connection to a piping subcircuit is inadequate to ensure circulation. A combination of two booster pumps, one with a pressure rise of $p_k^B = B\mathcal{P}$ in pipe k and another with $p_j^{1-B} = (1 - B)\mathcal{P}$ in j are used to provide a total pressure rise \mathcal{P} . B is a partition parameter that allocates the total pressure rise between the two pumps.

7.1.2 Thermal modeling

At the cooling coil, chilled water flowing inside the tubes removes heat from the hot air flowing over it. Heat transfer rates are modeled using inside and outside coefficients of heat transfer and temperatures differences between each fluid and the body of the heat exchanger. The correlations used are those in Equations (2.6) and (2.7) taken from an experimental study of a single-row heat exchanger. On the air side of the cooling coil the heat transfer by convection is

$$\dot{m}_a c_a (T_a^E - T_a^L) = h_a A_a (T_a - T_t). \quad (7.1)$$

The equation is valid for the dry region of the coil. At the coil the heat transfer by convection with both fluids is expressed as

$$h_a A_a (T_a - T_t) - h_w A_w (T_t - T_w) = 0. \quad (7.2)$$

The heat exchanger geometry corresponds to the one used by Zhao (1995). On the water side the energy equation is

$$\dot{m}_w c_w \frac{dT_w}{dx} = h_w \pi d (T_t - T_w). \quad (7.3)$$

The fluid temperatures are taken to be the averages between inlet and outlet.

7.1.3 Network principles

To model the network the individual components are combined using the following principles: the sum of the mass flow rate at every junction is zero, the advective

heat flow to each junction is also zero and the sum of the pressure drops around every closed loop must be zero.

7.2 Statement of problem

Figure 7.1 shows the piping network subcircuit to be analyzed, nowadays this is one of the most simple and typical layouts used in *HVAC* systems. Each of the piping branches is identified by a number. The water is driven by a fixed pressure drop between the subcircuit supply and return junctions of 5000 N/m^2 . The total booster pump pressure used is also $\mathcal{P} = 5000 \text{ N/m}^2$.

At junction a chilled water is supplied at a constant temperature $T_w^S = 5^\circ\text{C}$. At junction b the supply water either splits up to feed the cooling coil and to bypass it, or blends with the water coming from the coil outlet to feed the coil inlet. The bypass flow direction depends on the load and location of the pumps. At junction f chilled water returns at a higher temperature T_w^R to the network to be circulated back to the chiller (or bank of chillers) on the main circuit. The length of the pipes and their diameter are 1 m and 0.01905 m , respectively. To remove heat from the air flow, chilled water regulated by the valve runs through the cooling coil. The air flows over the coil at a uniform velocity of 5 m/s with an entering temperature of $T_a^E = 30^\circ\text{C}$

One control valve and two booster pumps are the hardware to be placed in the subcircuit. The purpose of the present study is to explore the discrete space of possibilities in order to suggest the best.

7.2.1 Hardware configurations

The hardware elements, control valve V and booster pumps P with partition B , can be placed on any of the subcircuit pipes. To avoid repetitions, the location and combination of elements are restricted to a specific set. A hardware configuration

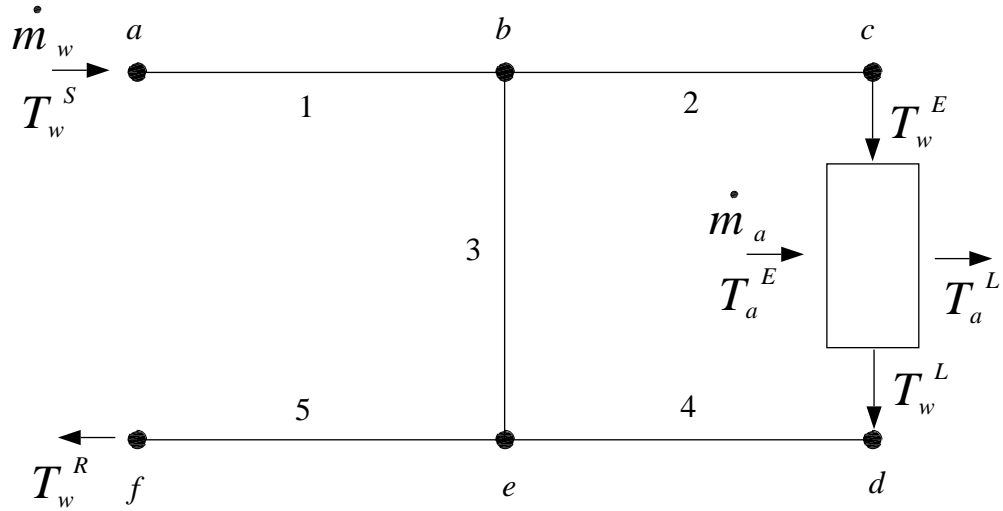


Figure 7.1. Subcircuit layout.

can be specified as a vector $[i, j, k, B]$, where the first three indices specify the pipe where the valve, the first booster pump and the second booster pump are located, respectively, and the last the value of the partition parameter. This represents all possible hardware configurations. However, because of the network geometry there are equivalent configurations like $[1, j, k, B] = [5, j, k, B]$, where placing the control valve on either the supply pipe 1 or the return pipe 5 produces the same effect to the network and its control. In fact this is also true for the pumps. The same symmetry is present between the coil inlet pipe 2 and outlet pipe 4. Therefore, to avoid repetitions the possible location of the hardware is confined to pipes 1, 2, and 3. Ten B values were used for the pumps; to vary B for a specific configuration from its minimum to maximum value implies a gradual change in the pumping head from pipe j to k . When a pump is placed on the bypass the direction of the pumping is from e to b . In some cases it is not large enough to change the flow direction but does modify the bypass flow rate. Looking at all possible independent combinations, there are a total of 90 different hardware configurations that must be considered.

Computations for all combinations were performed in order to address the problem of the optimal location of components.

7.2.2 Bounded thermal control

Open-loop control is used to determine the range of response of the thermal-hydraulic network and its control system. This is a single input single output control system in which a valve is used as the control element and the outlet air temperature T_a^L is the control variable. In fact, since it is open-loop control, the system has a specific single control input and several options for the control output. The most common practice is to use the outlet air temperature with closed-loop control since that is usually what the purpose of the heating or cooling system is; however, the inlet and outlet water temperature at the cooling coil and the pressure drop at the bypass are also possible candidates.

A change in the valve closing parameter v modifies the water mass flow rate and the inlet water temperature T_w^E to the heat exchanger, the latter depending on the location of the pumps and load. The control action is bounded because $0 \leq v_i \leq 1$, which defines an operational range of flow rates and thus a reachable set of temperatures T_a^L . The water flow rates and the pressure at the junctions constitute the state variables of the control system and the air outlet temperature T_a^L is the output variable. The change $\Delta T_a^L = |T_a^L(v_{op}) - T_a^L(v_{cl})|$, where v_{op} and v_{cl} are the open and closed valve positions, is the range of temperatures that can be reached.

7.2.3 Network performance

A thermal-hydraulic network, specially if it is large, almost never operates at design conditions. However, the closer the system is to such conditions, the more efficient it is. To drive the network to different operational states in order to achieve

the control task produces hydraulic and thermal changes that affect the entire system; for instance changes in the pressure drop Δp_w^{SR} or in the water temperature difference between the supply and the return ΔT_w^{SR} . The smaller the change in ΔT_w^{SR} the better it is, since the impact on the entire piping system is less. Though the chiller provides chilled water at a constant temperature to the complete piping network, the water returns to it at different temperatures. If the return water temperature decreases it is true that the further the temperature is from its design value, the more the chiller needs to extract heat. In the design and operation of chilled water plants an important point of concern is the chiller ΔT , which is the difference in temperature of the water entering and leaving the chiller. A common situation during the operation of a chilled water plant is that the temperature difference in the main loop is not at the design value, but is below the capacity of the selected equipment. As a consequence extra pumps and chillers are used to meet, in an inefficient fashion, the thermal load. The literature reports situations where this problem arises and provides practical recommendations to prevent and overcome it. Furthermore, the control system at the terminal user has an impact on the chiller performance (Franco *et al.*, 2003b). Therefore a smaller water return temperature difference $\Delta T_w^R = |T_w^R(v_{op}) - T_w^R(v_{cl})|$, is better for the network.

7.3 Computations

Computations for $v_{op} = 0$ and $v_{cl} = 0.9$ were performed in order to assess the range of response of the network and control system to a specific hardware configuration.

Figure 7.2 shows the difference in the air outlet temperature at the coil and of the water return temperature at the subcircuit, as a result of modifying v_i for all possible configurations. The figure shows mainly three different clusters $[1, j, k, B]$, $[2, j, k, B]$

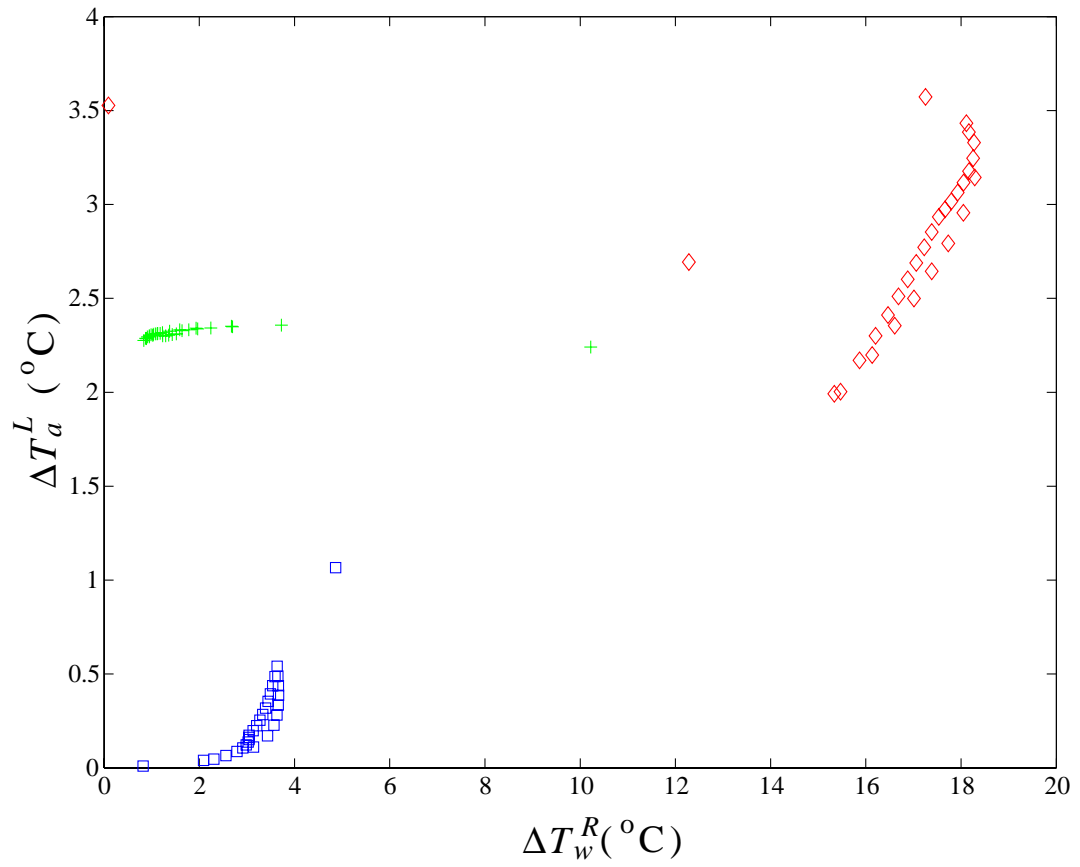


Figure 7.2. ΔT_w^R and ΔT_a^L for different v ; $\diamond = [1, j, k, B]$, $+$ = $[2, j, k, B]$, $\square = [3, j, k, B]$.

and $[3, j, k, B]$, which have different valve locations indicated by a difference in the first index.

Configurations within cluster $[1, j, k, B]$ with the valve in supply pipe 1 are mainly located on the upper right area of Figure 7.2 (there is one exception that will be discussed later). Physically what happens is the following. When the valve closes, water is restricted to the subcircuit and is recirculated through the bypass. The trickling flow picks up heat from the air which raises considerably the return water temperature T_w^R . The air outlet temperature T_a^L experiences only a small change because of the low water flow rate. On the other hand when the valve opens, water is allowed to the entire subcircuit at higher flow rates and there is no recirculation; T_a^L and T_w^R decrease. Therefore there are significant changes in the air outlet temperature and in the water return temperature in response to the opening and closing of the valve. Consider now the cluster $[2, j, k, B]$ with the valve in coil inlet pipe 2. When the valve closes, water is restricted to the cooling coil but not to the subcircuit; hence most of the water bypasses the coil. The trickling flow to the coil produces a small change to the air outlet temperature. When the valve opens a larger water flow runs through the coil reducing the air outlet temperature. There are no drastic variations in the subcircuit return water temperature since chilled water runs through the bypass at any time. For the cluster $[3, j, k, B]$ with the valve in bypass pipe 3, flow rate variations are small in any pipe except the bypass. Therefore changes in the temperature of the air and water are small. We will now take a closer look at each of these clusters.

7.3.1 Control valve on supply pipe

The pump locations are varied. The results correspond to Figure 7.3.

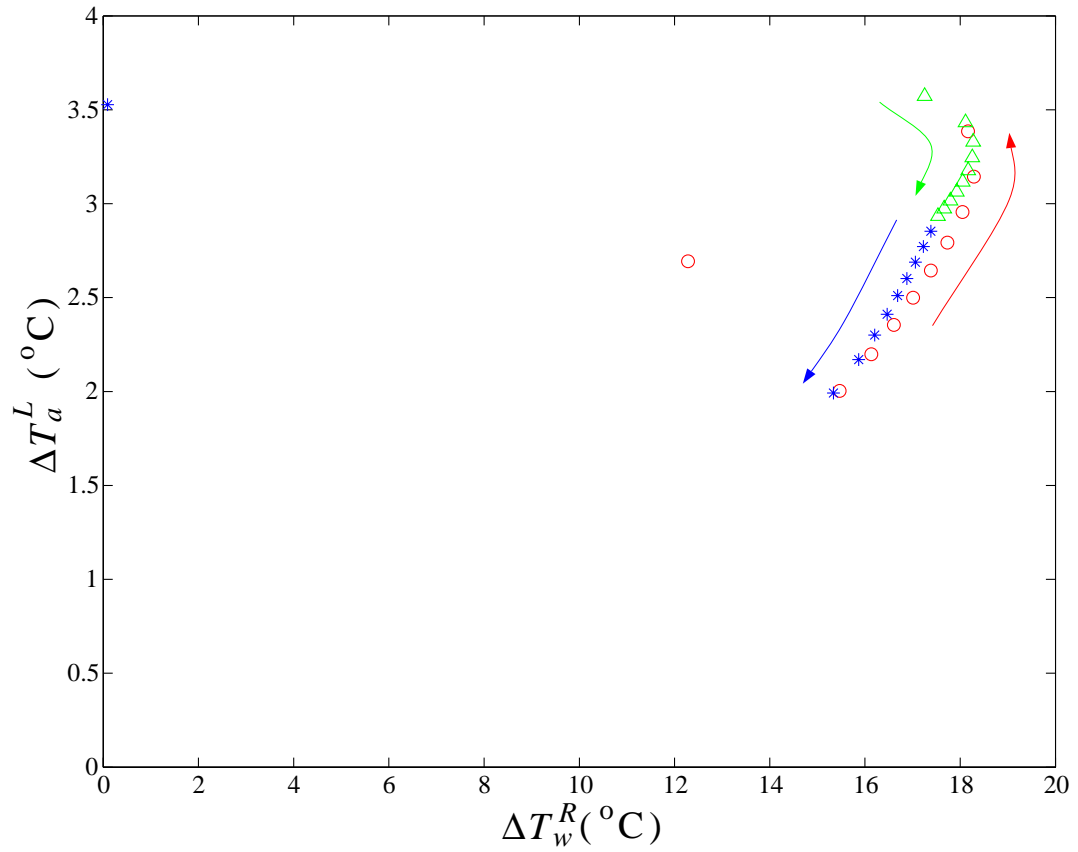
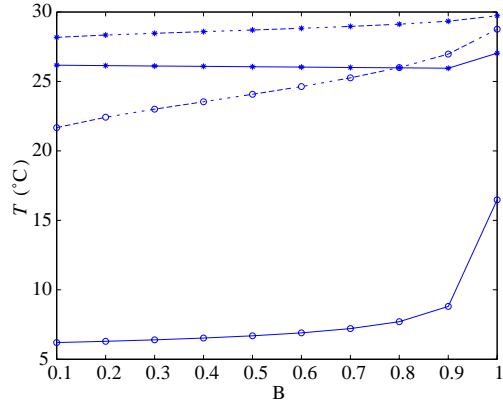


Figure 7.3. ΔT_w^R and ΔT_a^L for different v ; $\circ = [1, 1, 3, B]$, $* = [1, 2, 1, B]$, $\Delta = [1, 3, 2, B]$. Arrows indicate direction of increasing B .

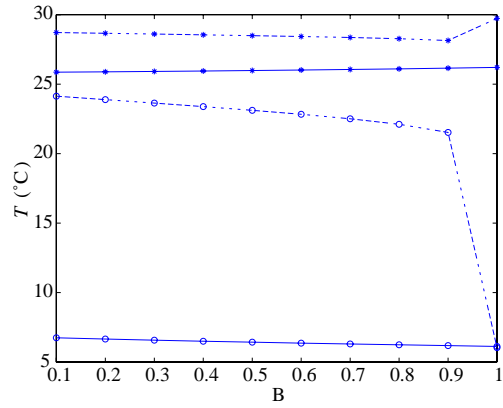
[1, 1, 3, B]: The pumping location is transferred from the supply pipe to the bypass pipe. When the valve is opened the water supply splits to the bypass and coil inlet. As B increases the bypass pumping increases but not enough to change the flow direction; the bypass total pressure drop decreases reducing the bypass flow yielding a higher water flow to the coil. Thus $T_a^L(v_{op})$ decreases and $T_w^R(v_{op})$ increases. When the valve is closed the bypass pumping changes the flow direction. As B increases the blending increases, thus $T_a^L(v_{cl})$ increases and $T_w^R(v_{cl})$ also increases since the trickling flow picks up the heat. The $T_w^R(v_{cl})$ increment slope is steeper than $T_w^R(v_{op})$. Therefore ΔT_a^L and ΔT_w^R increase with the partition parameter as shown in Figure 7.4(a). The exception is $B = 1$ since the pumping at the bypass is large enough to change the flow direction even when the valve is totally open.

[1, 2, 1, B]: The pumping location is transferred from the coil inlet to the supply pipe. When the valve is opened the water splits to the bypass and coil inlet. As the partition parameter increases, the flow at the inlet pipe diminishes but at the supply and bypass increases. Thus $T_a^L(v_{op})$ does not change significantly and $T_w^R(v_{op})$ decreases. When the valve is closed the water is recirculated through the bypass because pumping is on the coil inlet. As B increases the recirculated flow decreases but supply increases, so that $T_a^L(v_{cl})$ and $T_w^R(v_{cl})$ decrease. The $T_w^R(v_{cl})$ decrement slope is steeper than $T_w^R(v_{op})$. Therefore ΔT_a^L and ΔT_w^R decrease as the partition parameter increases as in Figure 7.4(b). If $B = 1$ there is no recirculation when the valve is closed because the pumping is at the supply pipe.

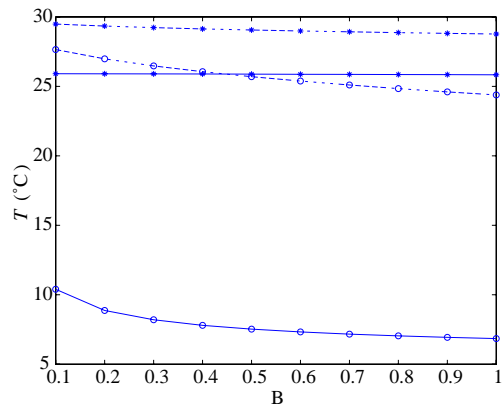
[1, 3, 2, B]: The pumping location is transferred from the bypass to the coil inlet pipe. When the valve is opened the water splits at the bypass and coil inlet. As B increases flow to the subcircuit and at bypass increases while flow to the coil does not change. Thus $T_a^L(v_{op})$ does not vary and $T_w^R(v_{op})$ drops. When the valve is closed, water is recirculated through the bypass, as B increases recirculated flow at



(a)



(b)



(c)

Figure 7.4. Temperatures as a function of B for $[1, j, k, B]$: $*- T_a^L(v_{op})$, $*- - T_a^L(v_{cl})$,
 $\circ- T_w^R(v_{op})$, $\circ- - T_w^R(v_{cl})$.

the bypass decreases, at the supply pipe increases and at the coil inlet remains the same thus $T_a^L(v_{cl})$ and $T_w^R(v_{cl})$ decrease. Therefore ΔT_a^L and ΔT_w^R decrease as the partition parameter increases, as shown in Figure 7.4(c).

7.3.2 Control valve on coil inlet pipe

The results for this subset are shown in Figure 7.5.

[2, 1, 3, B]: The pumping location is transferred from the supply to the bypass pipe. When the valve is either opened or closed the water supply splits to the bypass and coil inlet; there is no change in flow direction. If $v = v_{op}$, as B increases the bypass pumping increases but not enough to change the flow direction; the bypass total pressure drop decreases reducing the bypass flow yielding a higher water flow to the coil. $T_a^L(v_{op})$ decreases and $T_w^R(v_{op})$ increases. If $v = v_{cl}$ the situation is the same but with smaller flows to the coil. Therefore ΔT_a^L maintains practically its value and ΔT_w^R scarcely increases as the partition parameter increases, as Figure 7.6(a) shows. If $B = 1$ the pumping the bypass is large enough to change the flow direction even when the valve is totally open.

[2, 2, 1, B]: The pumping location is transferred from the coil inlet to the supply pipe. When the valve is either open or closed the water supply splits to the bypass and coil inlet. Thus both scenarios are similar. As B increases the pumping at the coil inlet decreases but water to the subcircuit increases. Flows to the coil do not vary in a significant way. ΔT_a^L maintains its value and ΔT_w^R scarcely decreases as the partition parameter increases as shown in Figure 7.6(b).

[2, 3, 2, B]: The pumping location is transferred from the bypass to the coil inlet. When the valve is either open or closed, the water supply splits to the bypass and coil inlet. As B increases the flow at the supply and bypass increases. Thus the flow

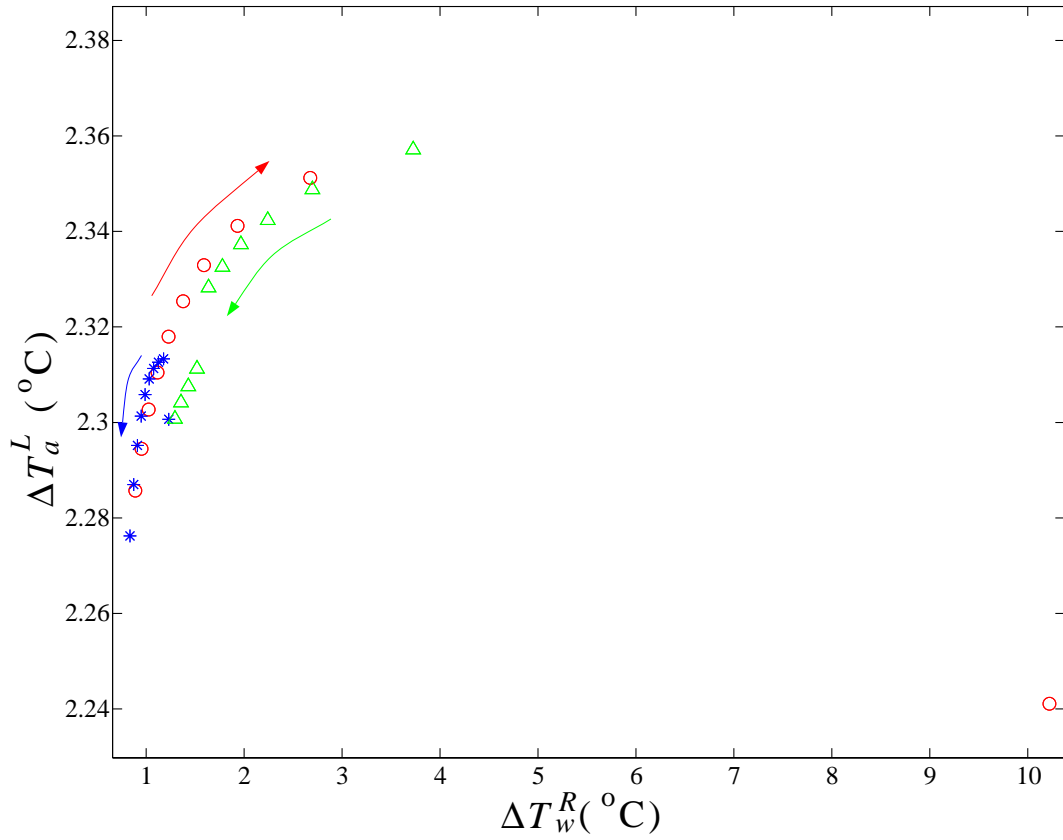
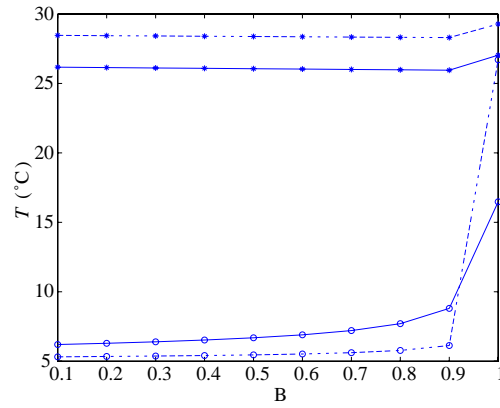
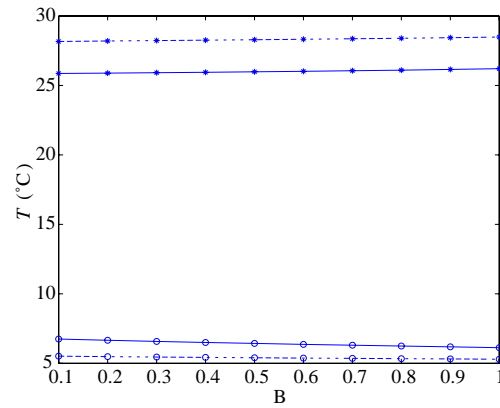


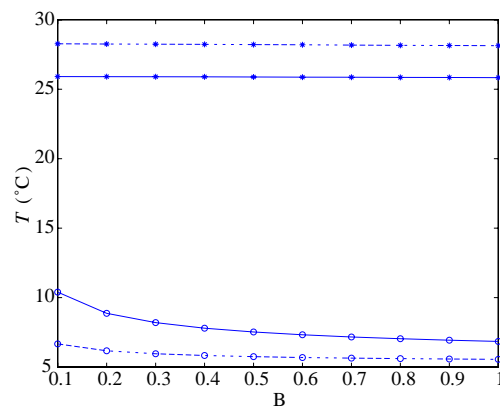
Figure 7.5. ΔT_w^{af} and ΔT_a^L for different v ; $\circ = [2, 1, 3, B]$, $* = [2, 2, 1, B]$, $\triangle = [2, 3, 2, B]$. Arrows indicate direction of increasing B .



(a)



(b)



(c)

Figure 7.6. Temperatures as a function of B for $[2, j, k, B]$: $*- T_a^L(v_{op})$, $*- T_a^L(v_{cl})$,
 $\circ- T_w^R(v_{op})$, $\circ- T_w^R(v_{cl})$.

rates to the coil does not change. ΔT_a^L and ΔT_w^R scarcely decrease as the partition parameter increases. This is shown in Figure 7.6(c).

7.3.3 Control valve on bypass pipe

The results are shown in Figure 7.7.

[3, 1, 3, B]: The pumping location is transferred from the supply to the bypass pipe. When $v = v_{cl}$ the chilled water splits to the coil and bypass. As B increases, the water flows to the subcircuit, coil and bypass decrease. Thus T_a^L and T_w^R increase. Therefore ΔT_a^L and ΔT_w^R decrease as the partition parameter increases, as in Figure 7.8(a). To place the valve on the bypass results in larger flow rates to the coil when the valve is closed than when is open. For the other two valve locations the converse is true. At $B = 1$ there is a change in the flow direction at the bypass.

[3, 2, 1, B]: The pumping location is transferred from the coil inlet to the supply pipe. When $v = v_{cl}$ the chilled water splits to the coil and bypass. As B increases, the flows to the subcircuit and inlet pipes keep the same value. T_a^L and T_w^R remain constant. Therefore ΔT_a^L and ΔT_w^R increase as the partition parameter does which is indicated in Figure 7.8(b).

[3, 3, 2, B]: The pumping location is transferred from the bypass pipe to the coil inlet. When $v = v_{cl}$ the chilled water splits to the coil and bypass. As B increases, the flow to the subcircuit and inlet pipe increases. T_a^L does not change and T_w^R scarcely decrease. Therefore ΔT_a^L and ΔT_w^R increase as the partition parameter decreases, as in Figure 7.8(c).

7.4 Optimal configuration

From the results shown, an optimal configuration within the discrete space defined by the specified piping layout and hardware elements can be inferred for the open loop steady state control case. In accordance with the comparison criteria

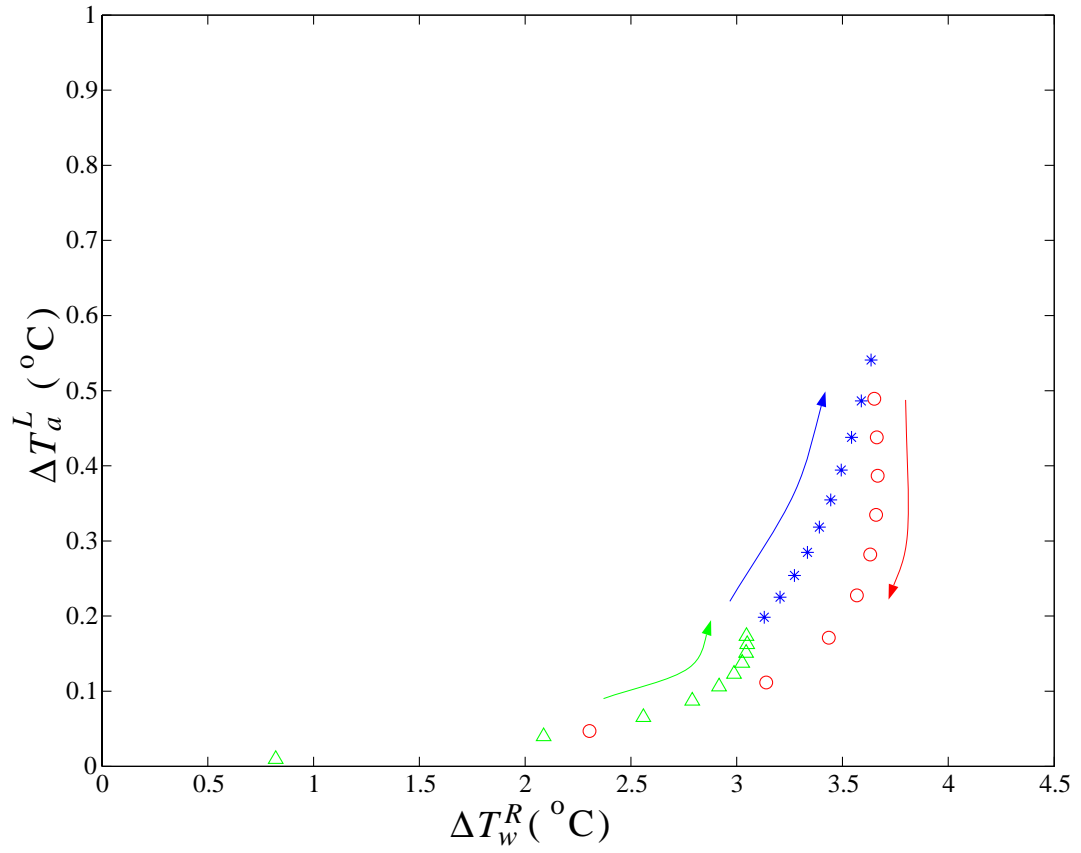
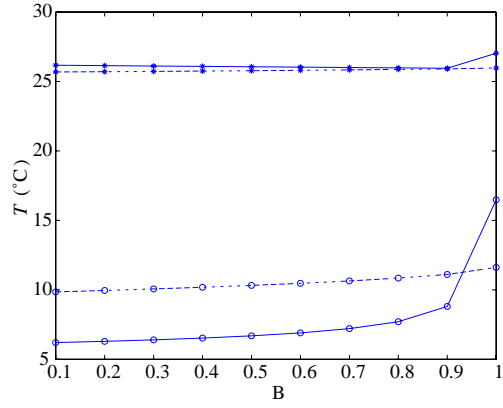
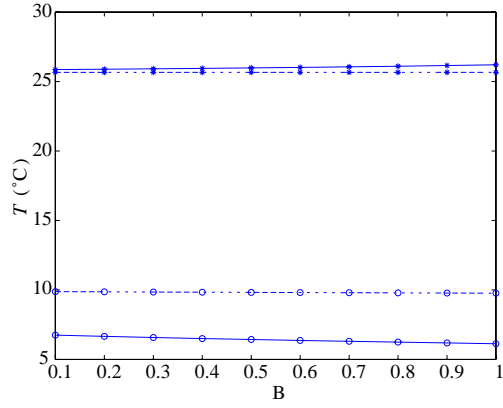


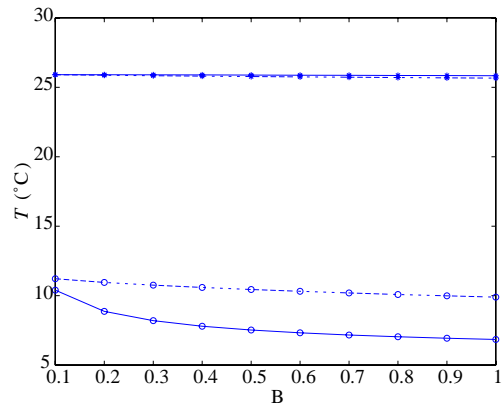
Figure 7.7. ΔT_w^{af} and ΔT_a^L for different v ; $\circ = [3, 1, 3, B]$, $* = [3, 2, 1, B]$, $\triangle = [3, 3, 2, B]$. Arrows indicate direction of increasing B .



(a)



(b)



(c)

Figure 7.8. Temperatures as a function of B for $[3, j, k, B]$: $*- T_a^L(v_{op})$, $*- - T_a^L(v_{cl})$,
 $\circ- T_w^R(v_{op})$, $\circ- - T_w^R(v_{cl})$.

chosen the best configuration is one with a wide reachability range and operation close to the design conditions; that is a high $\Delta T_a^L(v)$ and a low $\Delta T_w^R(v)$. This corresponds to configuration $[1, 2, 1, 1]$ which is the diamond operating point located on the upper left corner of Figure 7.2 corresponding to control valve and booster pump located on the supply pipe 1. Since the partition parameter B is equal to one there is just one pump. This solution has the characteristics of the cluster $[1, j, k, B]$ explained above: when the valve is closed small chilled water flows circulate the subcircuit, when it is opened higher chilled-water flows are allowed into the subcircuit, so that ΔT_a^L is high. However, the difference between this configuration and the rest of the points in the same cluster is the location of the booster pumps: for this configuration all the pumping is on the subcircuit supply pipe while in the rest some pumping is done either on the coil inlet or the supply pipe. The latter means that there is recirculation when v_{cl} while in this case the trickling flow is bypassed when $v = v_{cl}$. Consequently all the configurations in $[1, 2, 1, 1]$ have a low change in ΔT_w^R .

7.5 Discussion

Most *HVAC* optimization studies consider either the piping network or the control system at the terminal users. Furthermore, the control studies usually are about the algorithm or controller. However, even for an optimized network with optimal controllers at the terminal users the overall system performance can be seriously affected by the location of the control hardware. In this chapter the problem of optimal placement of control hardware in a terminal user subcircuit with a specific piping layout is addressed. To assess the relative advantages between different placement configurations the range of output of the control system and its effect on the hydronic network are computed.

The location of the hardware components in a piping subcircuit has an impact on the operation of the system since parameters like the water temperature difference at the subcircuit are drastically affected. In like manner the hardware location affects the thermal control at the subcircuit, the system reachability may be narrowed or broadened. As a consequence there is an optimal location of components for a specific hydronic network design and thermal control task. In fact the results showed that there are several configurations which have very similar performances, so that a new parameter, like cost, can be used to make a further selection between them.

CHAPTER 8

HYDRODYNAMICS OF REGULAR TREE NETWORKS

Studies of small, irregular and closed fluid networks have been presented in Chapters 5, 6 and 7. In this Chapter the study of fluid networks is extended to large systems. As a consequence the level of complexity of the problem increases. It is necessary to make assumptions in the geometry of the network in order to have a starting point for a feasible analysis. The problem considered in this Chapter is that of flow dynamics in large, regular and self-similar networks configured in the form of a branching tree. Each branch of the tree bifurcates with a constant diameter and length ratio. The global stability of the flow is demonstrated for friction laws satisfying certain condition. When the condition does not hold it is shown that there is a transition regime where the flow is not stable. In a sufficiently large tree network with an entering turbulent flow downstream branches may be trapped in the transition regime provoking the network flow to oscillate. In addition the control properties of the flow network are investigated using valves and pumps as the manipulated variables to control branch flow rates and nodal pressures. Because of the nature of the problem the mathematical model results in a system of DAE which is reduced to a dynamical system in order to show that the network hydrodynamics are only partially controllable if individual pumps are used to control the pressure at the junctions. In this Chapter, variables with star are dimensional and without it nondimensional; these are volumetric flow q , pressure terms p and \mathcal{P} , resistance

F and time t . Physical properties, ν and ρ , and geometric parameters, d and l , are dimensional. Some of the material presented in this Chapter has been published in proceedings (Sen *et al.*, 2002).

8.1 Topology

The tree to be studied is schematically shown in Figure 8.1. Each branch in a given generation bifurcates into two in the following generation. There are a total of N_g generations, where N_g is assumed to be large. If i indicates the generation number of a branch and j the branch number within that generation, then each branch can be represented uniquely as a pair of integers (i, j) where $1 \leq i \leq N_g$ and $1 \leq j \leq r_i = 2^{i-1}$. r_i is the number of branches in generation i . Thus the branch (i, j) bifurcates into branches $(i + 1, 2j - 1)$ and $(i + 1, 2j)$. An alternative notation where each branch is referred to a node k , where $k = r_i + j - 1$, will sometimes be used for purposes of compactness in analytical and computational representations. The junctions are similarly identified either by the indices (i, j) or the index k corresponding to the branch that leads *towards* it. There are a total of $N_b = 2^{N_g} - 1$ branches with $N_n = 2^{N_g-1} - 1$ junctions in the tree.

The inlet to the tree is a pipe branch of diameter d , length l , and volumetric flow rate q . Each branch (i, j) is a circular pipe of diameter $d_{i,j}$ and length $l_{i,j}$ that carries a volume flow rate $q_{i,j}^*$. It bifurcates into two branches, each with diameter of $d_{i,j}/\beta$ and length of $l_{i,j}/\beta$. The diameter and length scaling is taken to be the same, and though in principle there is no geometrical restriction on β it is assumed here to be a constant for the entire tree and greater than unity in value. Thus $d_{i,j} = d/\beta^{i-1}$ and $l_{i,j} = l/\beta^{i-1}$ where $d = d_{1,1}$ and $l = l_{1,1}$. The pressure difference in branch (i, j) between its inlet and outlet is $\Delta p_{i,j}^*$.

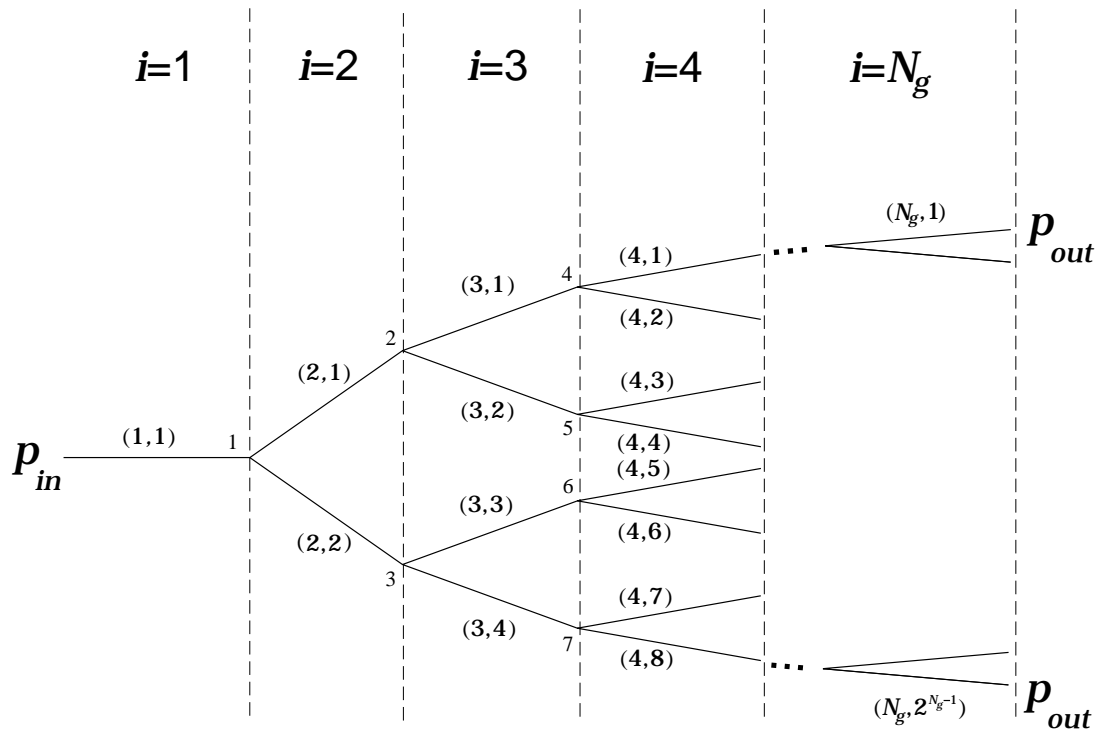


Figure 8.1. Schematic of tree with branches.

8.2 Mathematical model

A one-dimensional flow model is used to study the hydrodynamics of the network. The model is similar to the one developed in Section 2.1. It is assumed that the flow is fully developed, and inlet and exit effects are neglected. For a branch (i, j) the momentum equation is

$$\frac{dq_{i,j}^*}{dt^*} + F_{i,j}^*(q_{i,j}^*) - \frac{\pi d_{i,j}^2}{4\rho l_{i,j}} \Delta p_{i,j}^* = 0, \quad (8.1)$$

where t^* is time, and ρ is fluid density. The three terms are the fluid acceleration, viscous resistance, and pressure force, respectively. The resistance term is different for laminar and turbulent flow and is given by

$$F_{i,j}^*(q_{i,j}^*) = \begin{cases} 32\nu q_{i,j}^*/d_{i,j}^2 & \text{for } Re_{i,j} < Re_c \text{ (laminar flow),} \\ 0.1894 \nu^{1/4} q_{i,j}^{*7/4}/d_{i,j}^{11/4} & \text{for } Re_{i,j} \geq Re_c \text{ (turbulent flow).} \end{cases} \quad (8.2)$$

The Reynolds number of the flow in branch (i, j) is $Re_{i,j} = 4q_{i,j}^*/\pi d_{i,j}\nu$, and Re_c is the critical Reynolds number for transition. The turbulent friction factor is modeled using the Blasius formula for flow in a smooth pipe.

The fluid is assumed to be incompressible, so that continuity at the junction (i, j) can be expressed as

$$q_{i,j}^* - q_{i+1,2j}^* - q_{i+1,2j-1}^* = 0. \quad (8.3)$$

The equations are nondimensionalized using

$$q_{i,j} = \frac{q_{i,j}^*}{\nu d}, \quad p_{i,j} = \frac{\pi d^3}{128\nu^2 \rho l} p^*, \quad t = \frac{32\nu}{d^2} t^*. \quad (8.4)$$

This gives

$$\frac{dq_{i,j}}{dt} + F_{i,j}(q_{i,j}) - \frac{1}{\beta^{i-1}} \Delta p_{i,j} = 0, \quad (8.5)$$

$$q_{i,j} - q_{i+1,2j} - q_{i+1,2j-1} = 0, \quad (8.6)$$

where

$$F_{i,j}(q_{i,j}) = \begin{cases} \beta^{2(i-1)} q_{i,j} & \text{for } Re_{i,j} < Re_c, \\ C \beta^{11/4(i-1)} q_{i,j}^{7/4} & \text{for } Re_{i,j} \geq Re_c, \end{cases} \quad (8.7)$$

with $C = 0.005926$.

8.3 Steady-state analysis

Since all branches of a generation are identical, there is at least one solution to the steady-state problem with no variation with j for a given i . The flow rate in each branch is then $q_{i,j} = q/r_i$, where $q = q_{1,1}$ is the nondimensional flow rate in the first branch. The Reynolds number $Re_{i,j} = (4q/\pi) (\beta/2)^{i-1}$ decreases if $\beta < 2$.

From equation (8.5) the steady-state pressure drop in generation i is

$$\Delta p_i = F\left(\frac{q}{r_i}\right) \beta^{i-1}. \quad (8.8)$$

Proceeding as Cohn (1954): if the inlet and outlet to the network are pressures p_{in} and p_{out} respectively, the pressure drop in each generation can be summed over all the generations from $i = 1$ to N_g to give the total pressure drop $p_{in} - p_{out}$.

8.3.1 Large networks

The local Reynolds number increases (if $\beta > 2$) or decreases ($\beta < 2$) monotonically from the first to the last generation from a value of $4q/\pi$ to $(4q/\pi)(\beta/2)^{N_g-1}$. The flow in the first and last branches is laminar or turbulent depending on whether the local Reynolds number is less than or greater than Re_c , respectively. Thus there are four possible cases.

(a) *First laminar-last laminar*: The flow is laminar in the entire network. The total pressure drop is

$$p_{in} - p_{out} = q \frac{1 - (\beta^3/2)^{N_g}}{1 - \beta^3/2}. \quad (8.9)$$

(b) *First turbulent-last turbulent*: The flow is turbulent everywhere and

$$p_{in} - p_{out} = q^{7/4} C \frac{1 - (\beta^{15/4}/2^{7/4})^{N_g}}{1 - \beta^{15/4}/2^{7/4}}. \quad (8.10)$$

(c) *First laminar-last turbulent*: The entrance is laminar, but there is transition to turbulent flow in some intermediate generation N_l . We have

$$p_{in} - p_{out} = q \frac{1 - (\beta^3/2)^{N_l}}{1 - (\beta^3/2)} + q^{7/4} C \frac{(\beta^{15/4}/2^{7/4})^{N_l} - (\beta^{15/4}/2^{7/4})^{N_g}}{1 - (\beta^{15/4}/2^{7/4})}. \quad (8.11)$$

(d) *First turbulent-last laminar*: The entrance is turbulent, but there is transition to laminar flow in some intermediate generation N_t . We have

$$p_{in} - p_{out} = q^{7/4} C \frac{1 - (\beta^{15/4}/2^{7/4})^{N_t}}{1 - (\beta^{15/4}/2^{7/4})} + q \frac{(\beta^3/2)^{N_t} - (\beta^3/2)^{N_g}}{1 - (\beta^3/2)}. \quad (8.12)$$

The last generation before the flow changes to a different regime is

$$N_t = \lceil 1 + \frac{\ln(\pi Re_{\pm\epsilon}/4q)}{\ln(\beta/2)} \rceil, \quad (8.13)$$

where $Re_{\pm\epsilon} = Re_c(1 \pm \epsilon)$. ϵ represents the difference between accelerated and decelerated flows: the upper and lower bounds are the critical threshold during the accelerating and decelerating phase, respectively.

8.3.2 Infinite networks

For $\beta < 2^{1/3}$ it is possible to have an infinite first laminar-last laminar tree since the required pressure drop $p_{in} - p_{out}$ is finite. An infinite first turbulent-last laminar tree exists if $\beta < 2^{1/3}$; i.e., $2^{1/3} < 2^{7/15}$ ($1.26 < 1.38$).

The total length, lateral area and duct volume of a N_g generations tree are respectively

$$l_{N_g} = \frac{1 - (2/\beta)^{N_g}}{1 - 2/\beta}, \quad (8.14)$$

$$A_{N_g} = \frac{1 - (2/\beta^2)^{N_g}}{1 - 2/\beta^2}, \quad (8.15)$$

$$S_{N_g} = \frac{1 - (2/\beta^3)^{N_g}}{1 - 2/\beta^3}, \quad (8.16)$$

where each variable has been scaled by its first branch value. Figure 8.2 shows l_{N_g} as a function of the scaling parameter for networks of different size. The critical value $\beta_c = 2$ is indicated by the vertical dashed line. If $\beta > 2$ the total length is finite for an infinite number of generations. Figure 8.3 illustrates A_{N_g} as a function of β . The critical value for the lateral area $\beta_c = 2^{1/2} (\simeq 1.414)$ is indicated by the dashed line. The total lateral area is finite in the infinite case if $\beta > 2^{1/2}$. The total volume S of the conduits material is calculated by using the same scaling factor β for the thickness of the duct. S as a function of the scale parameter is illustrated by Figure 8.4. The volume critical parameter is $\beta_c = 2^{1/3} (\simeq 1.26)$. In an infinite network, the volume of conduit material is finite when $\beta > 2^{1/3}$. As shown in Figures 8.2, 8.3 and 8.4, the selection of the scaling ratio and the number of generations are design parameters to consider for the construction of this type of networks. Let $R = (p_{in} - p_{out})/q$, this expression relates the pressure drop along the network to the volumetric flow q . Figure 8.5 shows R , when $\beta < 2^{1/3}$ the value of R is finite in an infinite tree. There is a tradeoff between R and the material needed. An infinite R implies that flow cannot circulate. An infinite S implies that the tree cannot be built. Curves S/R for different β and N_g are plotted in Figure 8.6.

8.4 Global stability of steady flow

It is shown in this section that for certain friction laws the steady flow in a network of two, three and N_g generations is stable to all perturbations, large or small. The alternative nodal index notation k is used in the analysis to represent the junctions. The flow resistance F is assumed to be a non-decreasing (single-valued) function of the volumetric flow rate. The flow is driven by the pressure difference between the network inlet and outlets.

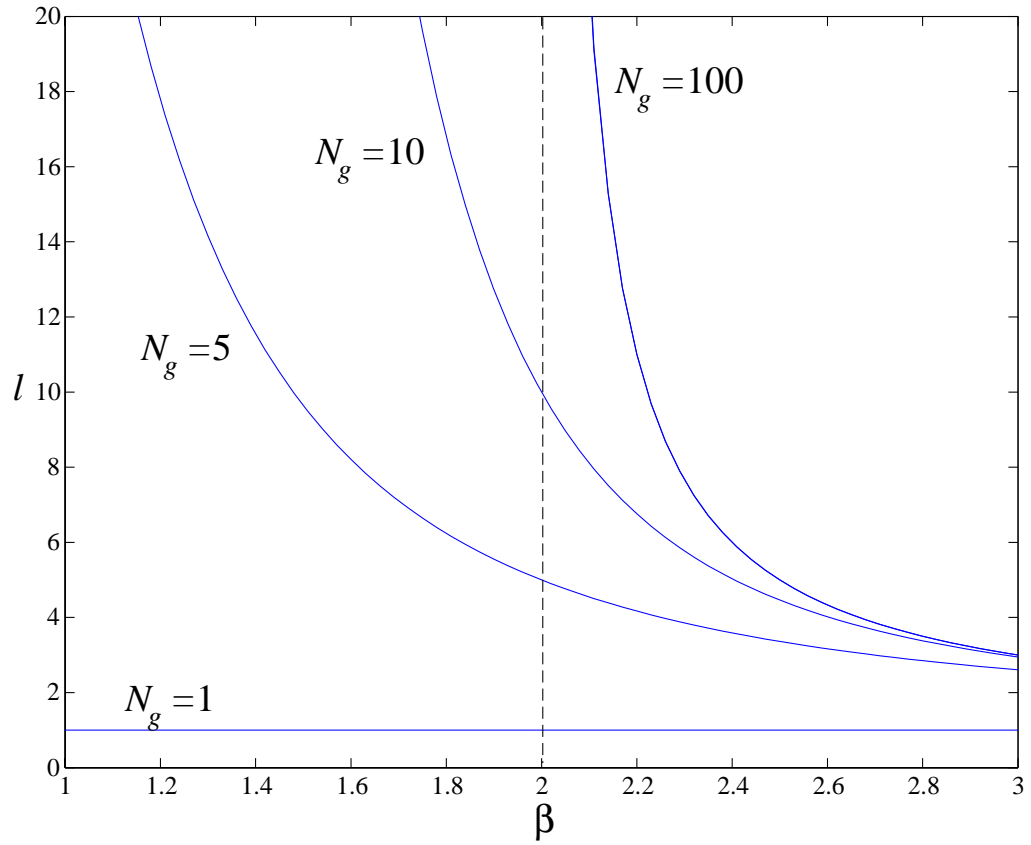


Figure 8.2. Length as function of scaling parameter.

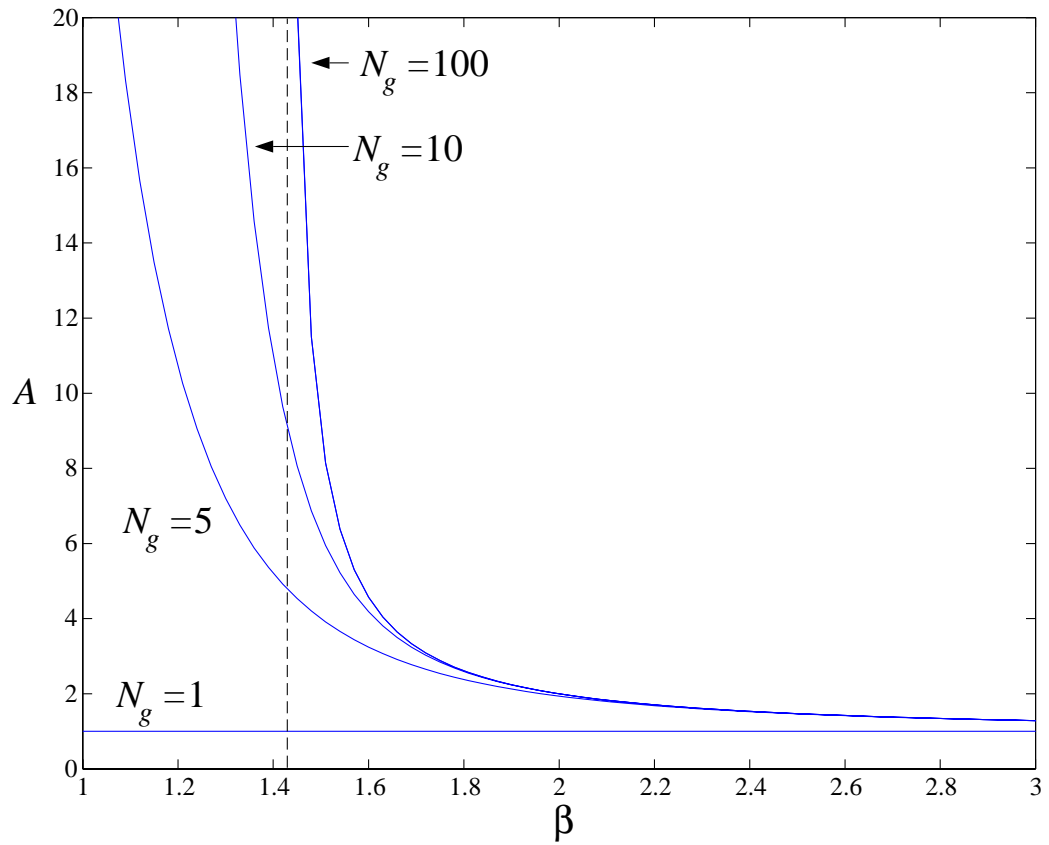


Figure 8.3. Lateral area as function of scaling parameter.

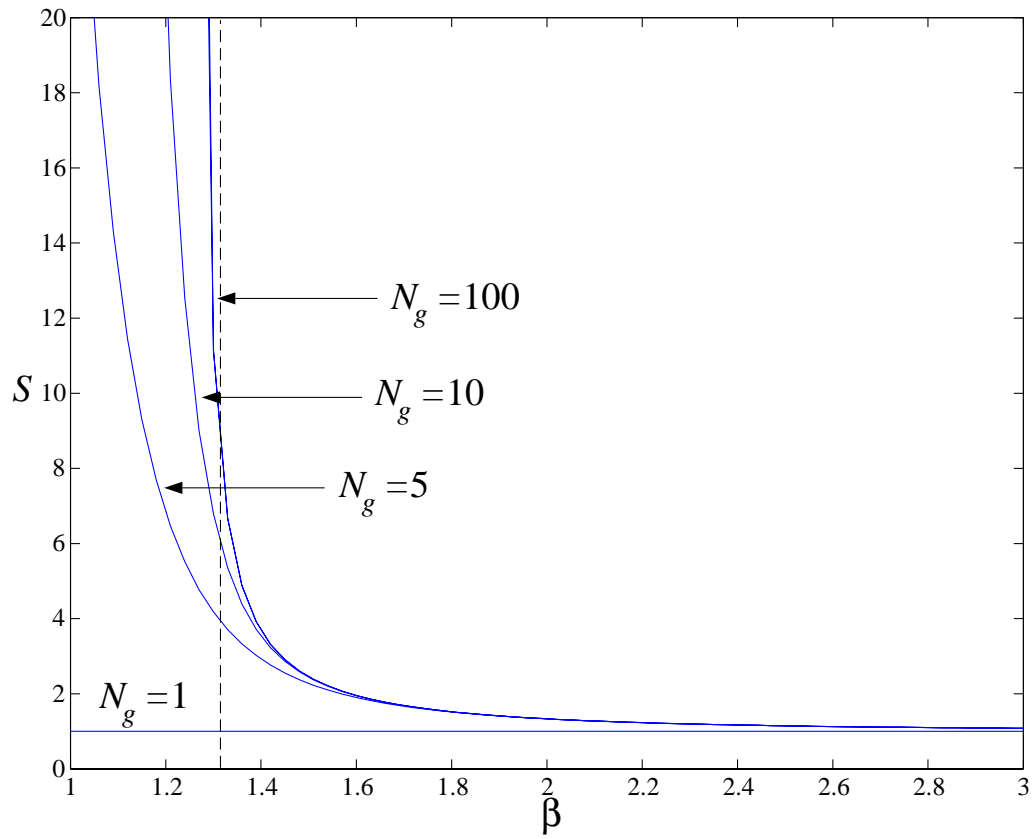


Figure 8.4. Tube volume as function of scaling parameter.

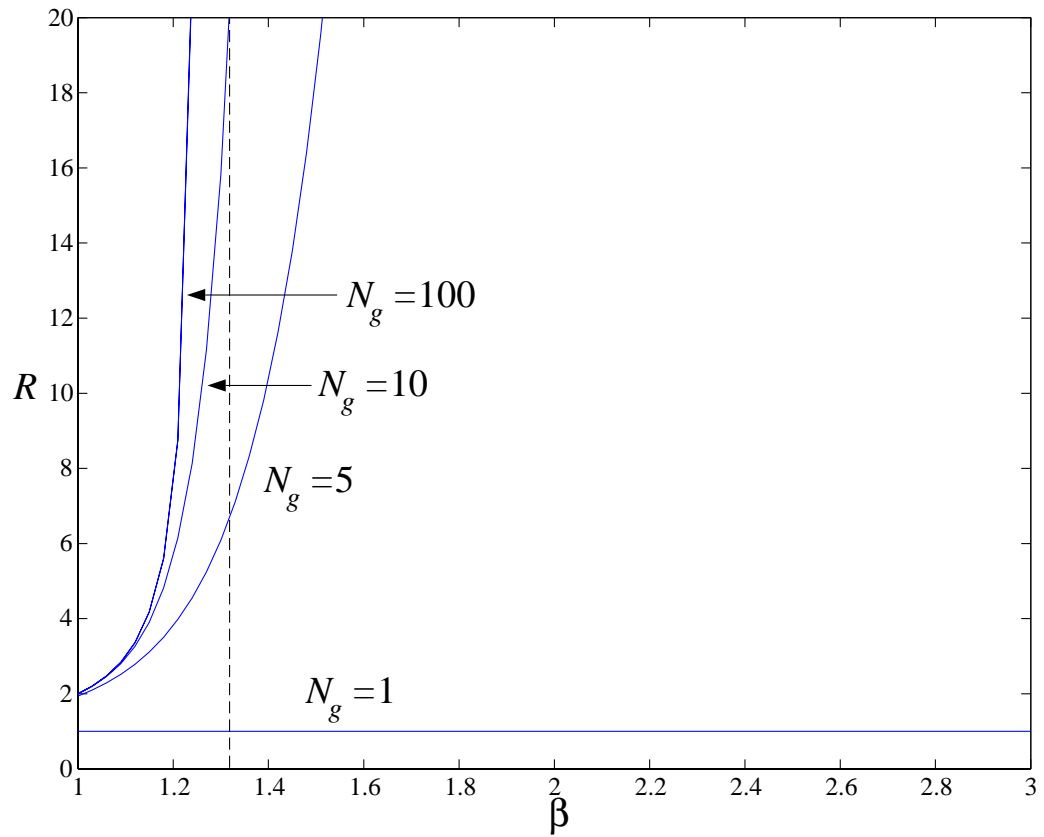


Figure 8.5. R as function of scaling parameter.

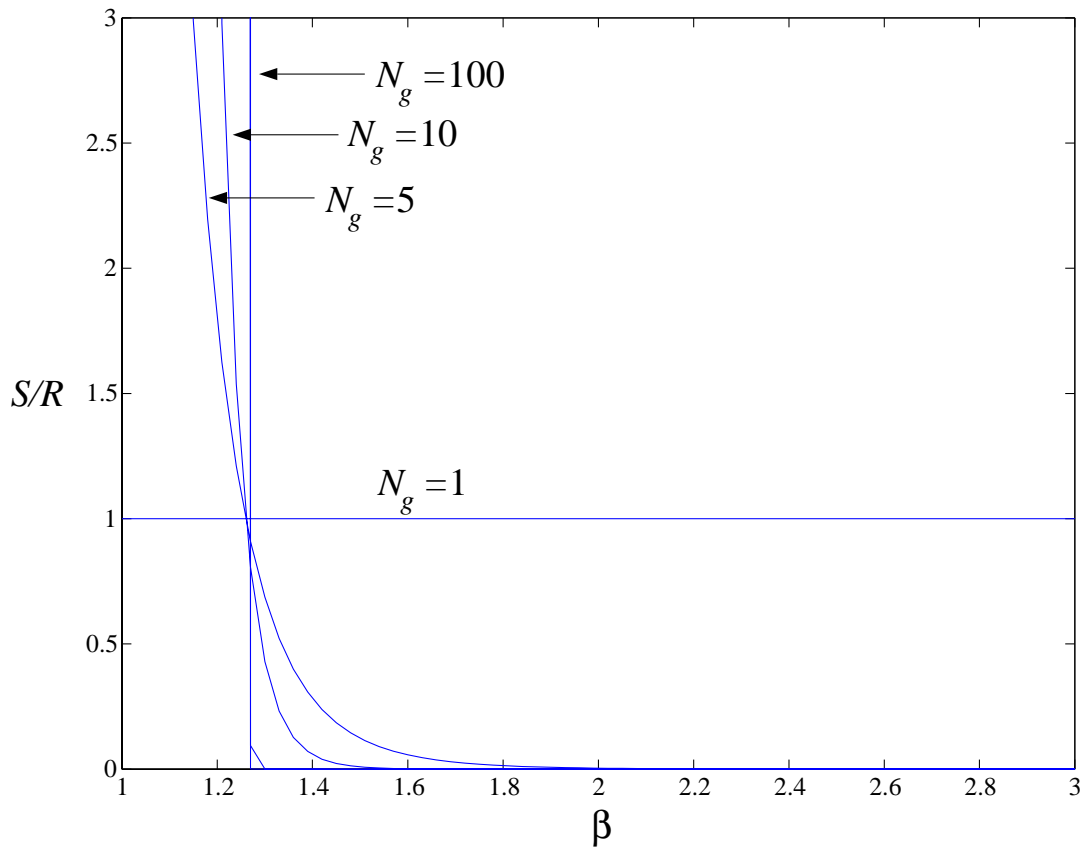


Figure 8.6. Ratio S/R as function of scaling parameter.

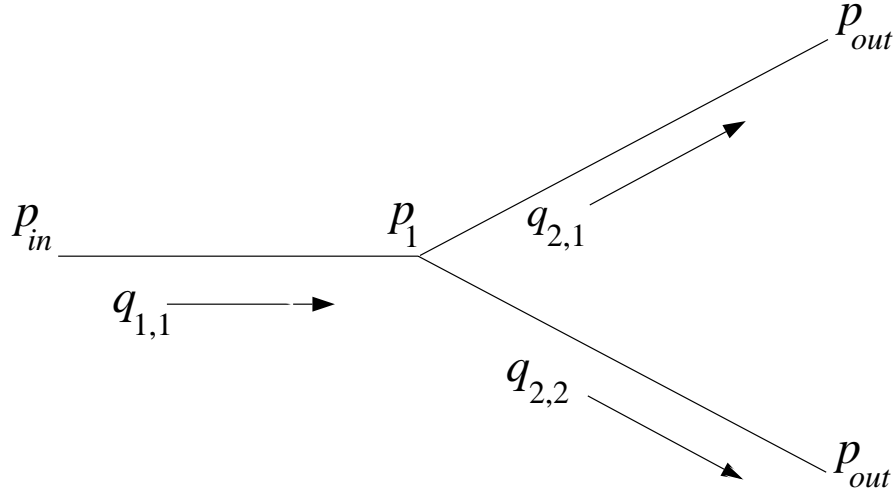


Figure 8.7. Network with two generations.

8.4.1 Network of two generations

Figure 8.7 illustrates a tree with two generations where an inlet flow splits in two outlet flows at junction 1. The inlet and outlet pressures are constant, and $p_{in} > p_{out}$. The arrows indicate the flow direction. Thus continuity at the junction is expressed as

$$q_{1,1} - q_{2,1} - q_{2,2} = 0. \quad (8.17)$$

The momentum equation of flow in each branch is given by

$$\frac{dq_{1,1}}{dt} + F(q_{1,1}) - (p_{in} - p_1) = 0, \quad (8.18)$$

$$\frac{dq_{2,1}}{dt} + F(q_{2,1}) - \frac{1}{\beta}(p_1 - p_{out}) = 0, \quad (8.19)$$

$$\frac{dq_{2,2}}{dt} + F(q_{2,2}) - \frac{1}{\beta}(p_1 - p_{out}) = 0. \quad (8.20)$$

Perturbing the flow rates and the pressure junction

$$q_{1,1} = \bar{q}_{1,1} + q'_{1,1}, \quad (8.21)$$

$$q_{2,1} = \bar{q}_{2,1} + q'_{2,1}, \quad (8.22)$$

$$q_{2,2} = \bar{q}_{2,2} + q'_{2,2}, \quad (8.23)$$

$$p_1 = \bar{p}_1 + p'_1, \quad (8.24)$$

where the bar denotes an equilibrium point and the prime a small perturbation. Substituting the perturbed variables in Equations (8.17), (8.18), (8.19) and (8.20), and subtracting the steady state the Equations become

$$q'_{1,1} - q'_{2,1} - q'_{2,2} = 0, \quad (8.25)$$

$$\frac{dq'_{1,1}}{dt} + F(\bar{q}_{1,1} + q'_{1,1}) - F(\bar{q}_{1,1}) + p'_1 = 0, \quad (8.26)$$

$$\frac{dq'_{2,1}}{dt} + F(\bar{q}_{2,1} + q'_{2,1}) - F(\bar{q}_{2,1}) - \frac{1}{\beta} p'_1 = 0, \quad (8.27)$$

$$\frac{dq'_{2,2}}{dt} + F(\bar{q}_{2,2} + q'_{2,2}) - F(\bar{q}_{2,2}) - \frac{1}{\beta} p'_1 = 0. \quad (8.28)$$

Consider the following function

$$V = \frac{1}{2} \left(q'^2_{1,1} + \beta q'^2_{2,1} + \beta q'^2_{2,2} \right). \quad (8.29)$$

Differentiating V respect to time and using Equations (8.26)–(8.28)

$$\begin{aligned} \frac{dV}{dt} &= q'_{1,1} \frac{dq'_{1,1}}{dt} + \beta q'_{2,1} \frac{dq'_{2,1}}{dt} + \beta q'_{2,2} \frac{dq'_{2,2}}{dt} \\ &= -q'_{1,1} \left(F(\bar{q}_{1,1} + q'_{1,1}) - F(\bar{q}_{1,1}) \right) \\ &\quad - \beta q'_{2,1} \left(F(\bar{q}_{2,1} + q'_{2,1}) - F(\bar{q}_{2,1}) \right) \\ &\quad - \beta q'_{2,2} \left(F(\bar{q}_{2,2} + q'_{2,2}) - F(\bar{q}_{2,2}) \right) \\ &\quad - p'_1 (q'_{1,1} - q'_{2,1} - q'_{2,2}). \end{aligned} \quad (8.31)$$

The last term vanishes because of flow conservation at the junction. Since $V \geq 0$ and $dV/dt \leq 0$, V is a Lyapunov function and the hydrodynamic steady state of a two generation network is globally stable and consequently also unique.

8.4.2 Network of three generations

Tree networks with three or more generations have three different types of generations: inlet, intermediate and outlet. The inlet and outlet have branches connected

to the exterior while the intermediate does not. A network of three generations has three junctions and seven branches. Continuity at the junction is expressed as

$$q_{1,1} - q_{2,1} - q_{2,2} = 0, \quad (8.32)$$

$$q_{2,1} - q_{3,1} - q_{3,2} = 0, \quad (8.33)$$

$$q_{2,1} - q_{3,3} - q_{3,4} = 0. \quad (8.34)$$

The momentum equation of each branch is given by

$$\frac{dq_{1,1}}{dt} + F(q_{1,1}) - (p_{in} - p_1) = 0, \quad (8.35)$$

$$\frac{dq_{2,1}}{dt} + F(q_{2,1}) - \frac{1}{\beta}(p_1 - p_2) = 0, \quad (8.36)$$

$$\frac{dq_{2,2}}{dt} + F(q_{2,2}) - \frac{1}{\beta}(p_1 - p_3) = 0, \quad (8.37)$$

$$\frac{dq_{3,1}}{dt} + F(q_{3,1}) - \frac{1}{\beta^2}(p_2 - p_{out}) = 0, \quad (8.38)$$

$$\frac{dq_{3,2}}{dt} + F(q_{3,2}) - \frac{1}{\beta^2}(p_2 - p_{out}) = 0, \quad (8.39)$$

$$\frac{dq_{3,3}}{dt} + F(q_{3,3}) - \frac{1}{\beta^2}(p_3 - p_{out}) = 0, \quad (8.40)$$

$$\frac{dq_{3,4}}{dt} + F(q_{3,4}) - \frac{1}{\beta^2}(p_3 - p_{out}) = 0. \quad (8.41)$$

Perturbing flows and pressures, substituting the perturbed variables in Equations (8.32)–(8.41), and subtracting the steady state the Equations become

$$q'_{1,1} - q'_{2,1} - q'_{2,2} = 0, \quad (8.42)$$

$$q'_{2,1} - q'_{3,1} - q'_{3,2} = 0, \quad (8.43)$$

$$q'_{2,2} - q'_{3,3} - q'_{3,4} = 0, \quad (8.44)$$

$$\frac{dq'_{1,1}}{dt} + F(\bar{q}_{1,1} + q'_{1,1}) - F(\bar{q}_{1,1}) + p'_1 = 0, \quad (8.45)$$

$$\frac{dq'_{2,1}}{dt} + F(\bar{q}_{2,1} + q'_{2,1}) - F(\bar{q}_{2,1}) - \frac{1}{\beta}(p'_1 - p'_2) = 0, \quad (8.46)$$

$$\frac{dq'_{2,2}}{dt} + F(\bar{q}_{2,2} + q'_{2,2}) - F(\bar{q}_{2,2}) - \frac{1}{\beta}(p'_1 - p'_3) = 0, \quad (8.47)$$

$$\frac{dq'_{3,1}}{dt} + F(\bar{q}_{3,1} + q'_{3,1}) - F(\bar{q}_{3,1}) - \frac{1}{\beta^2} p'_2 = 0, \quad (8.48)$$

$$\frac{dq'_{3,2}}{dt} + F(\bar{q}_{3,2} + q'_{3,2}) - F(\bar{q}_{3,2}) - \frac{1}{\beta^2} p'_2 = 0, \quad (8.49)$$

$$\frac{dq'_{3,3}}{dt} + F(\bar{q}_{3,3} + q'_{3,3}) - F(\bar{q}_{3,3}) - \frac{1}{\beta^2} p'_3 = 0, \quad (8.50)$$

$$\frac{dq'_{3,4}}{dt} + F(\bar{q}_{3,4} + q'_{3,4}) - F(\bar{q}_{3,4}) - \frac{1}{\beta^2} p'_3 = 0, \quad (8.51)$$

Consider the following function

$$V = \frac{1}{2} \left(q'^2_{1,1} + \beta q'^2_{2,1} + \beta q'^2_{2,2} + \beta^2 q'^2_{3,1} + \beta^2 q'^2_{3,2} + \beta^2 q'^2_{3,3} + \beta^2 q'^2_{3,4} \right). \quad (8.52)$$

Differentiating V respect to time and substituting Equations (8.45)–(8.51)

$$\begin{aligned} \frac{dV}{dt} &= q'_{1,1} \frac{dq'_{1,1}}{dt} + \beta q'_{2,1} \frac{dq'_{2,1}}{dt} + \dots + \beta^2 q'_{3,4} \frac{dq'_{3,4}}{dt} \\ &= -q'_{1,1} (F(\bar{q}_{1,1} + q'_{1,1}) - F(\bar{q}_{1,1})) \\ &\quad - \beta q'_{2,1} (F(\bar{q}_{2,1} + q'_{2,1}) - F(\bar{q}_{2,1})) \\ &\quad - \beta q'_{2,2} (F(\bar{q}_{2,2} + q'_{2,2}) - F(\bar{q}_{2,2})) \\ &\quad - \beta^2 q'_{3,1} (F(\bar{q}_{3,1} + q'_{3,1}) - F(\bar{q}_{3,1})) \\ &\quad - \beta^2 q'_{3,2} (F(\bar{q}_{3,2} + q'_{3,2}) - F(\bar{q}_{3,2})) \\ &\quad - \beta^2 q'_{3,3} (F(\bar{q}_{3,3} + q'_{3,3}) - F(\bar{q}_{3,3})) \\ &\quad - \beta^2 q'_{3,4} (F(\bar{q}_{3,4} + q'_{3,4}) - F(\bar{q}_{3,4})) \\ &\quad - p'_1 (q'_{1,1} - q'_{2,1} - q'_{2,2}) - p'_2 (q'_{2,1} - q'_{3,1} - q'_{3,2}) \\ &\quad - p'_3 (q'_{2,2} - q'_{3,3} - q'_{3,4}). \end{aligned} \quad (8.54)$$

The last three terms are zero because of continuity at the junctions. The remaining terms are negative for any flow value. The steady state hydrodynamics in a network of tree generations are globally stable since the Lyapunov function $V \geq 0$ and $dV/dt \leq 0$.

8.4.3 Network of N_g generations

Equation (8.6) for $i = 1, \dots, N_g$ and $j = 1, \dots, M_i$ represents the continuity equations in a network of N_g generations. At every node one volumetric flow splits in two. The momentum equation of the inlet branch is given by (8.18). where p_{in} is the pressure at the network inlet. The momentum equations of branches at intermediate generations are

$$\frac{dq_{i,j}}{dt} + F(q_{i,j}) - \frac{1}{\beta^{i-1}}(p_{\lfloor k/2 \rfloor} - p_k) = 0, \quad (8.55)$$

where $i = 2, \dots, N_g - 1$ and $j = 1, \dots, M_i$. The momentum equations of branches at the outlet generation are

$$\frac{dq_{N_g,j}}{dt} + F(q_{N_g,j}) - \frac{1}{\beta^{N_g-1}}(p_{\lfloor k/2 \rfloor} - p_{out}) = 0, \quad (8.56)$$

where $j = 1, \dots, 2^{N_g-1}$ and p_{out} is the pressure at the outlet of the network. Let $q_{i,j} = \bar{q}_{i,j} + q'_{i,j}$ and $p_k = \bar{p}_k + p'_k$. The bar denotes an equilibrium point and the prime a small perturbation. Substituting the perturbed variables in Equations (8.6), (8.18), (8.55) and (8.56), and subtracting the steady-state solution the system becomes

$$q'_{i,j} - q'_{i+1,2j-1} - q'_{i+1,2j} = 0 \quad (8.57)$$

$$\frac{dq'_{1,1}}{dt} + F(\bar{q}_{1,1} + q'_{1,1}) - F(\bar{q}_{1,1}) + p'_1 = 0 \quad (8.58)$$

$$\frac{dq'_{i,j}}{dt} + F(\bar{q}_{i,j} + q'_{i,j}) - F(\bar{q}_{i,j}) - \frac{1}{\beta^{i-1}}(p'_{\lfloor k/2 \rfloor} - p'_k) = 0 \quad (8.59)$$

$$\frac{dq'^{N_g}}{dt} + F(\bar{q}_{N_g,j} + q'_{N_g,j}) - F(\bar{q}_{N_g,j}) - \frac{1}{\beta^{N_g-1}}p'_{\lfloor k/2 \rfloor} = 0 \quad (8.60)$$

Consider the following function

$$V = \frac{1}{2} \sum_{i=1}^{N_g} \sum_{j=1}^{M_i} \beta^{i-1} q'^2_{i,j}. \quad (8.61)$$

Differentiating V respect to time and using Equations (8.58)–(8.60) we have

$$\frac{dV}{dt} = \sum_{i=1}^{N_g} \sum_{j=1}^{M_i} \beta^{i-1} q'_{i,j} \frac{dq'_{i,j}}{dt} \quad (8.62)$$

$$\begin{aligned}
&= - \sum_{i=1}^{N_g} \sum_{j=1}^{M_i} \beta^{i-1} q'_{i,j} (F(\bar{q}_{i,j} + q'_{i,j}) - F(\bar{q}_{i,j})) - q'_{1,1} p'_1 \\
&\quad + \sum_{i=1}^{N_g} \sum_{j=1}^{M_i} q'_{i,j} (p'_{[k/2]} - p'_k) + \sum_{j=1}^{2^{N_g-1}} q'_{N_g,j} p'_{[k/2]}. \tag{8.63}
\end{aligned}$$

The resistance term in the last equation, first term on the right hand side, is negative for any volumetric flow. Looking only at the pressure terms

$$\Pi = -q'_{1,1} p'_1 + \sum_{i=2}^{N_g-1} \sum_{j=1}^{M_i} q'_{i,j} (p'_{[k/2]} - p'_k) + \sum_{j=1}^{2^{N_g-1}} q'_{N_g,j} p'_{[k/2]}, \tag{8.64}$$

$$\begin{aligned}
&= -q'_{1,1} p'_1 + q'_{2,1} (p'_1 - p'_2) + q'_{2,2} (p'_1 - p'_3) + q'_{3,1} (p'_2 - p'_4) \\
&\quad + q'_{3,2} (p'_2 - p'_5) + \dots, \tag{8.65}
\end{aligned}$$

$$\begin{aligned}
&= p'_1 (-q'_{1,1} + q'_{2,1} + q'_{2,2}) + p'_2 (-q'_{2,1} + q'_{3,1} + q'_{3,2}) \\
&\quad + p'_3 (-q'_{2,2} + q'_{3,3} + q'_{3,4}) + \dots, \tag{8.66}
\end{aligned}$$

$$\begin{aligned}
&= p'_k (-q'_{i,j} + q'_{i+1,2j-1} + q'_{i,2j}), \\
&= 0. \tag{8.67}
\end{aligned}$$

It can be seen that every nodal pressure is associated to three flows that satisfy the continuity law, Equation (8.57), for that particular node by explicitly writing the first terms of Equation (8.64). Since $V \geq 0$ and $dV/dt \leq 0$, V is a Lyapunov function and the steady-state hydrodynamics of a tree network of N_g generations are globally stable and consequently also unique.

8.5 Unstable flow

The dynamics of a flow in a single branch driven by a pressure difference depend on the geometry, fluid physical properties, friction law and the pressure difference itself. For a branch with fixed geometry the pressure difference can be varied to drive the flow to a either laminar or turbulent equilibrium point and the transition zone has minimum relevance. However in a tree network with flow driven by the pressure

difference between the network inlet and outlet, provided that the flow is turbulent at the entrance, some generations may inevitable be trapped by the transition regime and, in fact, stay oscillating between the two regimes. To illustrate this phenomenon a single branch is considered before studying the network.

8.5.1 Single branch

Consider a conduit where the flow is driven by a pressure difference between the inlet and the outlet; Equation (8.5) for $i = 1$ and $Re_c = 2300(1 \pm \epsilon/2)$. The inlet and outlet pressure values are constant. The critical Reynolds number when the fluid is accelerated is not necessarily the same to the one when it is decelerated; the parameter ϵ represents this difference. Indeed the critical Reynolds number for the acceleration is higher than that for deceleration. This means that for some values of Δp exists a region where the flow is neither fully laminar nor fully turbulent and oscillates with hysteresis, since the accelerating and decelerating path are not the same. A local analysis of Equation (8.5) allows to derive an analytical expression for the period

$$\xi = \ln \left(\frac{\bar{q}_L - q_{-\epsilon}}{\bar{q}_L - q_{+\epsilon}} \right) + \frac{1}{b} \ln \left(\frac{q_{+\epsilon} - \bar{q}_T}{q_{-\epsilon} - \bar{q}_T} \right), \quad (8.68)$$

where

$$b = \frac{7}{4} C \bar{q}_T^{3/4}, \quad (8.69)$$

$$q_{\pm\epsilon} = \frac{\pi}{4} Re_c (1 \pm \epsilon/2), \quad (8.70)$$

$$\bar{q}_L = \Delta p, \quad (8.71)$$

$$\bar{q}_T = \left(\frac{\Delta p}{C} \right)^{4/7}. \quad (8.72)$$

Figure 8.8 shows the numerically and analytically computed dimensionless frequency ϕ as a function of ϵ . The amplitude of the oscillation depends on the size of ϵ ; if ϵ is zero the velocity oscillates with an infinite frequency. Figure 8.9 shows the pipe

dynamics for $\epsilon = 0.05$. The differential Equation (8.5) was numerically integrated using an implicit Euler scheme, the Matlab subroutine *fsolve* and the following parameters: time step of 0.01, $p_{in} = 2 \times 10^3$, $p_{out} = 0$ and $\beta = 1.1$.

It is clear that the condition for global stability stated in the previous section is being violated because F is not single valued. In a certain region, there are two possible resistance values for one q . Figure 8.10 shows the laminar and turbulence resistance curves as a function of the volumetric flow rate. The solid lines represent the resistance path or the flow regions where the curve is valid. The intersection point between the laminar and turbulent lines corresponds to a $Re \simeq 1187$. $q_{+\epsilon}$ and $q_{-\epsilon}$ are shown by the vertical lines. These points correspond respectively to the laminar and turbulent boundaries; the flow oscillates in between. The path and boundaries in Figure 8.10 correspond to the individual branch simulation shown in Figure 8.9. For different parameters similar representations can be drawn.

8.5.2 Branching network

Consider a laminar steady flow in a tree of four generations. At time $t = 0$ the pressure at the inlet rises. Because of the geometry flows at certain generations will enter the transition zone and may or may not stay in this region. Figures 8.11 and 8.12 show the volumetric flows and nodal pressures of the tree when the second generation is caught in the transition regime. The instability of generation two propagates upstream and downstream producing oscillations. The DAE (8.5) and (8.6) were integrated using the following parameters: a time step of 0.01, $p_{in} = 16 \times 10^3$, $p_{out} = 0$, $\beta = 1.1$ and $\epsilon = 0.05$.

The geometry has an impact on the nature of the flow. It is possible for the flow to be turbulent at some generation and laminar at the next one. Figure 8.13 shows the $\epsilon - \beta$ plane for a 10-generation tree where the flow at the inlet branch is

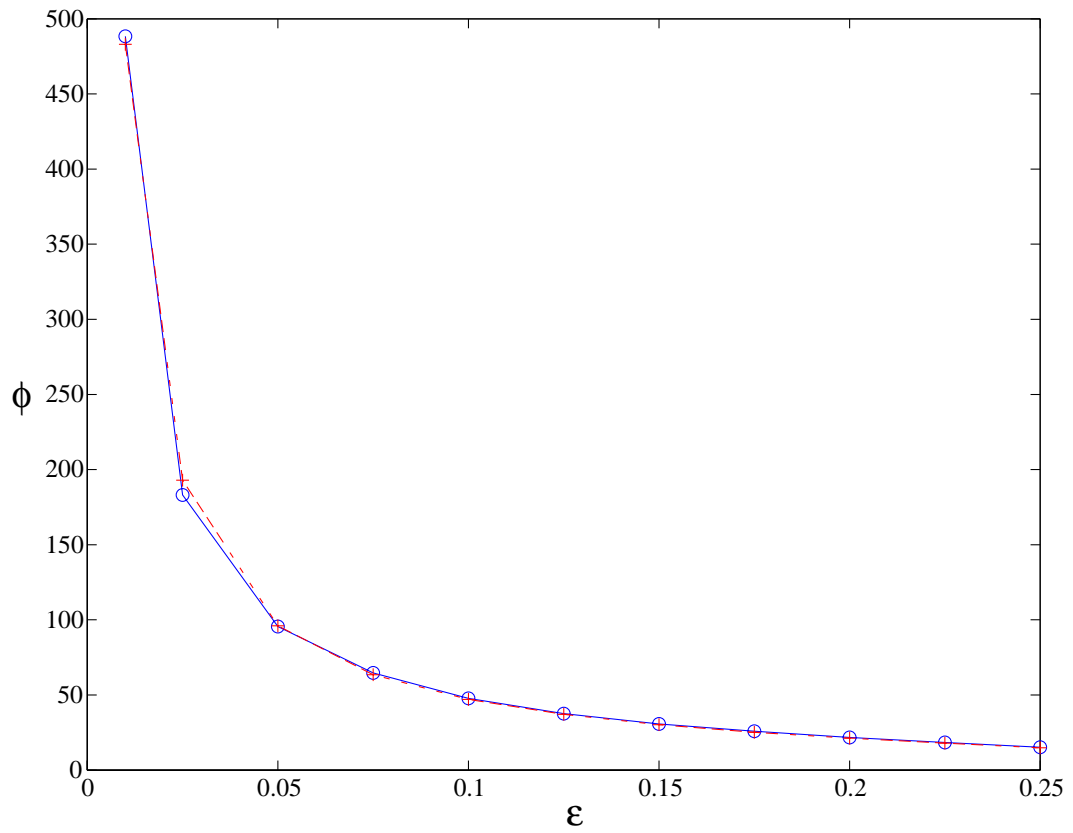


Figure 8.8. Analytical — + — and numerical — o — frequency as function of ϵ .

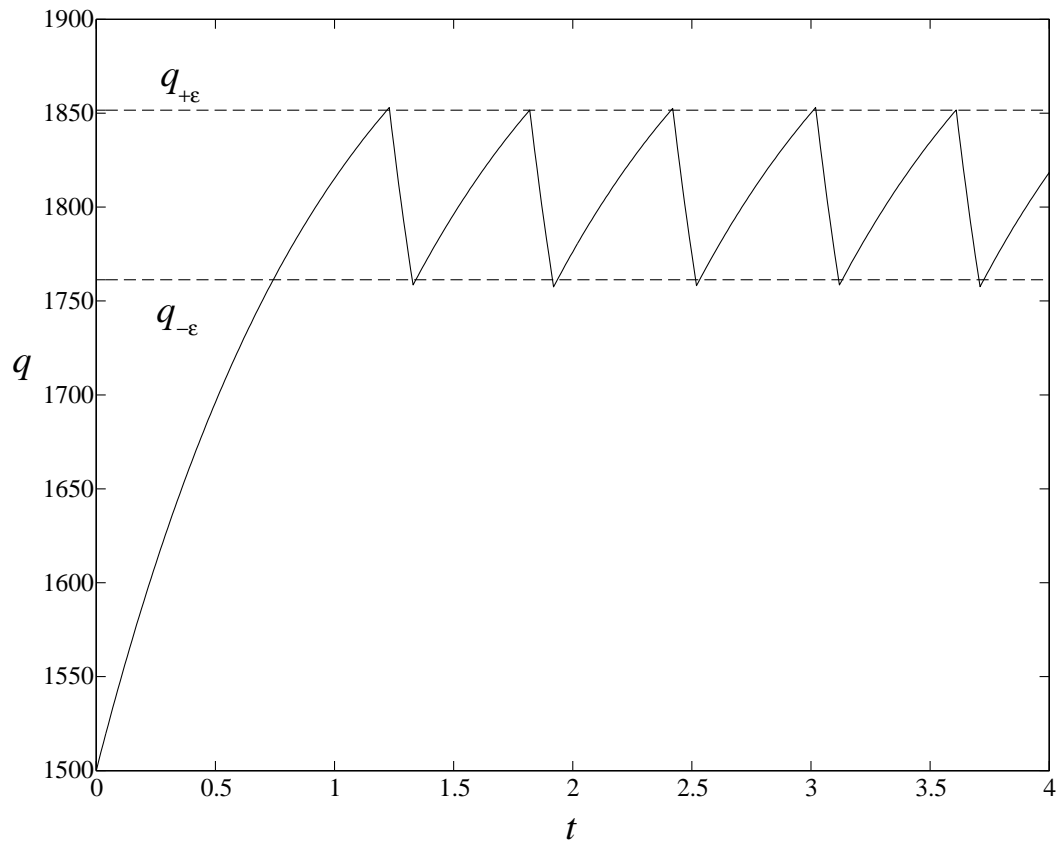


Figure 8.9. Pipe dynamics for $\epsilon = 0.05$.

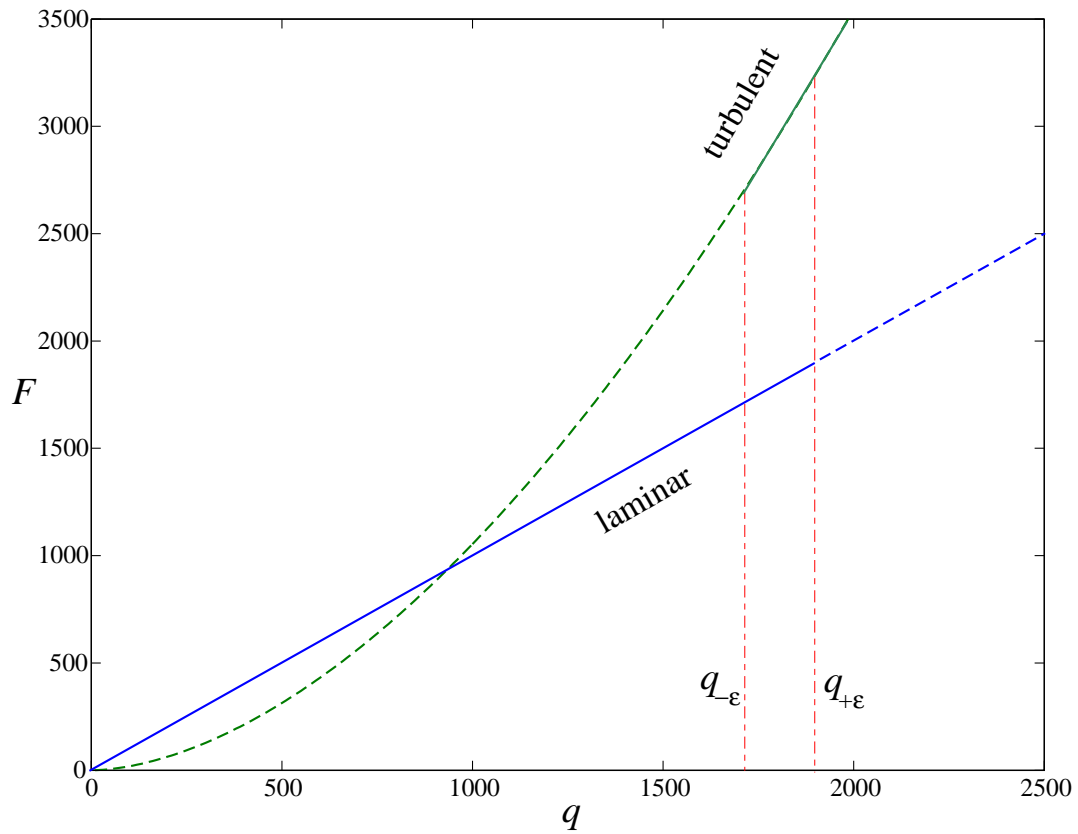


Figure 8.10. Pipe resistance F as function of q .

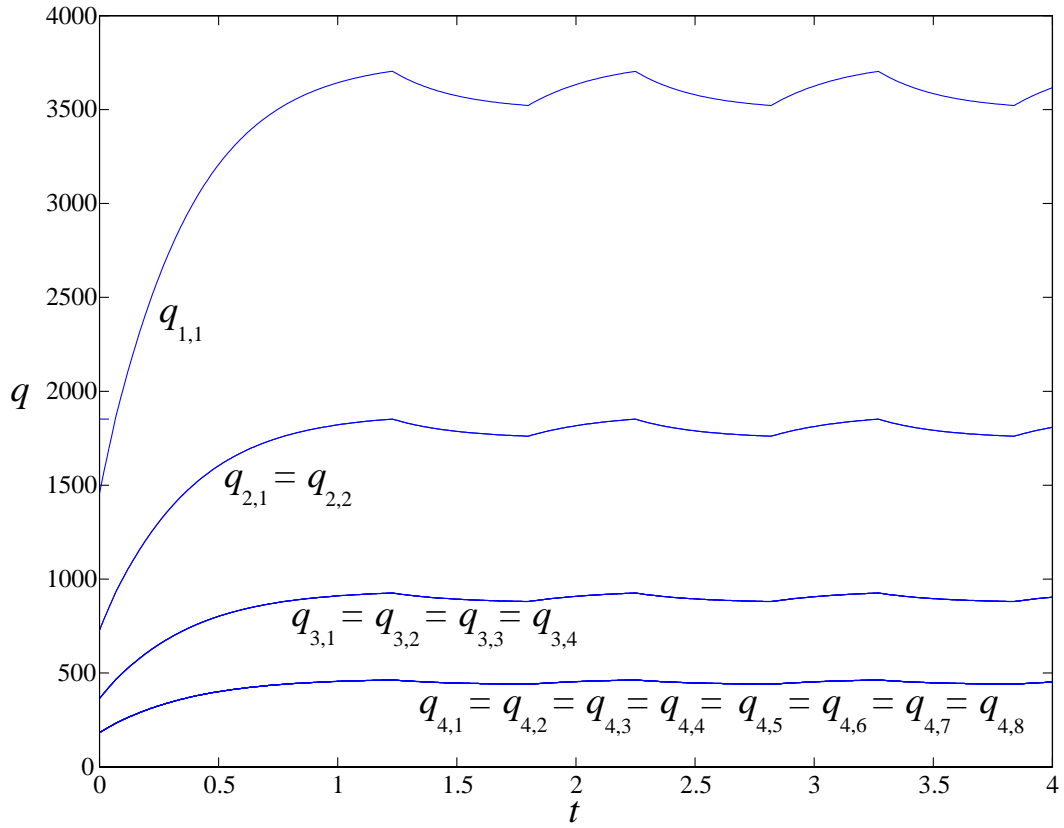


Figure 8.11. Flow rates for network with four generations when second generation oscillates.

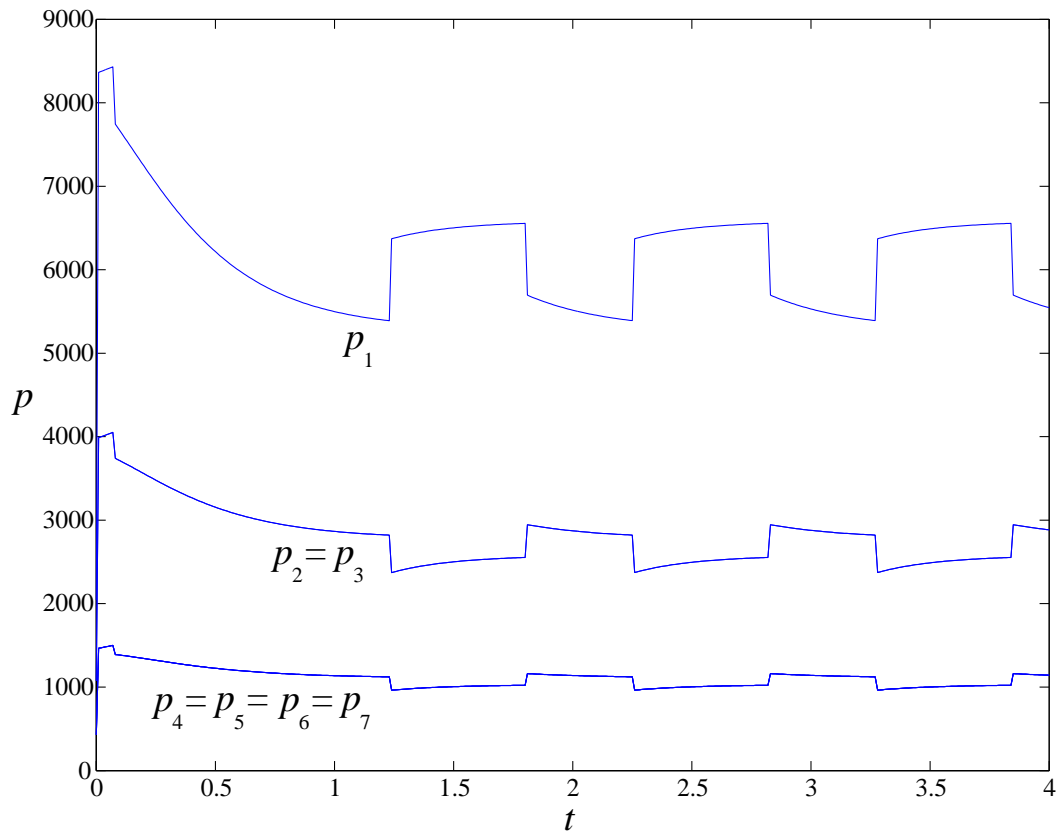


Figure 8.12. Nodal pressures for network with four generations when second generation oscillates.

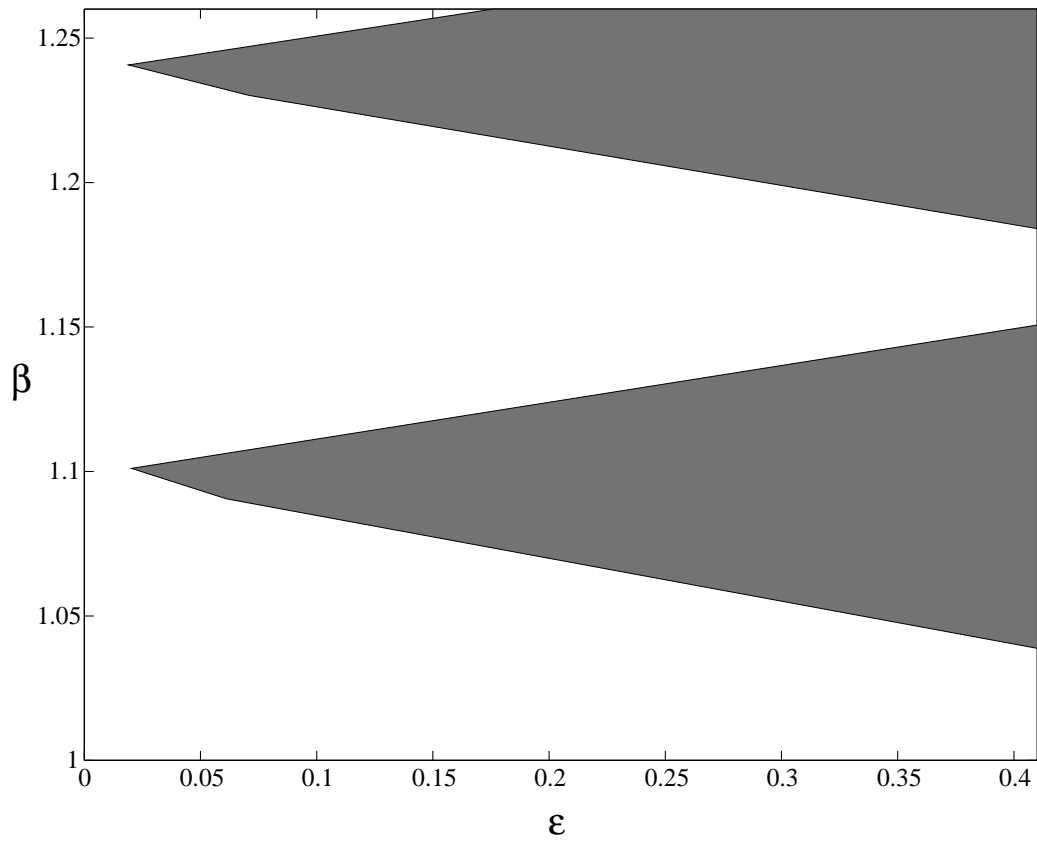


Figure 8.13. ϵ - β plane for 10 generation network where first branch Reynolds number is eleven times Re_c .

turbulent. The shaded area means that the flow value of at least one generation lies in the transition regime. Flows will oscillate for that choice of parameters. Outside of the shaded area the flow changes from turbulent to laminar in one generation, and the network is a first turbulent-last laminar tree.

8.6 Hydrodynamic control

In this section the hydrodynamic state and output controllability of a regular tree network is studied. Pumps are the most common devices used to transport fluid within large networks. To address the control problem pumps and valves are considered as the manipulated variables to control volumetric flow rates at branches and pressures at junctions.

The controllability theory for linear systems is well defined, as explained in Section 1.2, so that the flow will be assumed to be laminar here. Thus

$$\frac{dq_{i,j}}{dt} + \beta^{2(i-1)}q_{i,j} - \frac{1}{\beta^{i-1}}(\Delta p_{i,j} + \mathcal{P}_{i,j}) = 0, \quad (8.73)$$

where the added term $\mathcal{P}_{i,j}$ represents the pressure rise due to the pump. It is assumed that in generation i $\mathcal{P}_{i,j} = \mathcal{P}/\theta^{i-1}$, where θ is a scaling parameter and \mathcal{P} is the pressure rise of the pump at the inlet branch.

8.6.1 Control by means of valves

Consider flow in a large network driven by a constant pressure difference between the inlet and outlet. Valves are used as the manipulated variables to attempt to control the hydrodynamics.

By placing one valve in any branch of the tree the network is not controllable. The variables of state are the flows and pressures at every branch and junction, respectively. With one valve as control input the hydrodynamic variables cannot be prespecified and achieved. However the tree is output controllable if the output

of interest is just one flow or a pressure junction. Indeed it is output controllable within a range imposed by the driving force, geometry, friction and fluid physical properties. If a second valve is added the network is still not state controllable and it is output controllable in two variables. The output controllability range is affected by the valves themselves since each valve has an effect on the flow. If a valve is used in every branch the network state space is not controllable. Consider a two generation network like the one in Figure 8.7. The variables are the three flows and the pressure at the junction. Two flows may be specified but the third one cannot be chosen. This means that flows at the junctions in any tree network are not totally independent because of the continuity law. Mathematically, the algebraic relations impose a constraint on the differential variables.

A tree network with valves in every branch allows analysis of the problem of failure detection since valve changes in any branch have an effect in upstream, downstream and parallel flows. Consider a four generation tree with valves in every branch and flow driven by a pressure difference, i.e. $p_{in} - p_{out} \neq 0$. One branch at a time is completely blocked and the flow rates are computed for $\beta = 1.2$ and $\theta = 1.25$. A four generation tree has 15 branches. Only the seven branches within the first three generations are blocked. The columns of matrix \mathbf{R}_{out} represent the seven blockages. The elements of each column are the last generation flow rates, from top to bottom: $q_{4,1}$, $q_{4,2}$, $q_{4,3}$, $q_{4,4}$, $q_{4,5}$, $q_{4,6}$, $q_{4,7}$ and $q_{4,8}$.

By looking at the outlet flows it can easily be determined where the blockage occurred. The blockage in each column case is at the last common branch of those branches with no flow. The first common branch is (1,1). For instance, in column six the last common branch to branches (4,5) and (4,6) is (3,3); thus this branch is completely blocked. Furthermore, for n pairs of zero flow measurements the failure is going to be n generations upstream. If one branch is partially blocked

the downstream flows at the outlet are lower than the flow of the outlets without a blockage; the location of the partial block is determined as before. However if there is more than one partial blocking at a time it is not possible to locate the blockage by only looking at the outlet flows.

$$\mathbf{R}_{out} = \begin{bmatrix} 0.000 & 0.000 & 0.134 & 0.000 & 0.149 & 0.120 & 0.120 \\ 0.000 & 0.000 & 0.134 & 0.000 & 0.149 & 0.120 & 0.120 \\ 0.000 & 0.000 & 0.134 & 0.149 & 0.000 & 0.120 & 0.120 \\ 0.000 & 0.000 & 0.134 & 0.149 & 0.000 & 0.120 & 0.120 \\ 0.000 & 0.134 & 0.000 & 0.120 & 0.120 & 0.000 & 0.149 \\ 0.000 & 0.134 & 0.000 & 0.120 & 0.120 & 0.000 & 0.149 \\ 0.000 & 0.134 & 0.000 & 0.120 & 0.120 & 0.149 & 0.000 \\ 0.000 & 0.134 & 0.000 & 0.120 & 0.120 & 0.149 & 0.000 \end{bmatrix}$$

8.6.2 Control by means of individual pumps

As an alternative control method the use of individual pumps as inputs to manipulate the nodal pressures is studied in this section. Independent pumps that produce a pressure rise $\mathcal{P}_{i,j}$ may be placed in every branch of the tree.

The hydrodynamic network model constitutes a DAE system, Equations (8.73) and (8.6) must be recast into a dynamical system in order to investigate the control properties of the tree network. This is not a trivial task. DAE systems have been extensively studied, as pointed out in Section 1.4. In order to write a purely differential system, an option is to exclude the pipes whose flow rates are dependent on those of the others. Alternatively, one can write differential equations with the pressures at the junctions as the only unknowns. The procedure to recast the system is next presented for a two generation network; three differential momentum equations and one algebraic continuity equation are reduced to a one differential

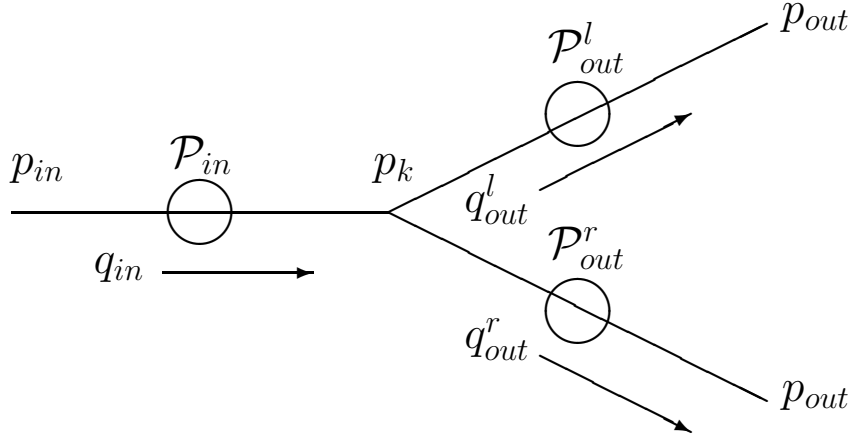


Figure 8.14. Flow into and out of junction k .

pressure equation. The procedure is then extended to larger networks so that differential pressure equations are written for a N_g generations tree network. Once the system is recast the state variables of the reduced system are the pressures at the junctions. Then the volumetric flow rates are elected to be the system output variables.

8.6.3 From differential algebraic to differential equations

The inflow, subscript in , and outflow, subscript out with superscripts l and r , to a single junction are shown in Figure 8.14 with the pressures at the junction, the flow rates in the inlet and outlet pipes, and the pressure rises due to the pumps marked. For the three pipes involved, the momentum equations are

$$\frac{dq_{in}}{dt} + \beta^{2(i-1)} q_{in} = \beta^{1-i} (p_{in}(t) - p_k(t) + \mathcal{P}_{in}(t)), \quad (8.74)$$

$$\frac{dq_{out}^l}{dt} + \beta^{2i} q_{out}^l = \beta^{-i} (p_k(t) - p_{out}^l(t) + \mathcal{P}_{out}^l(t)), \quad (8.75)$$

$$\frac{dq_{out}^r}{dt} + \beta^{2i} q_{out}^r = \beta^{-i} (p_k(t) - p_{out}^r(t) + \mathcal{P}_{out}^r(t)). \quad (8.76)$$

In addition we have mass conservation at the junction that can be written as

$$q_{in} - q_{out}^l - q_{out}^r = 0. \quad (8.77)$$

Adding Equations (8.75) and (8.76), subtracting the sum from (8.74), using (8.77) and differentiating the result is

$$\begin{aligned} \beta^{2(i-1)} \frac{dq_{in}}{dt} - \beta^{2i} \frac{d}{dt} (q_{out}^l + q_{out}^r) &= \beta^{1-i} \frac{d}{dt} (p_{in} - p_k + \mathcal{P}_{in}) \\ &+ \beta^{-i} \frac{d}{dt} (2p_k - p_{out}^l - p_{out}^r \\ &+ \mathcal{P}_{out}^l + \mathcal{P}_{out}^r). \end{aligned} \quad (8.78)$$

Dividing Equation (8.74) by $\beta^{2(i-1)}$ and subtracting the sum of (8.75) and (8.76) divided by β^{2i} gives

$$\begin{aligned} \frac{1}{\beta^{2(i-1)}} \frac{dq_{in}}{dt} - \frac{1}{\beta^{2i}} \frac{d}{dt} (q_{out}^l + q_{out}^r) &= \frac{\beta^{1-i}}{\beta^{2(i-1)}} (p_{in} - p_k + \mathcal{P}_{in}) \\ &- \frac{\beta^{-i}}{\beta^{2i}} (2p_k - p_{out}^l - p_{out}^r \\ &+ \mathcal{P}_{out}^l + \mathcal{P}_{out}^r). \end{aligned} \quad (8.79)$$

Dividing Equation (8.78) by $\beta^{2(i-1)}$ and subtracting from (8.79) multiplied by $\beta^{2(i-1)}$, the equation becomes

$$\begin{aligned} \frac{(\beta^{2i})^2 - (\beta^{2(i-1)})^2}{\beta^{2(i-1)}\beta^{2i}} \frac{d}{dt} (q_{out}^l + q_{out}^r) &= -\frac{\beta^{1-i}}{\beta^{2(i-1)}} \frac{d}{dt} (p_{in} - p_k + \mathcal{P}_{in}) \\ &+ \beta^{1-i} (p_{in} - p_k + \mathcal{P}_{in}) \\ &+ \frac{\beta^{-i}}{\beta^{2(i-1)}} \frac{d}{dt} (2p_k - p_{out}^l - p_{out}^r + \mathcal{P}_{out}^l + \mathcal{P}_{out}^r) \\ &- \frac{\beta^{-i}\beta^{2(i-1)}}{\beta^{2i}} (2p_k - p_{out}^l - p_{out}^r + \mathcal{P}_{out}^l + \mathcal{P}_{out}^r). \end{aligned} \quad (8.80)$$

In a similar way from Equations (8.78) and (8.79) the following equation arises

$$\frac{(\beta^{2i})^2 - (\beta^{2(i-1)})^2}{\beta^{2(i-1)}\beta^{2i}} \frac{dq_{in}}{dt} = -\frac{\beta^{1-i}}{\beta^{2i}} \frac{d}{dt} (p_{in} - p_k + \mathcal{P}_{in})$$

$$\begin{aligned}
& + \frac{\beta^{1-i}\beta^{2i}}{\beta^{2(i-1)}} (p_{in} - p_k + \mathcal{P}_{in}) \\
& + \frac{\beta^{-i}}{\beta^{2i}} \frac{d}{dt} (2p_k - p_{out}^l - p_{out}^r + \mathcal{P}_{out}^l + \mathcal{P}_{out}^r) \\
& - \beta^{-i} (2p_k - p_{out}^l - p_{out}^r + \mathcal{P}_{out}^l + \mathcal{P}_{out}^r). \quad (8.81)
\end{aligned}$$

The difference of the last two equations eliminates the flow rates to give

$$\begin{aligned}
\beta^{1-i} \frac{dp_{in}}{dt} - \beta^{-i}(\beta + 2) \frac{dp_k}{dt} + \beta^{-i} \frac{dp_{out}^l}{dt} + \beta^{-i} \frac{dp_{out}^r}{dt} = \\
- \beta^{1+i} p_{in} + \beta^{i-1}(\beta^2 + 2\beta^{-1}) p_k - \beta^{i-2} p_{out}^l - \beta^{i-2} p_{out}^r \\
- \left(\beta^{1+i} \mathcal{P}_{in} - \beta^{i-2} \mathcal{P}_{out}^l - \beta^{i-2} \mathcal{P}_{out}^r + \beta^{1-i} \frac{d\mathcal{P}_{in}}{dt} - \beta^{-i} \frac{d\mathcal{P}_{out}^l}{dt} - \beta^{-i} \frac{d\mathcal{P}_{out}^r}{dt} \right), \quad (8.82)
\end{aligned}$$

which is the differential equation that relates the pressures at neighboring junctions.

The original DAE is of index 2 since two differentiations are necessary to obtain a set of ODEs.

Equation (8.82) can be written for each one of the N_n junctions in the tree to form a system of equations. The variables to be controlled are the pressures at the junctions which can be written as a vector $\mathbf{X} = [p_1 \ p_2 \ \dots \ p_{N_n}]^T \in \mathbb{R}^{N_n}$. The control inputs are the pump pressure rise terms which can also be written as $\mathbf{u} = [\mathcal{P}_1 \ \mathcal{P}_2 \ \dots \ \mathcal{P}_{N_p}]^T \in \mathbb{R}^{N_p}$ and $\dot{\mathbf{u}} = [d\mathcal{P}_1/dt \ d\mathcal{P}_2/dt \ \dots \ d\mathcal{P}_{N_p}/dt]^T \in \mathbb{R}^{N_p}$. Thus

$$\mathbf{E}\dot{\mathbf{X}} = \mathbf{F}\mathbf{X} + \mathbf{G}\mathbf{u} + \mathbf{H}\dot{\mathbf{u}} + \mathbf{a}, \quad (8.83)$$

where $\mathbf{E} \in \mathbb{R}^{N_n \times N_n}$, $\mathbf{F} \in \mathbb{R}^{N_n \times N_n}$, $\mathbf{G} \in \mathbb{R}^{N_n \times N_p}$, $\mathbf{H} \in \mathbb{R}^{N_n \times N_p}$ and the vector $\mathbf{a} \in \mathbb{R}^{N_n}$ contains the known inlet and outlet pressures of the tree.

For example, for the 4-generation, 15-pipe, 7-junction tree in Figure 8.1, it can be shown that

$$\mathbf{E} = \begin{bmatrix} -\tilde{\beta} & \beta^{-1} & \beta^{-1} & 0 & 0 & 0 & 0 \\ \beta^{-1} & -\beta^{-1}\tilde{\beta} & 0 & \beta^{-2} & \beta^{-2} & 0 & 0 \\ \beta^{-1} & 0 & -\beta^{-1}\tilde{\beta} & 0 & 0 & \beta^{-2} & \beta^{-2} \\ 0 & \beta^{-2} & 0 & -\beta^{-2}\tilde{\beta} & 0 & 0 & 0 \\ 0 & \beta^{-2} & 0 & 0 & -\beta^{-2}\tilde{\beta} & 0 & 0 \\ 0 & 0 & \beta^{-2} & 0 & 0 & -\beta^{-2}\tilde{\beta} & 0 \\ 0 & 0 & \beta^{-2} & 0 & 0 & 0 & -\beta^{-2}\tilde{\beta} \end{bmatrix}$$

$$\mathbf{F} = - \begin{bmatrix} -\hat{\beta} & \beta^{-1} & \beta^{-1} & 0 & 0 & 0 & 0 \\ \beta^3 & -\beta\hat{\beta} & 0 & 1 & 1 & 0 & 0 \\ \beta^3 & 0 & -\beta\hat{\beta} & 0 & 0 & 1 & 1 \\ 0 & \beta^4 & 0 & -\beta^2\hat{\beta} & 0 & 0 & 0 \\ 0 & \beta^4 & 0 & 0 & -\beta^2\hat{\beta} & 0 & 0 \\ 0 & 0 & \beta^4 & 0 & 0 & -\beta^2\hat{\beta} & 0 \\ 0 & 0 & \beta^4 & 0 & 0 & 0 & -\beta^2\hat{\beta} \end{bmatrix}$$

$$\mathbf{a}^T = \begin{bmatrix} -\beta^2 & 0 & 0 & -2\beta & -2\beta & -2\beta & -2\beta \end{bmatrix}$$

where $\tilde{\beta} = 1 + 2/\beta$ and $\hat{\beta} = \beta^2 + 2/\beta$. \mathbf{G} and \mathbf{H} are known 7×15 matrices that are too large to be shown here. The matrix \mathbf{E} is found to be symmetric and non-singular.

Multiplying by \mathbf{E}^{-1} and writing $\mathbf{x} = \mathbf{X} + \mathbf{A}^{-1}\mathbf{b}$, Equation (8.83) takes the form

$$\dot{\mathbf{x}} = \mathbf{A}\mathbf{x} + \mathbf{B}\mathbf{u} + \mathbf{Z}\dot{\mathbf{u}}, \quad (8.84)$$

where $\mathbf{A} = \mathbf{E}^{-1}\mathbf{F}$, $\mathbf{B} = \mathbf{E}^{-1}\mathbf{G}$, $\mathbf{Z} = \mathbf{E}^{-1}\mathbf{H}$ and $\mathbf{b} = \mathbf{E}^{-1}\mathbf{a}$. In summary, the vector of state variables $\mathbf{x}(t)$ contains the junction pressure terms $p_k(t)$ and the vectors of

inputs $\mathbf{u}(t)$ and $\dot{\mathbf{u}}(t)$ contain the pressure rise terms \mathcal{P}_k and $d\mathcal{P}_k/dt$ produced by the control branch pumps, respectively. The vector of outputs $\mathbf{y}(t)$ of the system is taken to be the branch volumetric flows $q_k(t)$.

8.6.4 State R-controllability and output controllability

Defining

$$\mathbf{v} = \mathbf{B}\mathbf{u} + \mathbf{Z}\dot{\mathbf{u}}, \quad (8.85)$$

Equation (8.84) becomes

$$\dot{\mathbf{x}} = \mathbf{A}\mathbf{x} + \mathbf{v}, \quad (8.86)$$

where $\mathbf{v} \in \mathbb{R}^{N_n}$ is temporarily the input variable. The system has the form of Equation (1.2). The vector \mathbf{x} is controllable if the matrix

$$\mathbf{M} = \left[\mathbf{I} : \mathbf{A}\mathbf{I} : \mathbf{A}^2\mathbf{I} : \dots : \mathbf{A}^{N_n-1}\mathbf{I} \right], \quad (8.87)$$

where $\mathbf{M} \in \mathbb{R}^{N_n \times N_n N_n}$ and \mathbf{I} is the identity matrix, is of rank N_n and \mathbf{v} exists. \mathbf{B} and \mathbf{Z} are rectangular matrices within $\mathbb{R}^{N_n \times N_p}$. Since $N_n < N_p$ the vector \mathbf{v} is not unique and the controllability depends on the matrix \mathbf{A} . From Equation (8.85), \mathbf{u} can be determined for any given \mathbf{v} , indicating that the system is also controllable for \mathbf{u} as the input variable.

Let the column vector $\mathbf{Y} \in \mathbb{R}^{N_o}$ contain N_o volumetric flows, hence flows as a function of pressures can be written as

$$\mathbf{Y} = \mathbf{C}\mathbf{x} + \mathbf{D}\mathbf{u}, \quad (8.88)$$

where $\mathbf{C} \in \mathbb{R}^{N_o \times N_n}$ and $\mathbf{D} \in \mathbb{R}^{N_o \times N_p}$. The vector of known inlet and outlet pressures, \mathbf{c} , has been eliminated by a change of variable, $\mathbf{y} = \mathbf{Y} + \mathbf{C}\mathbf{A}^{-1}\mathbf{b} + \mathbf{c}$. The flows are output controllable if

$$\mathbf{N} = \left[\mathbf{D} : \mathbf{C}\mathbf{I} : \mathbf{C}\mathbf{A}\mathbf{I} : \mathbf{C}\mathbf{A}^2\mathbf{I} : \dots : \mathbf{C}\mathbf{A}^{N_n-1}\mathbf{I} \right], \quad (8.89)$$

Table 8.1. RANKS OF CONTROLLABILITY MATRICES.

N_g	N_b	N_n	N_o	Rank of \mathbf{M}	Rank of \mathbf{N}
2	3	1	2	1	2
3	7	3	4	3	4
4	15	7	8	7	8
5	31	15	16	15	16
6	63	31	32	31	32

where $\mathbf{N} \in \mathbb{R}^{N_o \times (N_n+1)N_n}$, is of rank N_o .

Due to the fact that the aforementioned DAE model has been reduced to a differential one, the reduced system, if controllable, would be partially controllable or *R-controllable* (Yip and Sincovec, 1981). The original state vector contains flow rates in addition to pressure terms.

Numerical calculations were performed for networks of 2, 3, 4, 5 and 6 generations with pumps in every branch. Calculations are summarized in Table 8.6.4 where the number of generations, branches, nodes and output flows determine the rank of the state and output controllability matrices. A two generation tree, Figure 8.14, is the smallest possible network within such topology; there is one junction and three branches, that is, one nodal pressure, three flows and three pumps. Using pumps in every branch the two generation tree is state controllable and only two flows are output controllable. The third flow cannot be specified because of its dependence on the other two. In a three generation network pumps in every branch make it state controllable, this is also true for four, five and six generations networks. This means that using N_b individual control pumps in a N_g network tree the N_n pressure junctions are state controllable and 2^{N_g-1} flows are output controllable. By individual is meant that there is only one pump per branch.

The system is state controllable by using the total number of available pumps. One pump is the minimum control input device. In the minimum case only a two

generation network is state controllable, i.e. pressure junctions in a $N_g > 2$ tree network are not controllable by manipulating one pump.

8.7 Discussion

In this Chapter large, regular tree networks are considered. Simple but realistic assumptions are made regarding their geometrical self-similarity and hydrodynamics. The scaling of the geometry plays an important role in the design and construction of bifurcating networks. It determines the total length, lateral area and volume of the conduit material. The scaling parameter β has an effect on the flow resistance; for certain values an infinite network has a finite resistance. Because of the branching and scaling the local Reynolds number changes from one generation to the next one. Then if the inlet flow is laminar the outlet flows may be laminar or turbulent. If the inlet flow is turbulent the outlet flows may be laminar or turbulent. The nature of the outlet flows depends on the choice of β .

It is shown that the hydrodynamics of a network of two generations are globally stable when the flow resistance due to the friction is a non-decreasing function of the flow rate. When the condition does not hold the flow may get caught in the transition zone that exists between laminar and turbulent flow. If this is the case the flow oscillates at a frequency proportional to the difference between the upper and lower boundaries. The boundaries are imposed by the difference between critical Reynolds number when flow is accelerating and the critical Reynolds number when flow is decelerating. In an individual branch, the unstable zone may easily be avoided by modifying the driving force in such a way that the flow is taken to the desired regime. In a branching network as the geometry changes some generations may inevitably fall into the transition zone. Instabilities propagate upstream and downstream and the flows oscillate. For this situation to occur the inlet flow must

be turbulent. It is also possible that the flow changes from turbulent to laminar from one generation to the next one so that the flows do not oscillate. This depends on the driving force and the scaling parameter.

Control is introduced to the network and the flow control characteristics of the tree are determined for different choices of manipulated variables: valves on one or every branch, a pump located anywhere in the network, and individual pumps placed on every branch. Considering valves as inputs the failure detection problem was explored. When partial or complete blockage of a branch within the tree occurs it is possible to locate the branch by looking at the outlet flows. If there is more than one blockage at a time the problem is more complex. In the control problem, the hydrodynamics of a tree are not fully controllable because of the continuity law. At every junction two out of three flows can be specified. In the linear case, it is possible to reduce the DAE model of the tree hydrodynamics to a differential model with the pressure at the junctions as the state variables. The pressures at the junctions are controllable by using individual pumps on every branch. The pressure rise and its derivative are the control inputs. The pumps allow control of a certain number of flow rates as system outputs. The number of output controllable flows depends on the size of the network.

CHAPTER 9

CONCLUSIONS AND RECOMMENDATIONS

9.1 Modeling, simulation and experiments in hydronic networks

A simple but realistic model based on first principles has been presented in Chapter 2. Simple models provide the flexibility needed for the simulation of large systems such that control and optimization problems in networks can be addressed. The model was successfully used to study small, irregular and closed cooling networks, as well as large, regular and open bifurcating fluid networks.

Experiments are as important as modeling and simulation. In fact experiments and analysis complement each other in a powerful way since experiments cannot go as far and fast as a simulation, and simulations cannot include all the complexity of the problem. The information provided by experiments may be overwhelming but a complementary theoretical analysis might throw new physical insights. The temperature changes and flow response obtained in the numerical simulation are similar to those obtained in the experimental investigation. Indeed similar conclusions can be independently drawn. However the experimental dynamics of the valve are very complex due to hysteresis effects, imperfect actuators, imperfect instruments, delay effects, etc.

9.2 Strategies for thermal control

Three commonly used control techniques for heating and cooling of buildings have been studied and compared through analytical models and experiments. Among

the three, the variable flow technique VF is the most simple and economic to implement. As the thermal load varies, this technique maintains the specified temperature at the conditioned space. However the return water temperature from the secondary loop and the supplied water flow show large deviations from their design value. The constant flow technique CF also maintains the specified temperature at the conditioned space as the thermal load varies. In addition the supplied water flow to the secondary loop is almost constant. The return water temperature shows large deviations from its design value. The constant temperature difference technique BT cannot maintain a constant temperature value at the conditioned space as the thermal load changes. The supplied flow water is variable but the return water temperature from the secondary loop is constant. The temperature of the water going back to the cooling plant is related to the energy consumed by the chillers; the larger the deviations of the water temperature at the chiller inlet from its design value the more heat is to be extracted. Therefore BT is a better choice regarding energy consumption by the chillers. CF is a good option for economy water pumping and comfort at the conditioned space. VF provides comfort and is economic in implementation but not in operation.

9.3 Selection and placement of control hardware

The selection and location of the hardware in fluid networks strongly affects the operation of the system and thermal control. The placement of two pumps and a control valve within a specific secondary loop layout has been explored. Among several configurations there is an optimum that maximizes the reachability range of the leaving air temperature and minimizes the change in the return water temperature. This configuration reduces the energy consumption at the chillers and has a broad range of temperature targets for cooling down the air. In general, to achieve a

cooling or heating task there are several possible configurations regarding the piping arrangement, hardware selection and placement, and variables to be controlled.

9.4 Bifurcating networks

The flow dynamics of large regular fluid networks within a tree topology have been investigated by means of theoretical models and principles. A scaling parameter defines the geometry of the tree. Therefore the choice of this parameter plays a key role in the design of the network and flow hydrodynamics. In addition the control properties of tree networks have been studied for a variety of control elements.

9.4.1 Flow dynamics

For a fixed pressure drop, the regime of the flow at the inlet branch and the scale factor determine the regime at the outlet branches. As the fluid flows downstream the geometry of the branches change, as well as the local Reynolds number. There are four cases: laminar-laminar, laminar-turbulent, turbulent-turbulent and turbulent-laminar.

It has been demonstrated that flows within a network of two generations are globally stable if the resistance to the flow by friction is a non-decreasing, single-valued function of the flow. If the condition for the flow resistance does not hold, the flow may stay in the transition regime, becoming unstable and oscillating. In a large network the flow can be turbulent at the entrance and as the geometry changes laminarization may occur in downstream generations. Laminarization may happen from one generation to the next one; the flow is turbulent at generation i and laminar at $i + 1$, and the change depends on the driving pressure force and the geometry scaling. However it is also possible that at generation $i + 1$ the flow falls into the transition regime and the flow in every branch of the tree oscillates.

9.4.2 Control properties

In this dissertation the control properties of hydrodynamics in large tree networks have been determined. The pressure at the junctions are controllable by placing control pumps on every branch. The pump input variables are the pressure rise and its derivative. The derivative input arises as a consequence of the DAE nature of the system. Flows are never all controllable because of their mutual dependence, as expressed by the continuity equation. Therefore the hydrodynamics of large tree networks are only partially controllable. However through varying the junction pressures a specific number of flow rates is output controllable.

9.5 Recommendations

In future experimental investigations it may be useful to extract information about the complexity of hydronic system components such as valves and pumps, and use the information to develop more accurate but simple dynamic models, for instance to extract time constants of valves when opening and closing. Model-free simulations, such as Artificial Neural Networks and Fuzzy Logic, may also be used to account for the complexity of the components.

It is also interesting to investigate the coupled dynamics in a hydronic network. Using simple controllers, minimum control hardware and basic piping layout a simple primary-secondary system may be emulated, for instance a heat exchanger within a secondary loop with a two-way valve, no bypass and a proportional controller. All the secondaries should be similar to each other and there should be at least two along with one primary loop. Changes in the thermal load at any heat exchanger will change the operational conditions in the network affecting the control in the rest of the secondaries. The coupling situation raises concerns about the response

and stability of the hydronic network. The proposed problem can be experimentally investigated by using the experiment described in Chapter 4.

In the experimental results presented in Chapter 6, it was observed that at low hot water flows CF and BT become unstable, and VF reaches a control bound. It is important to address in future studies problems like stability, reachability and controllability of thermal and fluid networks. A study of the flow stability in the experimental network may also be of interest. The hydrodynamics could be modeled as was done in Chapter 2 resulting in a system of DAE. To study the stability of such system the control theory outlined in Section 1.4 will be useful.

In the problem of optimal placement and selection of components, an optimization algorithm may be used to address a more general situation in which there are more components, there is no restriction on the piping arrangement and different variables of control are used. Properties relevant to the system implementation and operation should be regarded as optimization criteria, for instance control properties, energy consumption, dynamic response, cost, etc. Genetic Algorithms and Simulated Annealing are potential tools for this problem since the optimum lies on a discrete space.

It may be of interest in bifurcating fluid networks to study the hydrodynamics of pulsatile flow; transport phenomena, such as heat transfer; hydrodynamic and thermal effects of movable walls, like vibrating or viscoelastic walls, and bifurcation effects, such as wave reflexion. In the control of branching fluid networks it is relevant to investigate alternative control mechanisms, such as vibrating walls, and control properties of the network as a thermal system.

9.6 Significance of this research

The significance of this research is to incorporate the control problem into the complexity of thermal and fluid networks. In addition networks are identified as an emerging field that has been barely explored in thermal sciences.

REFERENCES

- Alotaibi, S. 2003: *Temperature controllability in cross-flow heat exchangers and long ducts*. Ph.D. thesis, Department of Aerospace and Mechanical Engineering, University of Notre Dame, Notre Dame, Indiana.
- Alotaibi, S., Sen, M., Goodwine, B., Yang, K. T. 2002: Numerical simulation of the thermal control of heat exchangers. *Numerical Heat Transfer, Part A*, volume 41, no. 3, pp. 229–244.
- Asiedu, Y., Besant, R. W., Gu, P. 2000: HVAC duct system design using genetic algorithms. *HVAC & R RESEARCH*, volume 6, no. 2, pp. 149–173.
- Åström, K. J., Hägglund, T. 1984: Automatic tuning of simple regulators with specifications on phase and amplitude margins. *Automatica*, volume 20, no. 5, pp. 645–651.
- Åström, K. J., Karl, J. 1995: *Adaptive control, filtering, and signal processing*. Springer-Verlag.
- Avery, G. 1998: Controlling chillers in variable flow systems. *ASHRAE Journal*, volume 40, no. 2, pp. 42–45.
- Avery, G. 2000: Selecting valves and piping coils. *ASHRAE Journal*, volume 42, no. 4, pp. 23–26.
- Avery, G. 2001: Improving the efficiency of chilled water plants. *ASHRAE Journal*, volume 43, no. 5, pp. 14–18.
- Balakrishnan, R., Ranganathan, K. 2000: *A textbook of graph theory*. Springer-Verlag.
- Barabási, A. L. 2002: *Linked*. Perseus Publishing.
- Bejan, A. 2000: *Shape and structure, from engineering to nature*. Cambridge University Press, New York, first edition.
- Bejan, A., Errera, M. 1997: Deterministic tree networks for fluid flow: geometry for minimal flow resistance between a volume and one point. *Fractals*, volume 5, no. 4, pp. 685–695.
- Berne, R., Levy, M. 1998: *Physiology*. Mosby, US, first edition.
- Biggs, N. L., Lloyd, E. K., Wilson, R. J. 1976: *Graph Theory 1736-1936*. Oxford University Press.

- Boguña, M., Satorras, R. P., Vespignani, A. 2003: Absence of epidemic thresholds in scale free networks with degree correlations. *Physical Review Letters*, volume 90, no. 2. 028701.
- Brenan, K., Campbell, S., Pezold, L. 1996: *Numerical solution of initial-value problems in differential-algebraic equations*. Society for Industrial and Applied Mathematics, Philadelphia.
- Brion, L., Mays, L. 1991: Methodology for optimal operation of pumping stations in water distribution-systems. *Journal of Hydraulic Engineering-ASCE*, volume 117, no. 11, pp. 1551–1569.
- Capps, R. W. 1995: Select the optimum pipe size. *Chemical Engineering*, volume 102, no. 7, pp. 128–132.
- Carlson-Skalak, S., White, M. D., Teng, Y. 1998: Using an evolutionary algorithm for catalog design. *Research in Engineering Design-Theory Applications and Concurrent Engineering*, volume 10, no. 2, pp. 63–83.
- Chen, Y., Cheng, P. 2002: Heat transfer in fractal tree-like micro-channels for cooling of electronic chips. *International Journal of Heat and Mass Transfer*, volume 45, no. 13, pp. 2643–2648.
- Cohn, D. 1954: Optimal systems: the vascular system. *Bulletin of mathematical biophysics*, volume 16, pp. 59–74.
- Coker, A. K. 1991: Determine process pipe sizes. *Chemical Engineering Progress*, volume 87, no. 3, pp. 33–39.
- Costa, A. L. H., Medeiros, J. L. D., Pessoa, F. L. P. 2000: Optimization of pipe networks including pumps by simulated annealing. *Brazilian Journal of Chemical Engineering*, volume 17, no. 4-7, pp. 887–895.
- Csete, M. E., Doyle, J. C. 2002: Reverse engineering of biological complexity. *Science*, volume 295, pp. 1664–1670.
- Dager, R., Zuazua, E. 2001: Controllability of tree shaped networks of vibrating strings. *Comptes Rendus de l Academie des Sciences Serie I - Mathematique*, volume 332, no. 12, pp. 1087–1092.
- Dai, L. 1989: *Singular control systems*. Springer-Verlag Berlin, Heidelberg, Germany.
- Díaz, G. 2000: *Simulation and control of heat exchangers using artificial neural networks*. Ph.D. thesis, Department of Aerospace and Mechanical Engineering, University of Notre Dame, Notre Dame, Indiana.
- Dorini, D. K., Krist, G. D., Mannion, G. F., Mannion, J. R. 1994: Method and apparatus for controlling the flow of process fluids. U.S. Patent 5,318,106.
- Fiorino, D. P. 1999: Achieving high chilled-water delta ts. *ASHRAE Journal*, volume 41, no. 11, pp. 24–30.

- Franco, W., Sen, M., Yang, K. T. 2003a: Optimization of control hardware placement in a thermal-hydraulic network. In *Proceedings of the 6th ASME-JSME Thermal Engineering Joint Conference*. TED-AJ03-239.
- Franco, W., Sen, M., Yang, K. T., McClain, R. L. 2002: Modeling and control of a thermal-hydraulic network. In *Proceedings of ASME 35th National Heat Transfer Conference*. NHTC2001-20156.
- Franco, W., Sen, M., Yang, K. T., McClain, R. L. 2003b: Comparison of thermal-hydraulic network control strategies. *Proceedings of the Institution of Mechanical Engineers, Part I: J Systems and Control Engineering*, volume 217, pp. 35–47.
- Franco, W., Sen, M., Yang, K. T., McClain, R. L. 2003c: Dynamics of thermal-hydraulic network control strategies. *Experimental Heat Transfer*. Submitted to review.
- Gafiychuk, V., Lubashevsky, I. 2001: On the principles of the vascular network branching. *J. theor. Biol.*, volume 212, pp. 1–9.
- Gantmacher, F. R. 1974: *The Theory of Matrices*, volume 2. Chelsea.
- Grasman, J., Brascamp, J. W., Van Leeuwen, J. L., Van Putten, B. 2003: The multifractal structure of arterial trees. *J. theor. Biol.*, volume 220, no. 12, pp. 75–82.
- Greenblatt, D., Moss, E. 1999: Pipe-flow relaminarization by temporal acceleration. *Physics of Fluids*, volume 11, no. 11, pp. 3478–3481.
- Gutierrez, W. 2002: Volume integration of fractal distribution networks. *Physical Review E*, volume 66. 041906.
- Harary, F., Norman, R. Z., Cartwright, D. 1965: *Structural Models: An Introduction to Theory of Directed Graphs*. J. Wiley & Sons.
- Hausdorff, F. 1919: Dimension and äusseres. *Math. Ann.*, volume 79, pp. 159–79.
- Hordeski, M. F. 2001: *HVAC control in the new millennium*. The Fairmont Press, INC.
- Iida, O., Nagano, Y. 1998: The relaminarization mechanisms of turbulent channel flow at low reynolds numbers. *Flow, Turbulence and Combustion*, volume 60, pp. 193–213.
- Incropera, F. P., DeWitt, D. P. 1996: *Fundamentals of heat and mass transfer*. Wiley.
- Kirsner, W. 1995a: Chilled water distribution problems. *Heating Piping Air Conditioning*, volume 67, no. 2, pp. 51–59.
- Kirsner, W. 1995b: Chilled water plant design. *Heating Piping Air Conditioning*, volume 68, no. 11, pp. 73–78.

- Krist, G. D. 1994: Method and apparatus for controlling the flow of process fluids. U.S. Patent 5,586,449.
- Kumar, A. 1999: *Control of nonlinear differential algebraic equation systems*. Chapman & Hall/CRC.
- Mannion, G. F., Mannion, J. R. 1994: Method and apparatus for controlling the flow of process fluids. U.S. Patent 5,138,845.
- Morillo, C., Villar, J. 1997: Neurogenic syncope. *Baillière's Clinical Neurology*, volume 6, no. 2, pp. 357–380.
- Narasimha, R., Sreenivasan, K. 1979: Relaminarization of fluid flows. *Advances in Applied Mechanics*, volume 19, pp. 221–309.
- Ohmi, M., Iguchi, M., Urahata, I. 1982a: Transition to turbulence in a pulsatile pipe flow part 1, wave forms and distribution of pulsatile velocities near transition region. *Bulletin of the Japan Society of Mechanical Engineers*, volume 25, no. 200, pp. 182–189.
- Ohmi, M., Iguchi, M., Urahata, I. 1982b: Transition to turbulence in a pulsatile pipe flow part 2, characteristics of reversing flow accompanied by relaminarization. *Bulletin of the Japan Society of Mechanical Engineers*, volume 25, no. 208, pp. 1529–1536.
- Pacheco-Vega, A. 2002: *Simulation of compact heat exchangers using global regression and soft computing*. Ph.D. thesis, Department of Aerospace and Mechanical Engineering, University of Notre Dame, Notre Dame, Indiana.
- Paraskevopoulos, P. 2002: *Modern Control Engineering*. Marcel Dekker, New York.
- Pedley, T. 2000: Blood flow in arteries and veins. In G. Batchelor, H. Moffatt, M. Worster, eds., *Perspectives of Fluid Dynamics*, chapter 3, pp. 395–574. Cambridge University Press, Cambridge, first edition.
- Pence, D. V. 2002: Reduced pumping power and wall temperature in microchannel heat sinks with fractal-like branching channel networks. *Microscale Thermophysical Engineering*, volume 6, pp. 319–330.
- Reinschke, K. 1988: *Multivariable control a graph-theoretic approach*. Springer Verlag, Germany.
- Reis, L. F. R., Porto, R. M., H. Chaudhry, F. 1997: Optimal location of control valves in pipe networks by genetic algorithm. *Journal of Water Resources planning and Management-ASCE*, volume 123, no. 6, pp. 317–326.
- Rinaldo, A., Rodriguez-Iturbe, I., Rigon, R. 1998: Channel networks. *Annu. Rev. Earth Planet Sci.*, volume 26, pp. 289–327.
- Romero-Méndez, R. 1998: *Study of external heat transfer mechanisms in single-row fin and tube heat exchangers*. Ph.D. thesis, Department of Aerospace and Mechanical Engineering, University of Notre Dame, Notre Dame, Indiana.

- Seebacher, F. 2000: Heat transfer in a microvascular network: the effect of heart rate on heating and cooling in reptiles (pogona barbata and varanus varius). *J. theor. Biol.*, volume 203, pp. 97–109.
- Sen, M., Franco, W., Alotaibi, S. 2002: Control of single and networked heat exchangers. In *Proceedings of the 9th Latin American Congress of Heat and Mass Transfer*, pp. 541–546.
- Söylemez, M. S. 2000: On the optimum channel sizing for hvac systems. *Energy Conversion and Management*, volume 42, pp. 791–798.
- Strogatz, S. H. 2001: Exploring complex networks. *Nature*, volume 410, pp. 268–276.
- Thorsen, T., Sebastian, J. M., Quake, S. R. 2002: Microfluidic large-scale integration. *Science*, volume 298, no. 5593, pp. 580–589.
- Tosun, I., Akşhin, I. 1993: Calculate critical piping parameters. *Chemical Engineering*, volume 100, no. 3, pp. 165–166.
- Varga, E., Hangos, K., Szigeti, F. 1995: Controllability of heat exchanger networks in the time-varying parameter case. *Control Engineering Practice*, volume 3, no. 10, pp. 1409–1419.
- West, G. B., Brown, J. H., Enquist, B. J. 1997: A general model for the origin of scaling laws in biology. *Science*, volume 276, no. 5309, pp. 122–126.
- Yip, E., Sincovec, R. 1981: Solvability, controllability, and observability of continuous descriptor systems. *IEEE Transactions on Automatic Control*, volume 26, no. 3, pp. 702–707.
- Yu, C. C. 1999: *Autotuning of PID Controllers*. Springer-Verlag.
- Zamir, M. 1999: On fractal properties of arterial trees. *J. theor. Biol.*, volume 197, pp. 517–526.
- Zamir, M. 2001: Fractal dimensions and multifractality in vascular branching. *J. theor. Biol.*, volume 212, pp. 183–190.
- Zhao, X. 1995: *Performance of a Single-Row Heat Exchanger at Low In-Tube Flow Rates*. Master's thesis, Department of Aerospace and Mechanical Engineering, University of Notre Dame, Notre Dame, Indiana.